8-1-2000

# Experimental Evaluation of the Composite Behavior of Precast Concrete Sandwich Wall Panels

Alexandar Mlynarczyk

Stephen Pessiki

# EXPERIMENTAL EVALUATION OF THE COMPOSITE BEHAVIOR OF PRECAST CONCRETE SANDWICH WALL PANELS

**Alexandar Mlynarczyk**

**Stephen Pessiki**

**August 2000**

## ATLSS Report No. 00-07

**ATLSS is a National Center for Engineering Research on Advanced Technology for Large Structural Systems**

117 ATLSS Drive
Bethlehem, PA 18015-4729

Phone: (610)758-3525
Fax: (610)758-5902

www.atlss.lehigh.edu
Email: inatl@lehigh.edu

# EXPERIMENTAL EVALUATION OF THE COMPOSITE BEHAVIOR OF PRECAST CONCRETE SANDWICH WALL PANELS

**Alexandar Mlynarczyk**
Graduate Research Assistant
Civil and Environmental Engineering

**Stephen Pessiki**
Associate Professor
Civil and Environmental Engineering

**August 2000**

## ATLSS Report No. 00-07

**ATLSS is a National Center for Engineering Research on Advanced Technology for Large Structural Systems**

117 ATLSS Drive
Bethlehem, PA 18015-4729

Phone: (610)758-3525
Fax: (610)758-5902

www.atlss.lehigh.edu
Email: inatl@lehigh.edu

# ACKNOWLEDGMENTS

This research was funded by the Pennsylvania Infrastructure Technology Alliance and by Lehigh University. Additional financial and technical support was provided by Composite Technologies Corporation, Dayton Superior Corporation, H. Wilden and Associates, High Concrete Structures Inc., Metromont Prestress Company, Morse Bros. Inc., Nitterhouse Concrete Products, Owens Corning, the Precast/Prestressed Concrete Institute, Stresscon Corporation, and Tindall Concrete. The support from the sponsors is gratefully acknowledged. The findings and conclusions presented in this report are those of the authors, and do not necessarily reflect the views of the sponsors.

# TABLE OF CONTENTS

# LIST OF TABLES

# LIST OF FIGURES

# ABSTRACT

To ensure sufficient composite action to meet structural strength and stiffness requirements in precast concrete sandwich wall panels, the designer must provide adequate shear transfer between concrete wythes. In a typical sandwich panel, shear transfer may be provided through several different mechanisms. These mechanisms include: (1) solid concrete regions; (2) mechanical connectors that pass through the insulation wythe; and, (3) bond between the concrete wythes and the insulation. The objective to the work presented in this report is to investigate the flexural behavior of sandwich panels and the contribution to composite action provided by regions of solid concrete, wythe connectors, and bond.

Tests were performed on four full-scale precast sandwich wall panels. A Prototype panel was tested, which included regions of solid concrete in the insulation wythe, metal wythe connectors, and no attempt was made to disrupt the bond between the concrete wythes and the insulation wythe. The degree of composite action developed by each of the different shear transfer mechanisms was then evaluated by testing three additional panels that included only one mechanism of shear transfer (solid concrete, wythe connectors, or bond).

It was found that, for the panel geometries and materials treated in this study, the solid concrete regions provide most of the strength and stiffness that contribute to composite behavior. Steel M-tie connectors and bond between the insulation and concrete contribute relatively little to composite behavior. Therefore, for design purposes, it is recommended that solid concrete regions be proportioned to provide all of the required composite action in a precast sandwich wall panel. A precast concrete sandwich wall panel constructed similarly to the Prototype panel treated in this study will behave as a fully composite panel in terms of service load-deflection behavior and flexural strength.

# CHAPTER 1
# INTRODUCTION

## 1.1 INTRODUCTION

Precast concrete sandwich wall panels are used throughout the construction industry due to their versatility and economical value. Precast concrete sandwich wall panels, often referred to as sandwich panels, provide a fast and easy means of meeting both structural and thermal requirements of a structure. As a result, sandwich panels are used as exterior and interior walls for many types of structures.

Sandwich panels are composed of two wythes of concrete separated by a wythe of insulation. Concrete wythes can take on many shapes such as flat slabs or double tees and may be designed to provide the structure with an architectural finish. Depending on the demands of handling and service loads, sandwich panels may be prestressed or non-prestressed. Panels can be load-bearing, supporting gravity loads such as roof and floor loads, or non-load bearing, transmitting wind loads to the structural frame and foundation.

In non-load bearing applications, sandwich panels can be attached to nearly any type of structural frame to provide a thermally efficient permanent wall system. The panels are cast at a precasting plant and trucked to the building site where they are erected using a crane and then are structurally connected to the building's structural framework. Sandwich panels typically span between building foundations and floors or roofs.

Sandwich panels can be designed to behave compositely where both concrete wythes act together structurally, or non-compositely, where both concrete wythes act independently. More commonly however, sandwich panels are designed semi-compositely where varying degrees of composite action are assumed during stripping, handling, and service. To ensure sufficient composite action to meet structural strength and stiffness requirements, the designer must provide adequate shear transfer between concrete wythes. In a typical sandwich panel, shear transfer may be provided through several different mechanisms. These mechanisms include: (1) solid concrete regions (i.e. regions where the insulation is intentionally omitted and replaced with concrete); (2) mechanical connectors that pass through the insulation wythe; and, (3) bond between the concrete wythes and the insulation.

## 1.2 OBJECTIVES

The work described in this report is part of an ongoing research program at Lehigh University on precast concrete sandwich wall panels. The work is directed at the development of design recommendations for the lateral load design of sandwich wall panels, and also explores the development of new types of sandwich panels with improved thermal and structural performance. The objective to the work presented in this report is to investigate the flexural behavior of sandwich panels and the contribution to composite action provided by regions of solid concrete, wythe connectors, and bond.

## 1.3 SUMMARY OF APPROACH

Tests were performed on four full-scale precast sandwich wall panels. The test panels were fabricated by High Concrete Structures Inc. of Denver, Pennsylvania according to normal practice of the precast industry. The first sandwich panel tested was a typical sandwich panel that would be produced for a building project. This panel included regions of solid concrete in the insulation wythe, metal wythe connectors, and no attempt was made to disrupt the bond between the concrete wythes and the insulation wythe. The degree of composite action developed by each of the different shear transfer mechanisms was then evaluated by testing three additional panels that included only one mechanism of shear transfer (solid concrete, wythe connectors, or bond).

All tests were conducted at the Center for Advanced Technology for Large Structural Systems (ATLSS) at Lehigh University. The panels were tested in a horizontal position with simple supports. A uniform pressure load was applied from beneath the panel and no axial load was applied.

## 1.4 SUMMARY OF FINDINGS

It was found that, for the panel geometries and materials treated in this study, the solid concrete regions provide most of the strength and stiffness that contribute to composite behavior. Steel M-tie connectors and bond between the insulation and concrete contribute relatively little to composite behavior. Therefore, for design purposes, it is recommended that solid concrete regions be proportioned to provide all of the required composite action in a precast sandwich wall panel.

A precast concrete sandwich wall panel constructed similarly to the Prototype panel treated in this study will behave as a fully composite panel in terms of service load-deflection behavior and flexural strength.

Panels with solid concrete regions placed intermittently along the span develop stress concentrations at the solid regions, do not exhibit plane section behavior through the depth of the panels, and develop strains that are not uniform across the width of the panels. These effects seem to contribute to early flexural cracking at service loads. Non-uniformity of strains across the width of the panel may also contribute to a reduction in the value of bending moment at which yielding of the prestressing steel occurs.

## 1.5 OUTLINE OF REPORT

The remainder of this report is separated into five chapters. Chapter 2 presents relevant background information, including a discussion of the general behavior of sandwich panels. Chapter 3 describes the experimental program. This includes descriptions of the test matrix, test panel details, test fixture, and the instrumentation. The procedure used to design the Prototype panel is summarized in this chapter and some sample design calculations for the Prototype panel are presented in Appendix A. The experimental results are presented in Chapter 4, and analyzed and discussed in Chapter 5. Finally, Chapter 6 presents the conclusions of this research, along with recommendations regarding composite action in the lateral load design of sandwich panels.

## 1.6 NOTATION

The following notation is used in this report:

$a$ = depth of equivalent rectangular stress block
$A_c$ = total area of concrete in cross-section (both wythes)
$A_{cs}$ = total area of concrete resisting horizontal shear
$A_p$ = area of prestressing steel
$b$ = width of test panel
$d_p$ = depth of prestressing steel
$D$ = dead load
$e_p$ = eccentricity of prestressing steel
$E_c$ = modulus of elasticity of concrete
$E_{ci}$ = modulus of elasticity of concrete at transfer of prestress
$E_p$ = modulus of elasticity of prestressing steel
$f'_c$ = unconfined concrete compressive strength
$f'_{ci}$ = unconfined compressive strength of concrete at transfer of prestress
$f_{pe}$ = effective prestress stress in the prestressing steel
$f_{pi}$ = initial prestress stress in the prestressing steel
$f_{pu}$ = specified tensile strength of the prestressing steel
$f_{ps}$ = stress in prestressing steel at nominal strength
$f_{py}$ = specified yield stress of the prestressing steel
$f'_r$ = modulus of rupture of concrete
$f_s$ = panel bending stress due to service load
$f_x$ = panel bending stress due to bending about panel x-axis
$f_y$ = panel bending stress due to bending about panel y-axis
$I$ = moment of inertia
$I_c$ = moment of inertia of composite concrete section
$I_{cr}$ = moment of inertia of fully cracked section transformed to concrete
$I_e$ = effective moment of inertia
$I_{exp}$ = experimentally determined moment of inertia
$I_g$ = moment of inertia of gross concrete section about centroidal axis, neglecting reinforcement
$I_{nc}$ = moment of inertia of non-composite concrete section
$I_{pc}$ = moment of inertia of partially composite concrete section
$L$ = span length of test panel
$L'$ = length of test panel
$M_a$ = maximum moment acting in span
$M_{cr}$ = cracking moment
$M_n$ = nominal moment capacity
$M_s$ = service load moment
$M_u$ = factored moment
$M_x$ = moment about the x-axis
$M_y$ = moment about the y-axis
$p$ = surface pressure load
$P$ = total load (link force)

$P_e$ = effective prestress force
$P_i$ = initial prestress force
$Q$ = first moment of inertia
$R$ = effectiveness ratio of prestress
$S_c$ = section modulus of a composite section
$S_{eff}$ = effective section modulus
$S_{nc}$ = section modulus of a non-composite section
$S_{pc}$ = section modulus of a partially composite section
$t$ = total panel thickness
$U$ = factored load
$V_{nh}$ = horizontal shear capacity
$w$ = uniformly distributed load
$W$ = wind surface pressure load
$x$ = distance along span
$\beta_1$ = equivalent rectangular stress block coefficient, equal to 0.85 for concrete with compressive strength equal to 6000 psi
$\Delta$ = midspan lateral deflection
$\phi$ = strength reduction factor, equal to 0.9 for bending
$\gamma_p$ = factor for type of prestressing tendon, equal to 0.28 for $f_{py}/f_{pu}$ not less than 0.90
$\kappa$ = factor to describe percent composite stiffness of a panel
$\rho_p$ = ratio of prestressed reinforcement

## 1.7 UNIT CONVERSION FACTORS

The following unit conversions are used in this report:

1 in. = 25.4 mm
1 ft. = 0.3048 m
1 $in.^2$ = 645 $mm^2$
1 lb. = 4.448 N
1 kip = 4.448 kN
1 ksi = 6.895 MPa
1 kip-in. = 0.113 kN-m

# CHAPTER 2
# BACKGROUND

## 2.1 INTRODUCTION

In general, sandwich panels behave similarly to other precast prestressed concrete members. However, due to the presence of the intervening wythe of insulation, sandwich panels do exhibit some unique characteristics and behavior. Present knowledge of the behavior of sandwich panels is based on observed field performance and limited laboratory testing. As a result, there is a lack of agreement among designers concerning degree of composite action and resulting panel performance. Much of the present understanding about the behavior and design of sandwich panels is presented in two recent reports. The first report, by Einea, Salmon, Fogarasi, Culp, and Tadros, titled "State-of-the Art of Precast Sandwich Wall Panels," was published in 1991. The second report, by the PCI Committee on Precast Sandwich Wall Panels, titled "State-of-the Art of Precast / Prestressed Sandwich Wall Panels" (hereafter referred to as the PCI State-of-the-Art Report), was published in 1997.

## 2.2 COMPOSITE, NON-COMPOSITE, AND PARTIALLY COMPOSITE PANELS

In this report, a fully composite sandwich panel is defined as a panel in which both wythes act integrally to resist flexure. In theory, a fully composite panel exhibits plane section behavior at any location along its span. Figure 2.1(a) shows an elevation view of a portion of a sandwich wall panel subjected to shear and bending moment. A fully composite panel exhibits the deformed shape and strain distribution shown in Figure 2.1(b). Full composite action is achieved by providing sufficient shear transfer between wythes to obtain plane section behavior throughout the entire panel depth. Shear transfer is provided through various types of shear transfer mechanisms, discussed in Section 1.1, including solid concrete regions, wythe connectors, and bond. For a panel to be considered fully composite, shear transfer mechanisms must have adequate strength and stiffness to resist the longitudinal shear force.

A non-composite sandwich panel is defined as a panel in which both concrete wythes act independently. In general one or both wythes can act as structural wythes, which resist lateral load. For non-composite action, there is no shear transfer between wythes. Any connectors provided between concrete wythes act solely to hold the wythes together. Figure 2.1(c) illustrates the deformed shape and strain distributions present in a non-composite panel under the action of shear and bending. In a non-composite panel, plane section behavior is obtained only individually in each wythe, and not through the entire panel depth. Because each wythe acts individually, relative movement occurs between wythes, as shown in Figure 2.1(c).

A partially or semi-composite panel is defined as a panel in which only some of the longitudinal shear forces are transferred between the concrete wythes. Alternate definitions for partially composite panels have been presented. Einea et al. (1991) have defined a partially composite panel as a panel in which the connectors can transfer between zero and 100 percent of the longitudinal shear required for a fully composite panel.

For a panel with a given geometry, a fully composite panel would exhibit the highest flexural stiffness, whereas a fully non-composite panel would exhibit the lowest flexural stiffness. This is also illustrated in Figure 2.1, where for a given bending moment, the fully composite panel exhibits smaller deformations than the non-composite panel. A partially composite panel would exhibit a flexural stiffness somewhere in the range in between that of a fully non-composite panel and that of a fully composite panel.

Finally, it is also possible for the degree of composite action to change throughout the loading history of a panel. For example, a panel may start out being fully composite, but as the flexural stresses are increased the longitudinal shear stresses will also increase. If sufficient load is applied, the shear connection between wythes may degrade as the strengths of the different mechanisms that contribute to shear resistance are overcome.

## 2.3 WYTHE CONNECTORS

Wythe connectors are used to tie the two concrete wythes together during stripping, handling, and service. According to the PCI State-of-the-Art Report, two types of connectors are used to construct sandwich panels. They are non-shear connectors and shear connectors.

The primary purpose of non-shear connectors is to transfer normal tension forces between wythes. Non-shear connectors are used to prevent the two concrete wythes and insulation from separating during the process of stripping the panel from the formwork. Non-shear connectors also help to maintain the integrity of the panel when it is being handled and transported. These connectors prevent the concrete wythes from separating during service if the panel is designed as a non-composite panel and no other connectors are present. Non-shear connectors come in several forms, including metallic and fiber composite pin connectors, and transverse welded wire ladder connectors.

The second type of wythe connector, shear connectors, also transfer normal tension forces between the wythes. In addition, shear connectors provide a longitudinal shear connection to develop composite action between the two concrete wythes. There are two different types of shear connectors. One-way shear connectors are stiff in one direction and flexible in the other. These connectors only resist shear in the longitudinal direction. Typical one-way shear connectors include M-ties and welded wire truss. Other shear connectors are stiff in at least two directions and resist both longitudinal and transverse shears. These types of connectors include solid blocks of concrete and cylindrical sleeve anchors (shear cans).

It is also known from experience that the friction bond developed between the insulation and the wythes provides a small amount of shear resistance. The amount of shear transfer provided is dependent on the type of insulation board used and the features of its surfaces. Generally, the amount of shear transferred by the bond between concrete and insulation is small and can only be counted on in early phases of the life of the panel. It has been observed that this bond degrades rapidly and is considered unreliable in the long term.

## 2.4 PREVIOUS STUDIES OF SANDWICH PANELS

In the past, other research projects have been conducted on precast sandwich wall panels. Pfeifer and Hanson (1964) tested several non-prestressed sandwich panels with varying wythe connectors in flexure under uniform loading. Approximately 50 panels were tested. Test panels measured 5 ft. by 3 ft., with thicknesses ranging from 2.25 in. to 6 in. Pfeifer et al. found that by varying the types of connectors and their spacing that different degrees of composite action could be achieved. It was shown that adequate shear connection between wythes was the key factor in achieving higher values of stiffness and resisting moment. It was observed that metal connectors with diagonal members, such as a welded wire truss, were more effective in transferring shear than those without diagonal members. However, it was also observed that concrete ribs provided better shear transfer than metal connectors.

Bush and Stine (1992) tested precast concrete sandwich panels with continuous truss connectors. The primary variables of the test program included the number, orientation, and spacing of the truss connectors. Six panels were tested. Each test panel measured 16 ft. by 8 ft. and was tested under uniform lateral pressure. Each panel was a total of 8 in. thick and consisted of two 3 in. thick concrete wythes with a 2 in. thick intervening insulation wythe. Results of the tests showed that a high degree of composite stiffness and flexural capacity could be achieved with truss connectors oriented longitudinally in the panels. The tests also showed that a significant amount of shear was transferred through stripping and handling inserts, as well as through solid concrete ribs. It was also shown that the friction bond between the insulation and the concrete provided a modest contribution to the overall shear transfer.

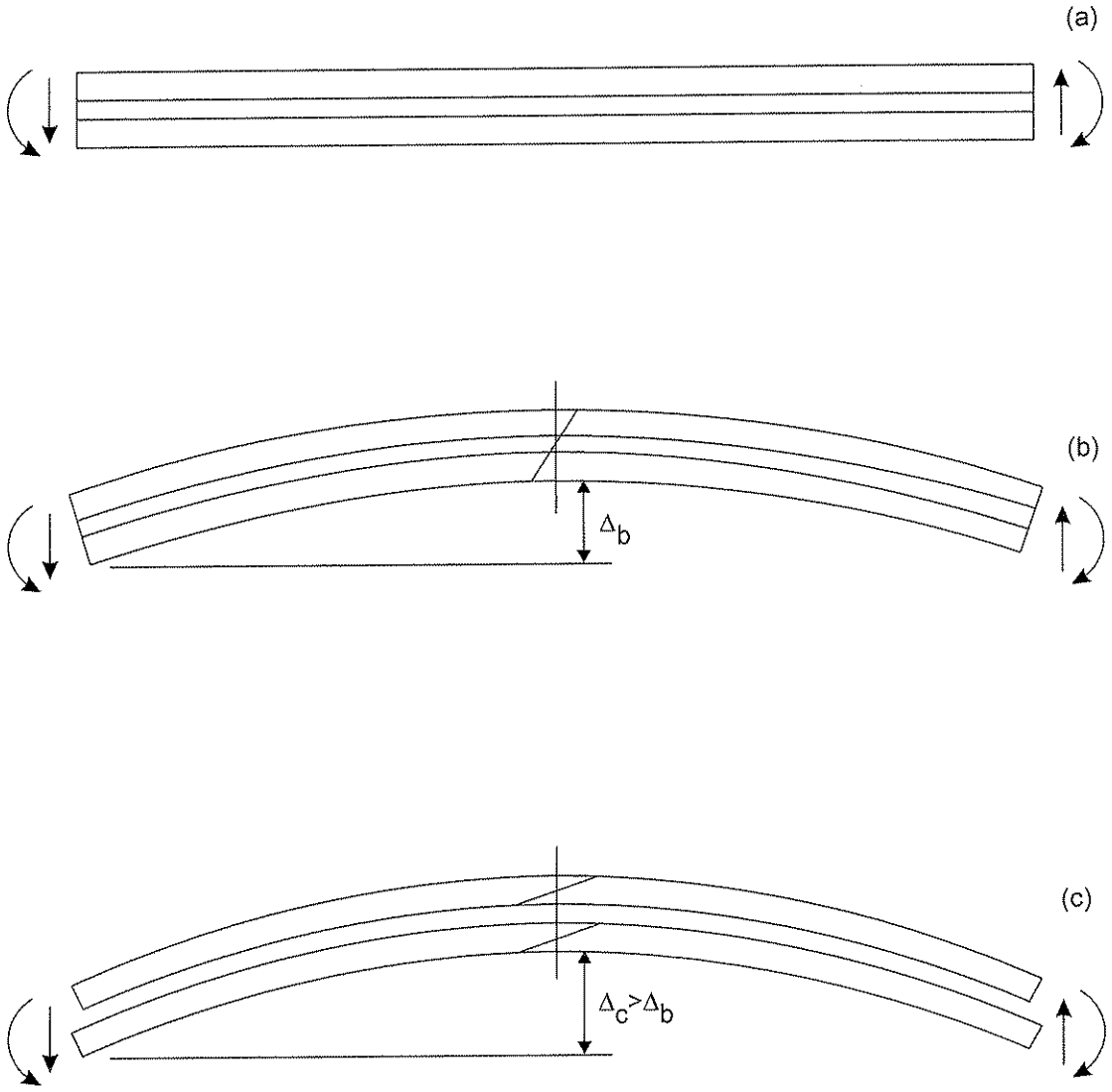


Figure 2.1 (a) Elevation view of a portion of a sandwich panel subjected to shear and bending moment; (b) Deformed shape and strain distribution in a fully composite panel; (c) Deformed shape and strain distribution in a non-composite panel.

# CHAPTER 3
# DESCRIPTION OF EXPERIMENTAL PROGRAM

## 3.1 INTRODUCTION

This chapter describes the experimental program. Section 3.2 presents the test matrix and Section 3.3 presents the design of the prototype panel. Section 3.4 describes the test panel details and Section 3.5 describes the construction of the panels. Sections 3.6 and 3.7 explain the fixture and instrumentation used for testing the sandwich panels. Finally, material properties of the test panels are presented in Section 3.8.

## 3.2 TEST MATRIX

As noted in Chapter 1, at least three potential mechanisms of shear transfer, which contribute to composite action, exist in sandwich panels. These mechanisms are: (1) solid concrete regions; (2) mechanical connectors that pass through the insulation wythe; and, (3) bond between the concrete wythes and the insulation. The test matrix for this experimental program, given in Table 3.1, was designed to investigate the degree of composite action contributed by each of these mechanisms. The test matrix consists of four precast concrete sandwich wall panels. Panel 1, the Prototype panel, was designed and fabricated as a panel which might be for commercial use. This panel contained all three mechanisms which contribute to shear transfer, namely solid regions, M-ties, and bond between the concrete wythes and the insulation. This panel was the control specimen for evaluating the total amount of composite action contributed by all components of the typical sandwich panel.

Each of the three remaining panels includes only one mechanism of shear transfer in attempt to isolate and quantify its contribution to the development of composite action. Table 3.1 shows that for Panel 2, only M-ties were provided as a mechanism of shear transfer, the regions of solid concrete were omitted, and the bond between the concrete and insulation was destroyed. Similarly, in Panel 3, only solid regions were provided as a mechanism of shear transfer, M-ties were omitted, and the bond was again destroyed. Finally, the only mechanism of shear transfer that was present in Panel 4 was the bond between the concrete and the insulation.

## 3.3 PROTOTYPE PANEL DESIGN

Some sample design calculations for Panel 1, the Prototype panel, are presented in Appendix A. Table 3.2 provides a summary of the key design parameters for this panel. The Prototype panel was designed as a partially composite panel. Fully composite behavior is assumed for stripping and handling, and 70 percent composite action is assumed for service.

The Prototype panel was designed with regard to the current provisions of the ACI Building Code Requirements for Structural Concrete (1999) (hereafter referred to as the ACI 318 Code), the Prestressed Concrete Design Handbook (1999) (hereafter referred to as the PCI Handbook), and the Guide for Precast Concrete Wall Panels (1996) (hereafter referred to as the ACI Committee 533 Report).

## 3.4 PANEL DETAILS

Each panel was 8 in. thick and consisted of two 3 in. concrete wythes separated by a 2 in. wythe of insulation (a 3-2-3 panel). Each of the panels measured 6 ft. by 37 ft. in plan. The design span of all test panels was 35 ft. In all panels, each concrete wythe was axially prestressed with four 7/16 in. diameter Grade 270 low-relaxation prestressing strands. Each wythe also contained #3 grade 60 reinforcing bars that were placed at 2 ft. on center transverse to the prestressing strands. All panels were designed using a concrete compressive strength, $f'_{ci}$=3500 psi at transfer and a 28-day compressive strength of $f'_c$=6000 psi. Each panel had eight lifting points for handling. As discussed later, lifting hardware varied based on the requirements of the test matrix. All lifting hardware was designed for lifting the panel in the flat position only.

Figure 3.1 shows the details of Panel 1. This panel was used to investigate the behavior of a typical sandwich wall panel. This panel contains a 1 ft. wide solid band of concrete at each end of the panel, which is used to anchor hardware for connections to the roof and foundation. These solid end regions are also reinforced as shown in Figure 3.1. There are also eight 1ft. square solid regions at various locations throughout the span of the panel. These solid regions provide locations for placement of lifting hardware (eight 4-ton capacity 4-3/4" long Dayton Superior Swift Lift lifting studs) and also provide connection between concrete wythes for shear transfer. This panel also contained steel M-tie connectors spaced at 2 ft. on center. A photograph of the M-tie connector used in this research is shown in Figure 3.5. No attempt was made to alter or disrupt the bond between the concrete wythes and the insulation.

Figure 3.2 shows the details of Panel 2. This panel was used to investigate the fraction of composite action provided by the steel M-tie connectors. This panel contained no solid regions and the bond between the concrete wythes and the insulation was destroyed using a plastic bond breaker at each concrete-insulation interface. Therefore, the only mechanism of shear transfer present was the steel M-ties. M-ties were spaced at 2 ft. on center, as in Panel 1.

Special lifting hardware was designed for this panel because the lack of solid concrete regions did not allow for the use of the same lifting hardware that was used in Panel 1. A photograph of the lifting hardware used in this panel is shown in Figure 3.6. For lifting, swivel plates were attached to removable rods which were threaded into coupling nuts that were anchored in the back and face wythes of concrete. During testing the threaded rods were removed. This lifting hardware allowed for no shear transfer mechanism between wythes at the lifting points.

Figure 3.3 shows the details of Panel 3. This panel was used to investigate the fraction of composite action provided by the solid concrete regions. This panel contained no M-tie connectors and the bond between the concrete wythes and the insulation was destroyed using a plastic bond breaker. The solid concrete regions provided the only mechanism of shear transfer. Since solid regions were provided, the lifting hardware used for this panel was the same as that used in Panel 1.

Figure 3.4 shows the details of Panel 4. This panel was used to investigate the fraction of composite action provided by the bond between the concrete wythes and the insulation. This

panel contained no M-ties or solid concrete regions. Lifting inserts the same as those used in Panel 2 were used for this panel, so no shear transfer mechanism was provided at the lifting points.

## 3.5 PANEL FABRICATION

The following is a description of the fabrication of Panel 1, which was the prototype panel. Panels 2 through 4 were constructed in a similar manner, with the exceptions as described in Section 3.3.

In this report, the following terminology is used to identify the two concrete wythes in a panel. The *face* wythe is the wythe that is on the bottom of the panel during fabrication. This is also the bottom wythe during testing, which is the compression side of the panel during testing. The *back* wythe is the wythe that is on top of the panel during fabrication and testing. Thus the back wythe is the tension side of the panel during testing.

Panel fabrication begins with the setup of the formwork on the long-line casting bed and the placement and tensioning of the prestressing strand for the face wythe of concrete. Mild steel transverse reinforcement for the face wythe is then tied to the top of the strand, mild steel is placed in the solid end regions, and the face wythe of concrete is then poured. Figure 3.7 shows the formwork for the panel with the prestressing and transverse reinforcing steel already in place.

Next, insulation board is placed on top of the freshly poured concrete. Any holes in the insulation necessary to create solid concrete regions are pre-cut into the insulation prior to placement on top of the concrete. Placement of the face wythe and the insulation are shown in Figure 3.8. The steel M-ties are then placed by punching them through the insulation and into the face wythe of wet concrete. Figure 3.9 shows the placement of the M-ties.

After the placement of the insulation, the prestressing steel for the back wythe is placed in the formwork and fully tensioned to the specified load. Figure 3.10 shows the prestressing strands after being placed in the formwork. The stressing operation is shown in Figure 3.11. All mild steel reinforcement for the back wythe is then tied into place. Figure 3.12 shows the transverse steel reinforcing bars being tied into place for the back wythe.

Following the placement of all steel, the back wythe of concrete is poured and screeded. Lifting hardware is then put into place and the surface of the back wythe is finished. Figure 3.13 shows the screeding of the back wythe and placement of the lifting inserts.

After completion, the panel is cured until it has reached sufficient strength for transfer of prestress and stripping.

## 3.6 TEST FIXTURE

Drawings of the test fixture are given in Figure 3.14. For this test program, each panel was tested in a horizontal position, with simply supported end conditions. Load was applied from beneath the panel as a uniform pressure using an air bladder. No axial load was applied to the panel.

End supports were provided by two reaction beams constructed from steel wide flange sections, which spanned across the width of the panel at each end. Each panel spanned 35 ft. center-to-center of the reaction beams.

The upward applied load was transmitted to the laboratory floor through a total of four tension links, one at each end of the two reaction beams. The tension links, which are shown in Figure 3.15, consisted of a high strength steel rod with a forged steel clevis threaded on each end. The links were instrumented as full bridge load cells, to measure the total upward force applied to the panel. As shown in Figures 3.16 and 3.17, the top ends of the tension links were pinned to tabs welded to the bottom flanges of the reaction beams. The bottom ends of the tension links were attached to steel tabs that were bolted to the laboratory floor.

At one end of the span, lateral movement of the panel was restrained to simulate a pinned end condition. The assembly of the reaction beam and the lateral brace is shown in Figure 3.16. Lateral movement of the panel was permitted at the opposite end of the panel, simulating a roller support.

A uniform pressure load was applied from beneath the panel using a two-cell air bladder constructed from a rubber coated heavy-duty fabric. The air bladder measured 32 ft. by 5 ft. in plan. Its two-cell construction allowed the air bladder to inflate to a vertical displacement of over 12 in. essentially without any significant loss of surface contact area. The air bladder was filled using compressed air from the laboratory. Airflow into the bladder was monitored and regulated using a pressure regulator. Precast concrete spacer blocks were used as a reaction surface for the air bladder and to reduce the required vertical displacement of the air bladder. Figure 3.18 shows the air bladder in place on the spacer blocks, prior to the placement of the test panel and reaction hardware.

Prior to loading, the test panel was supported around its perimeter on 3.5 in. x 3.5 in. wood blocks, which were set on top of the concrete spacer blocks. This prevented the test panel from resting directly on the air bladder. Figure 3.19 shows a test panel in place in the fixture. After the test panel is placed in the fixture, the reaction beams, tension links and lateral braces are installed. The test fixture is shown fully assembled in Figure 3.20. The fixture also includes several braces which were intended to limit the amount of sudden lateral and vertical movement of the panel in the case of catastrophic failure of the panel during testing.

## 3.7 INSTRUMENTATION

Several different types of instruments were utilized during testing. All test panels were instrumented in a similar manner, as shown in Figure 3.21. Electrical resistance strain gages were used to measure the distribution of strain through the thickness of the panel. Differential movement between the two concrete wythes was monitored using linear variable differential transformers (LVDTs). Vertical deflection of the panel was measured using displacement potentiometers. As noted earlier, load cells in the steel tension links were used to measure the force applied to the panel.

Strain gages were used to monitor strains throughout the panel depth so that plane section behavior could be evaluated. Strain gages manufactured by Measurements Group, Inc. of type EA-06-20CBW-120 were used. These gages have a 2 in. gage length to mechanically average the localized variations in strains that occur in regions of paste and aggregate. Strain gages were placed at five different locations along the span of the panel, with four strain gages at each location. Figure 3.22 shows the typical placement of the strain gages at one location along the span. As shown in the figure, two gages are attached to the back wythe, and two gages are attached to the face wythe. The gages were placed on the sides of the wythes and were attached directly to the concrete surface. Since only two gages were used on each wythe, plane section behavior is assumed within each individual wythe, and the strain measurements are used to evaluate plane section throughout the entire panel thickness.

LVDTs were placed at the same five locations as the strain gages along the span of the panel. These instruments were used to measure the relative displacement between the two wythes of concrete. As shown in Figure 3.22, a small amount of insulation was removed where each LVDT was located, and the instruments were placed between the two wythes. All LVDTs used in this test had a linear range of ±0.25 inch.

Displacement potentiometers attached to the top surface of the panel via a wire or string (string pots) were used to measure transverse displacements under load. All string pots were mounted to steel frames that spanned across the width of the panel as shown in Figure 3.23. There were four reference displacements that were measured, one at each corner of the test panel. These measurements were necessary because the panel experienced a certain amount of vertical displacement until the tension links began to engage and take on load. This vertical displacement is due to the air bladder overcoming the self-weight of the panel. After the tension links engaged, these values of reference displacement remained constant. These values form a reference for all other displacements of the panel at the quarter points and at midspan.

As shown in Figure 3.21, displacements of the sandwich panel were measured at the quarter points and at midspan of the panel using string pots. These displacements were used to determine the deflected shape of the panel.

Four load cells were used to measure the load applied to the panel by the air bladder. The total load measured by the load cells was converted to an equivalent pressure load in pounds per square foot.

## 3.8 MATERIAL PROPERTIES

### 3.8.1 Concrete

Concrete compressive strength was determined from compression tests of field-cured cylinders. Field-cured cylinders were prepared by the precaster according to ASTM C-31 procedures using plastic molds. The cylinders were cured under the same conditions as the sandwich panels. For each test panel, 3 cylinders were prepared from the face wythe concrete and 3 cylinders were prepared from the back wythe concrete.

All cylinders were tested in a 600 kip (2669 kN) capacity displacement controlled universal testing machine. The cylinders were tested at approximately the same age that the corresponding panel was tested. The cylinders were capped with a sulfur mortar compound according to ASTM C-617. All cylinders were tested according to ASTM C-39.

For each panel, the three face wythe and the three back wythe cylinders were tested and the average unconfined compressive strength was computed for each wythe. An average unconfined compressive strength of both wythes was also computed. The results of the cylinder tests for Panels 1 through 4 are presented in Table 3.3. The modulus of elasticity, $E_c$, is also presented. $E_c$ is computed based on unconfined concrete compressive strength using the equation

$$E_c = 57000\sqrt{f'_c} \tag{3.1}$$

### 3.8.2 Prestressing Steel

Grade 270 low-relaxation seven-wire strand was used in all test panels. Each wythe was prestressed with four 7/16 in. strands. No material property tests were performed on the prestressing steel. Instead, all material properties were taken from the PCI Handbook. The yield stress of the prestressing steel, $f_{py}$, was taken as 243 ksi and the ultimate strength of the prestressing steel, $f_{pu}$, was taken as 270 ksi. The modulus of elasticity, $E_p$, of the prestressing steel was taken as 28500 ksi.

### 3.8.3 Insulation

All test panels were made using an extruded polystyrene rigid foam insulation. The insulation was manufactured by Owens-Corning Co. and is designated as Foamular 250. No material property tests were performed on the insulation. Material strengths from the manufacturer's literature are as follows: the minimum compressive strength is specified as 25 psi, the minimum flexural strength is specified as 75 psi, and the modulus of elasticity is specified as 1.35 ksi.

### 3.8.4 Steel M-ties

Steel M-tie connectors were used in Panels 1 and 2. The steel M-tie connector, shown in Figure 3.5, measured 6 in. in height and 4 in. in width. The M-tie connectors are formed from 0.25 in. galvanized steel wire. No material property tests were performed on the steel M-ties.

| Panel | Connector Type | Bond | Solid Regions | Primary Variable |
|---|---|---|---|---|
| 1 | M-tie | Yes | Yes | Prototype panel. |
| 2 | M-tie | No | No | Fraction of composite action provided by M-tie connector. |
| 3 | None | No | Yes | Fraction of composite action provided by solid regions. |
| 4 | None | Yes | No | Fraction of composite action provided by bond between insulation and concrete. |

Table 3.1 Test matrix.

| | | |
|---|---|---|
| Dimensions | Width, b | 6 ft. |
| | Overall Length, L' | 37 ft. |
| | Span Length, L | 35 ft. |
| | Concrete Wythe Thicknesses | 3 in. |
| | Insulation Thickness | 2 in. |
| | Total Thickness | 8 in. |
| Section Properties | $A_c$ (both wythes) | 432 $in.^2$ |
| | I (fully composite), $I_c$ | 3024 $in.^4$ |
| | S (fully composite), $S_c$ | 756 $in.^3$ |
| | I (fully non-composite), $I_{nc}$ | 324 $in.^4$ |
| | S (fully non-composite), $S_{nc}$ | 216 $in.^3$ |
| Prestress Properties | $A_p$ | 0.92 $in.^2$ |
| | $e_p$ | 0 in. |
| | $E_p$ | 28500 ksi |
| | $f_{pu}$ | 270 ksi |
| | $f_{pi} = 0.70f_{pu}$ | 189 ksi |
| | $P_i$ | 174 kips |
| | R (assumed) | 0.87 |
| | $P_e$ | 151 kips |
| | $f_{pe}$ | 0.35 ksi |
| Concrete Properties | $f'_{ci}$ | 3500 psi |
| | $E_{ci}$ | 4750 ksi |
| | $f'_c$ | 6000 psi |
| | $E_c$ | 3372 ksi |

Table 3.2 Key design parameters for Panels 1 through 4.

| Panel | Age at Testing (days) | Face Wythe | | Back Wythe | | Average of Face and Back Wythes | |
|---|---|---|---|---|---|---|---|
| | | $f'_c$ (psi) | $E_c$ (ksi) | $f'_c$ (psi) | $E_c$ (ksi) | $f'_c$ (psi) | $E_c$ (ksi) |
| 1 | 30 | 7050 | 4790 | 6820 | 4710 | 6930 | 4750 |
| 2 | 28 | 8340 | 5210 | 9170 | 5460 | 8760 | 5340 |
| 3 | 175 | 8000 | 5100 | 4480 | 3820 | 6240 | 4500 |
| 4 | 152 | 7480 | 4930 | 6510 | 4600 | 7000 | 4770 |

Table 3.3 Concrete material properties for Panels 1 through 4.

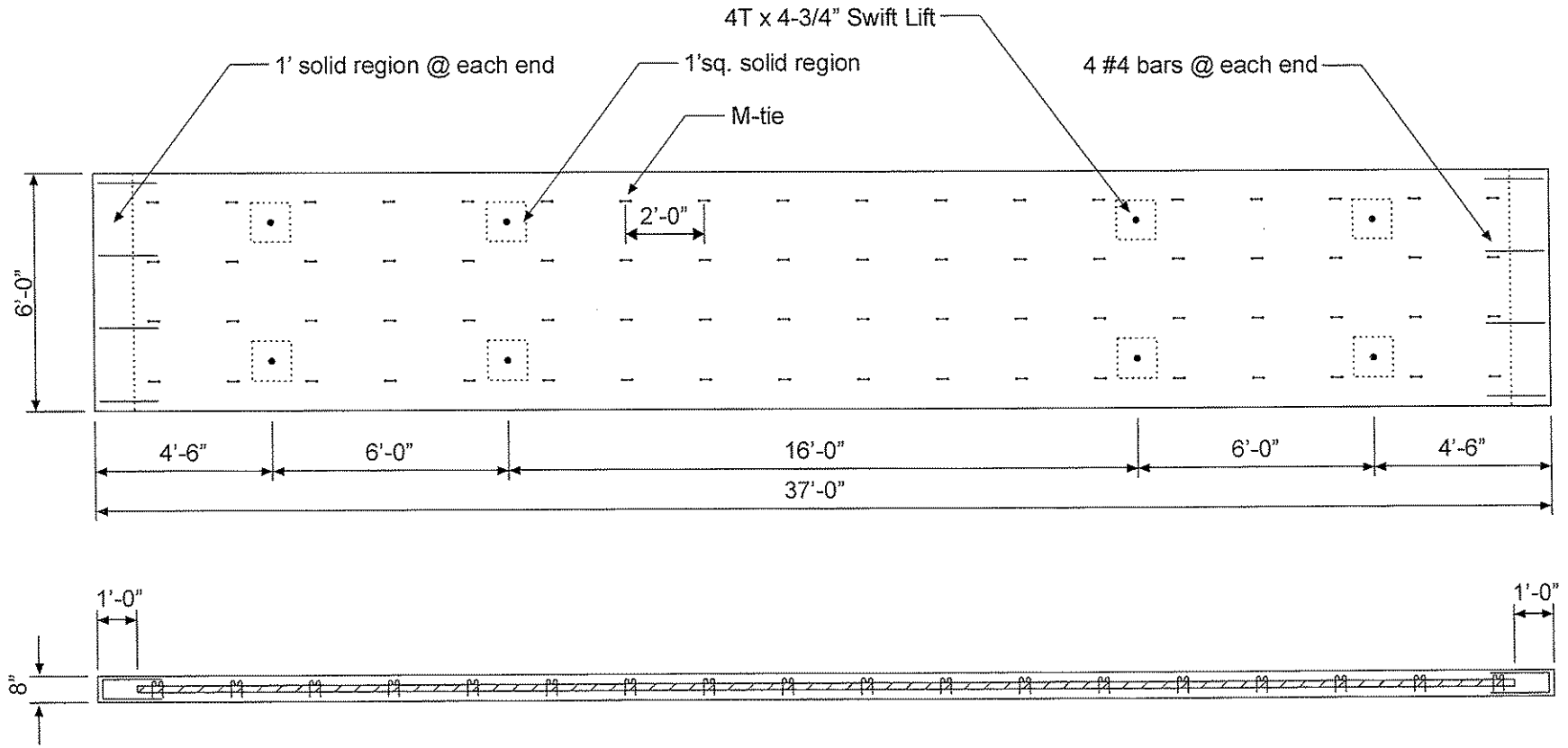


Figure 3.1 Plan view and longitudinal section of Panel 1.

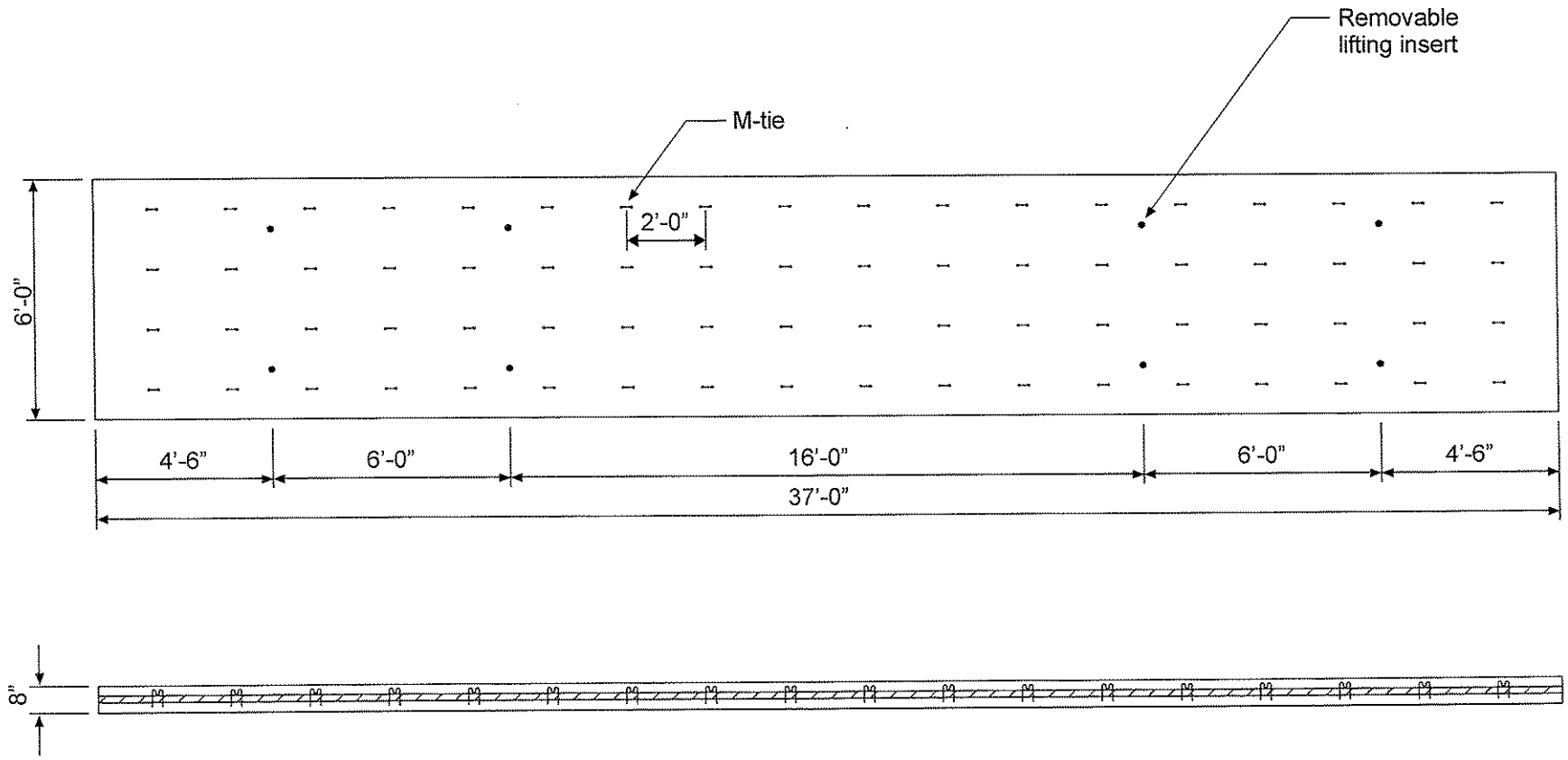


Figure 3.2 Plan view and longitudinal section of Panel 2.

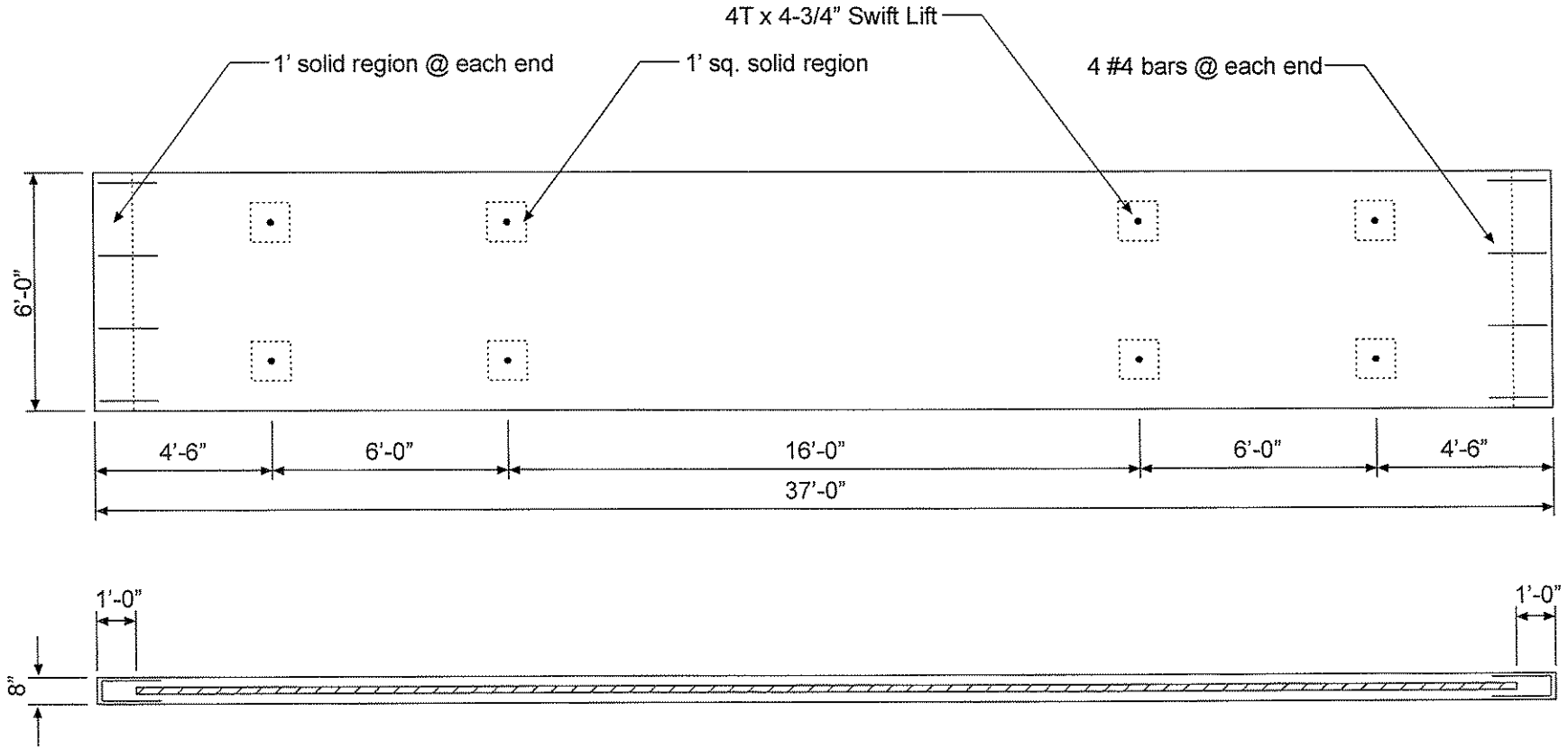


Figure 3.3 Plan view and longitudinal section of Panel 3.

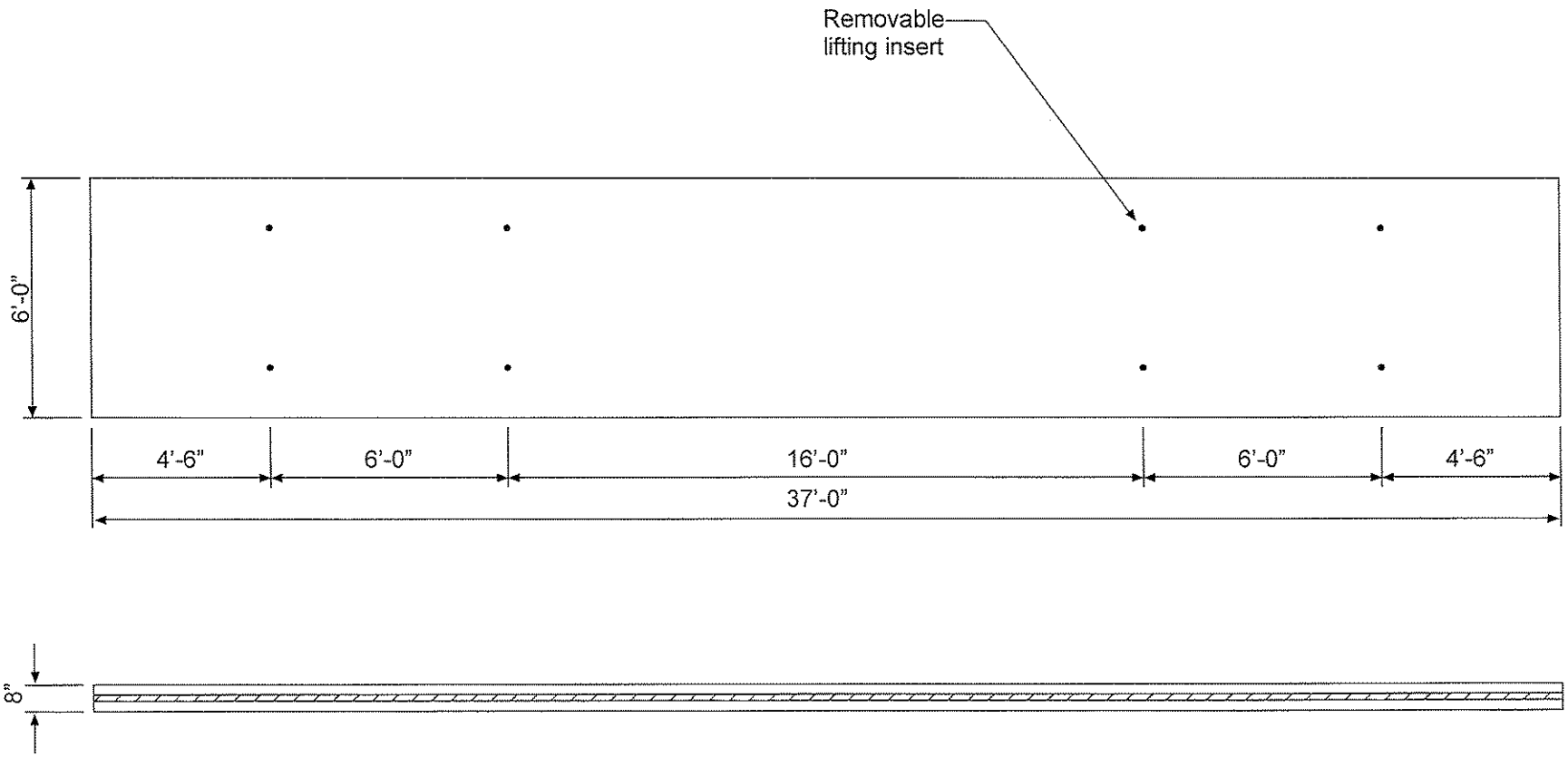


Figure 3.4 Plan view and longitudinal section of Panel 4.

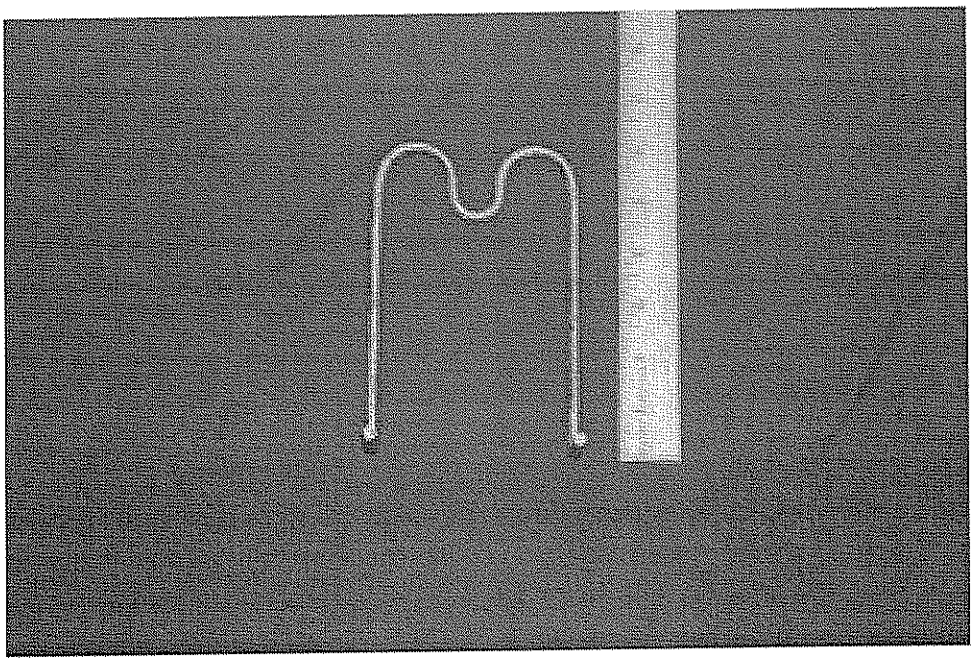

Figure 3.5 Steel M-tie connector.

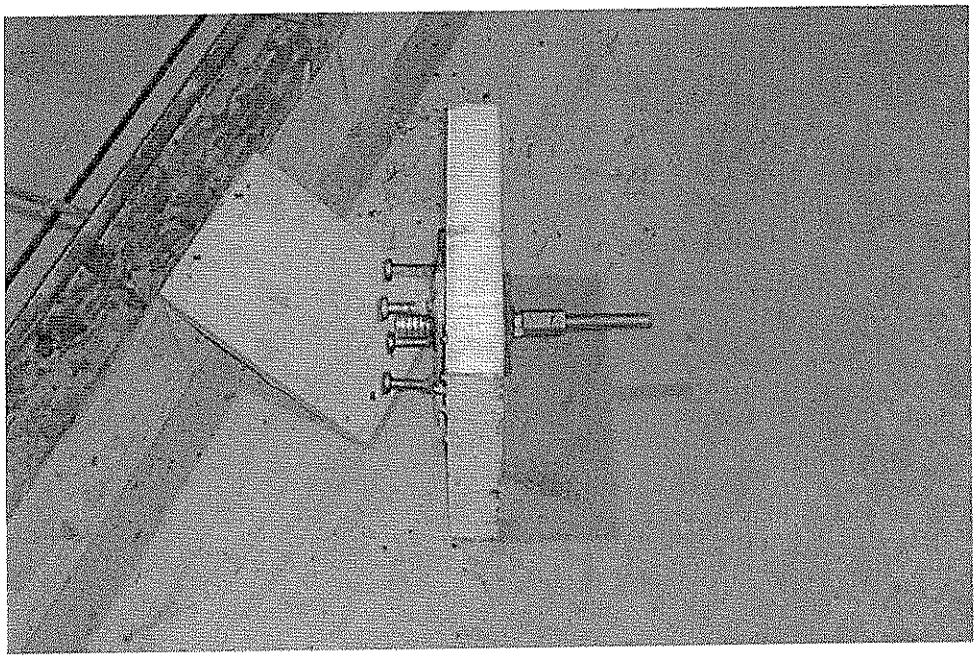

Figure 3.6 Removable lifting hardware used in Panels 2 and 4.

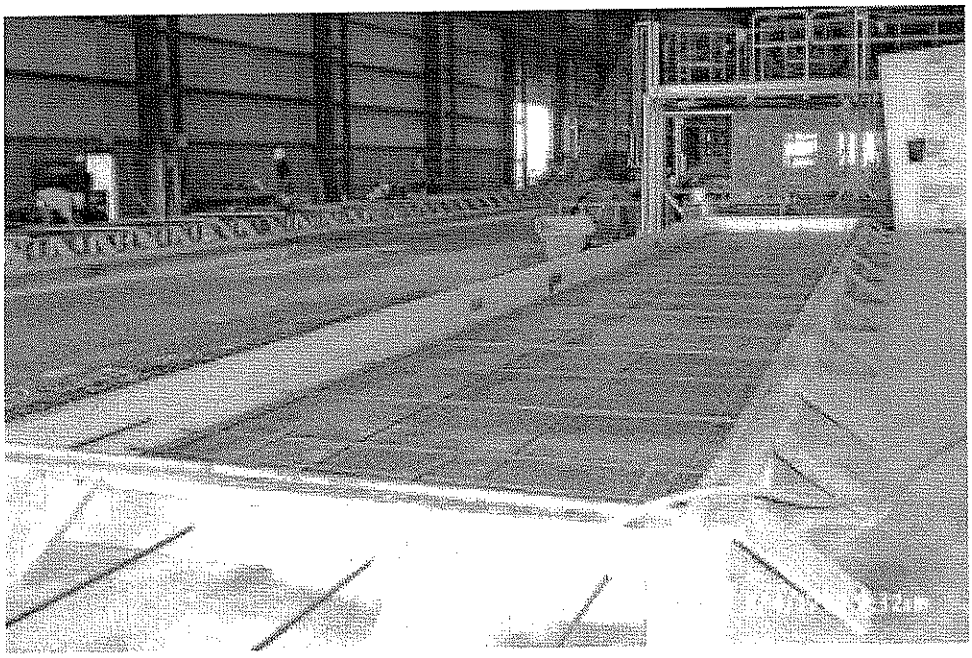

Figure 3.7 Panel formwork with face wythe prestressing strand and reinforcing steel in place.

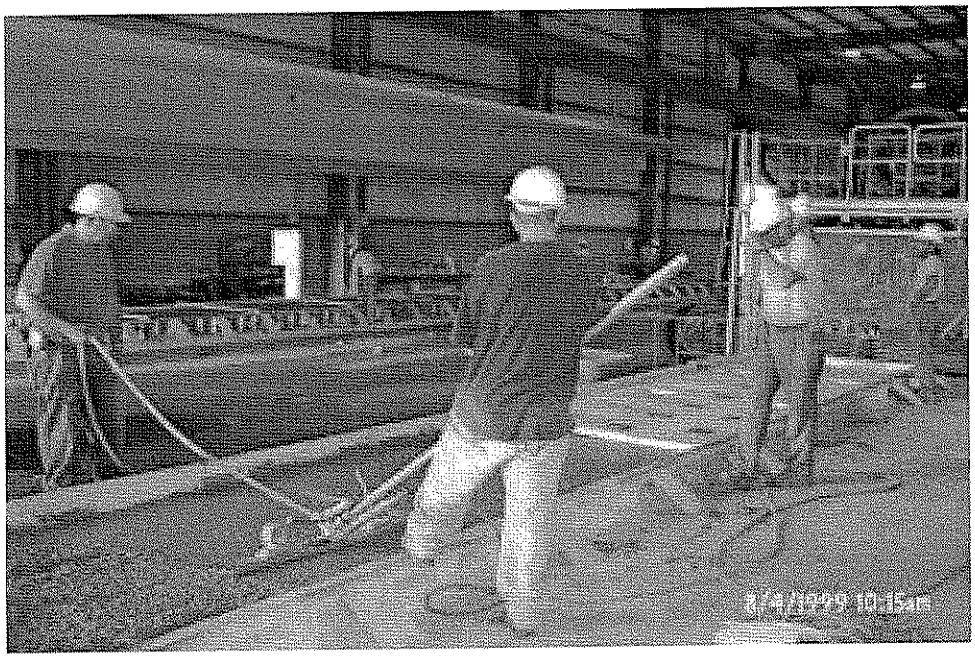

Figure 3.8 Placement of the face wythe concrete and the insulation board.

Figure 3.9 Placement of the steel M-tie connectors.

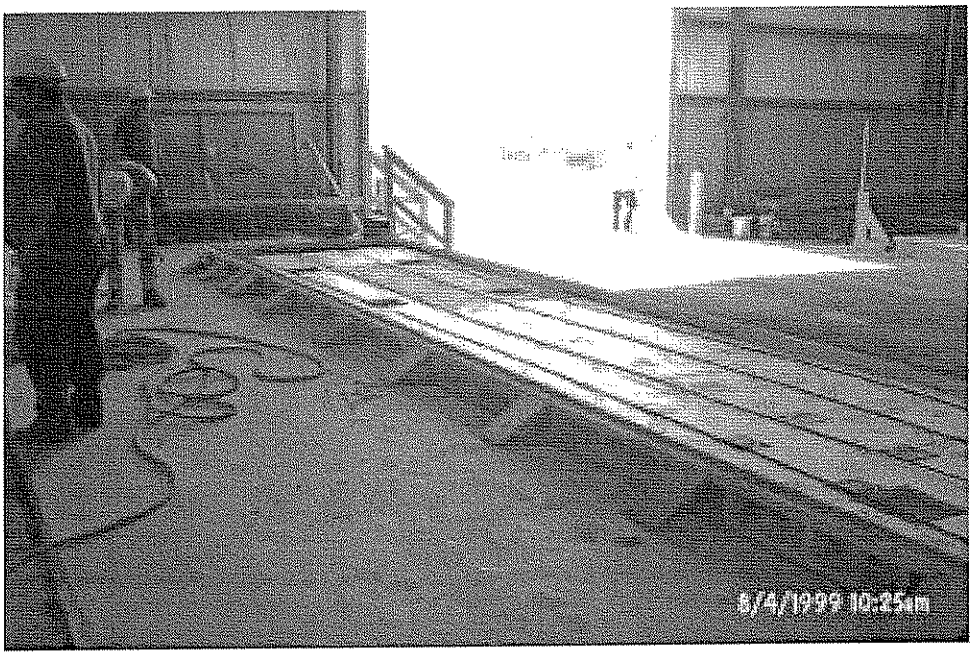

Figure 3.10 Placement of the back wythe prestressing strands.

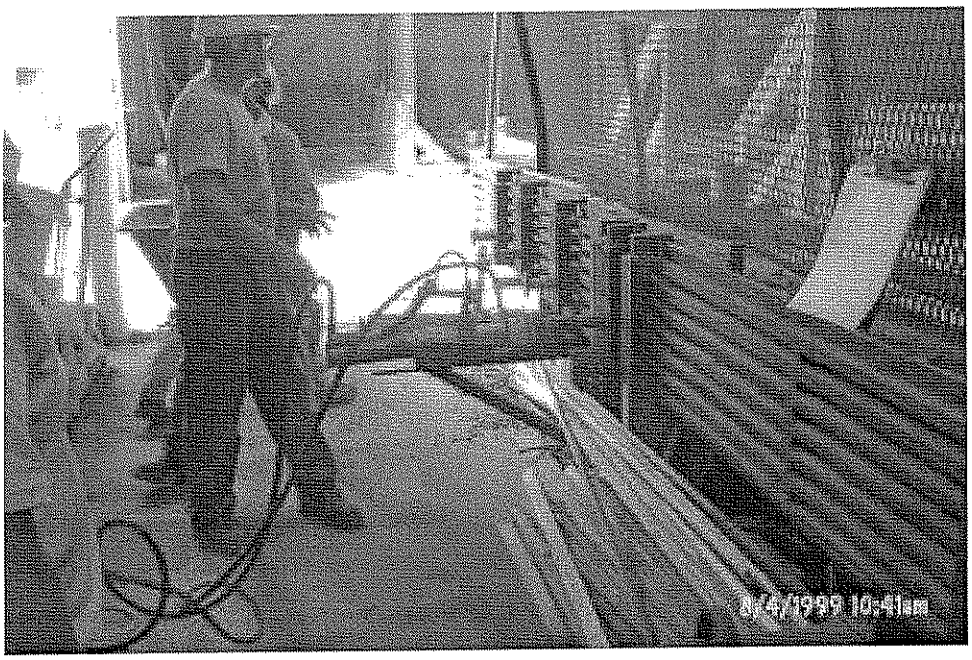

Figure 3.11 Stressing of the prestressing strands.

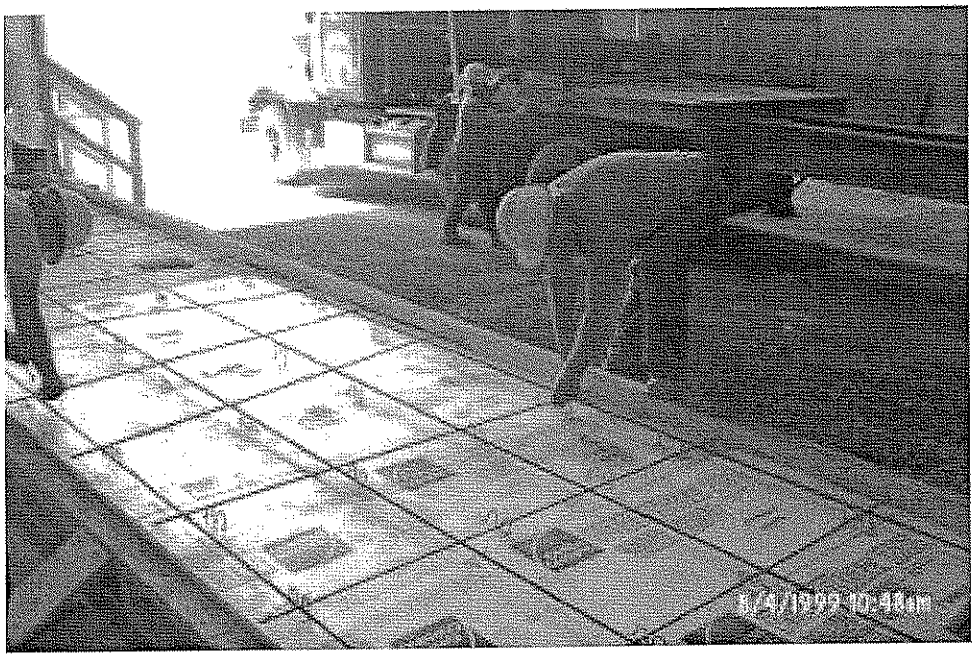

Figure 3.12 Placement of the back wythe transverse reinforcing steel.

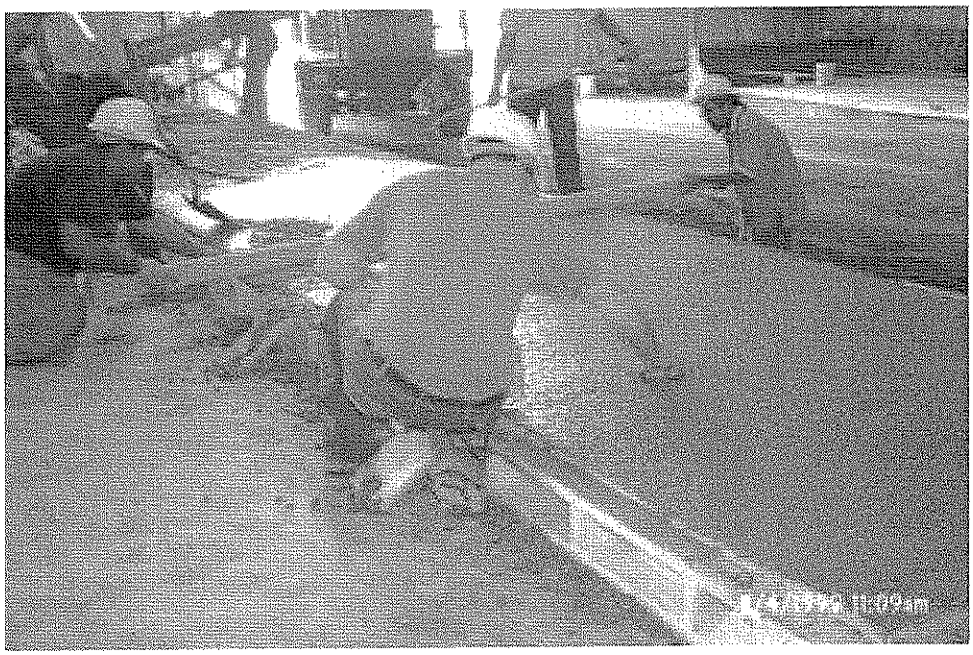

Figure 3.13 Screeding of the back wythe of concrete and placement of the lifting inserts.

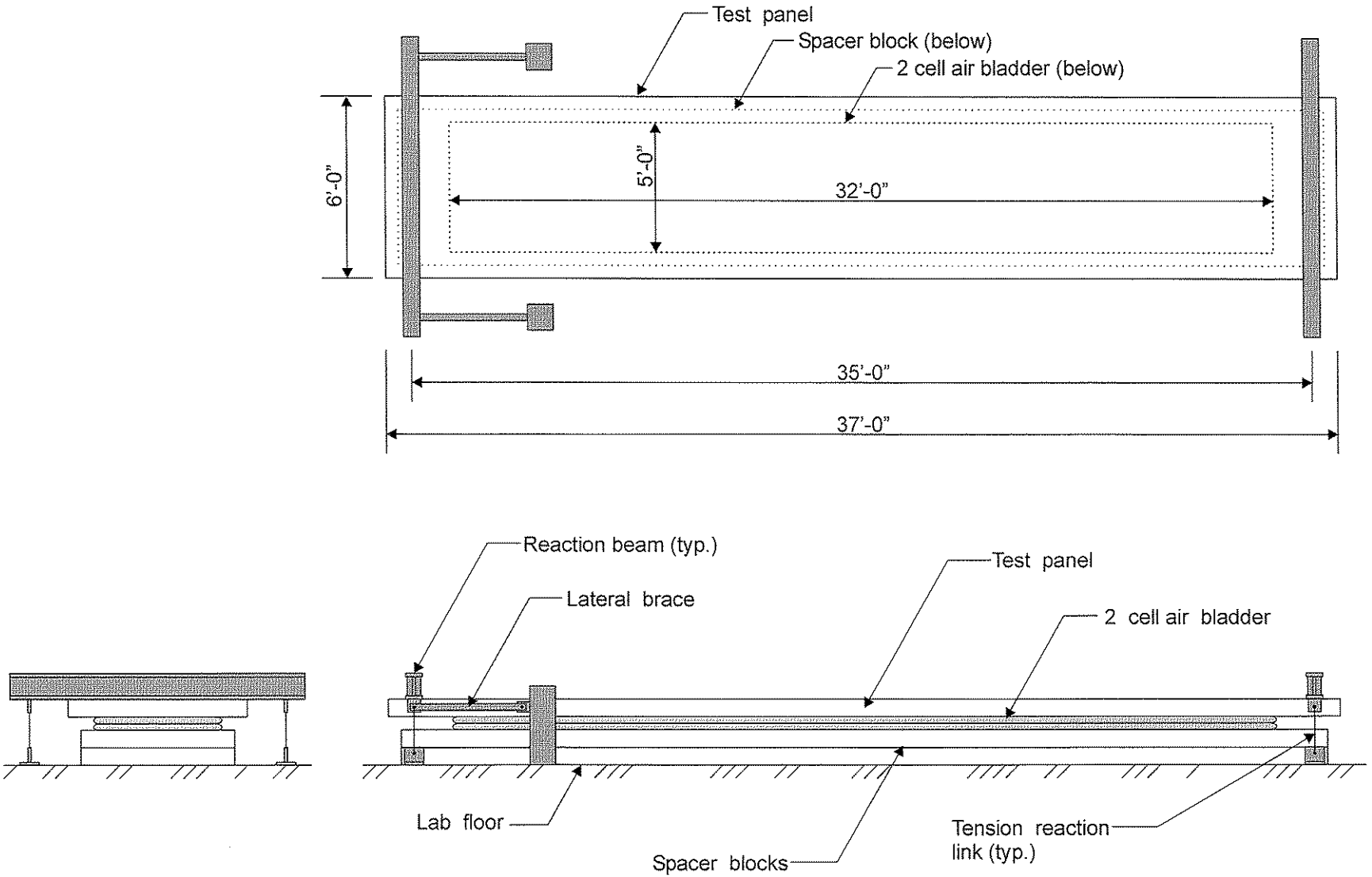


Figure 3.14 Test fixture.

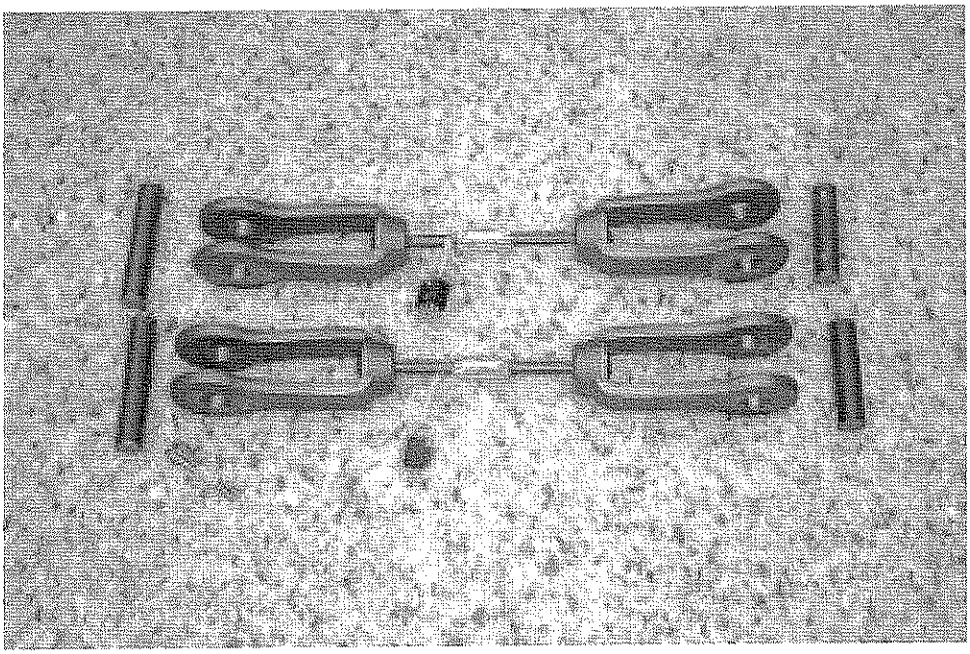

Figure 3.15 Steel tension links instrumented as a full bridge load cell.

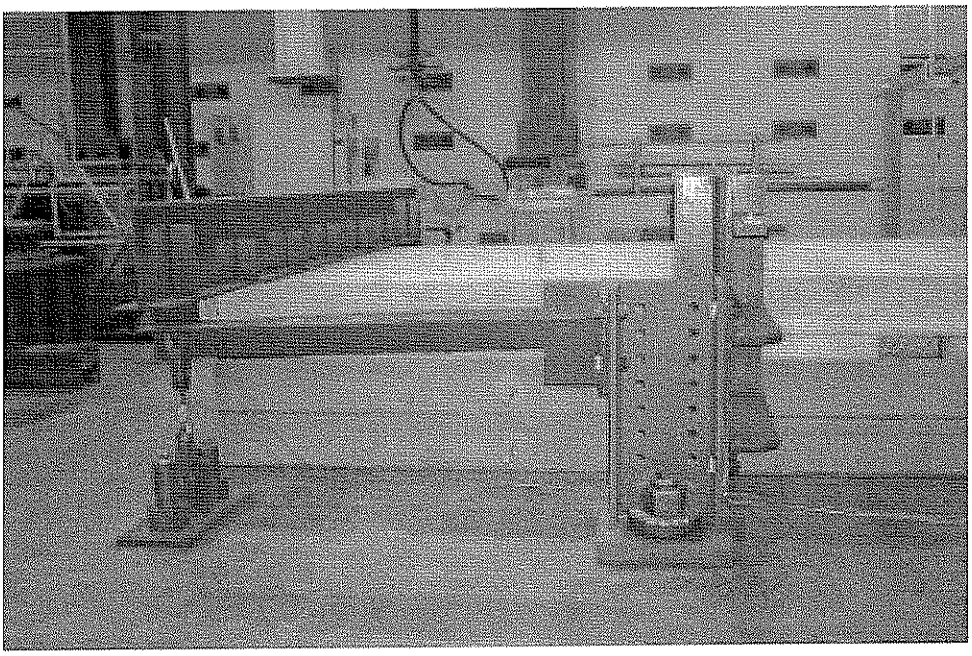

Figure 3.16 Assembly of the south end of the fixture with a test panel in place.

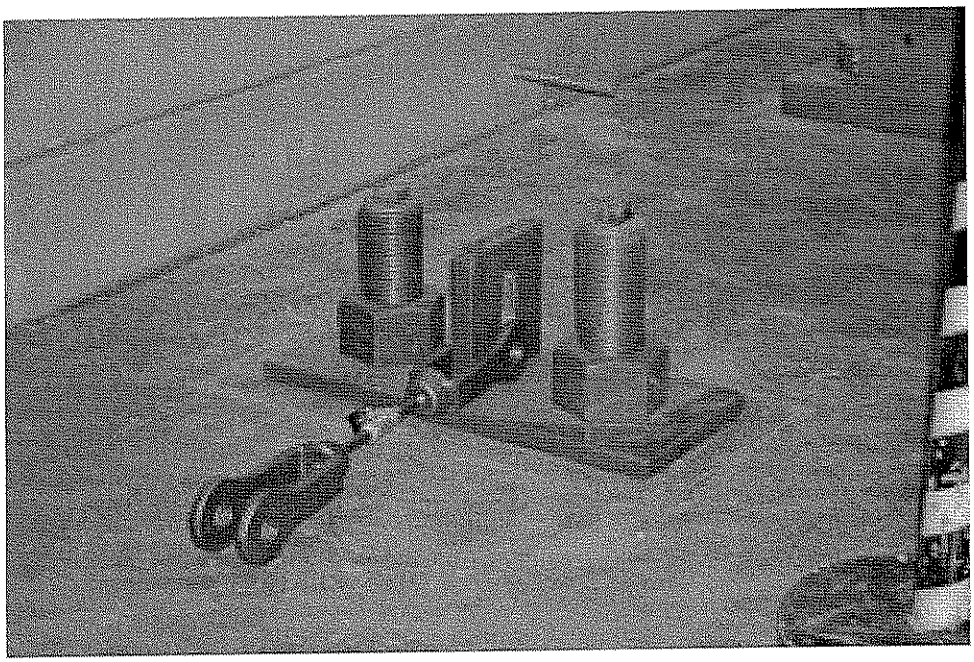

Figure 3.17 Steel tab to transmit load from the tension link to the laboratory floor.

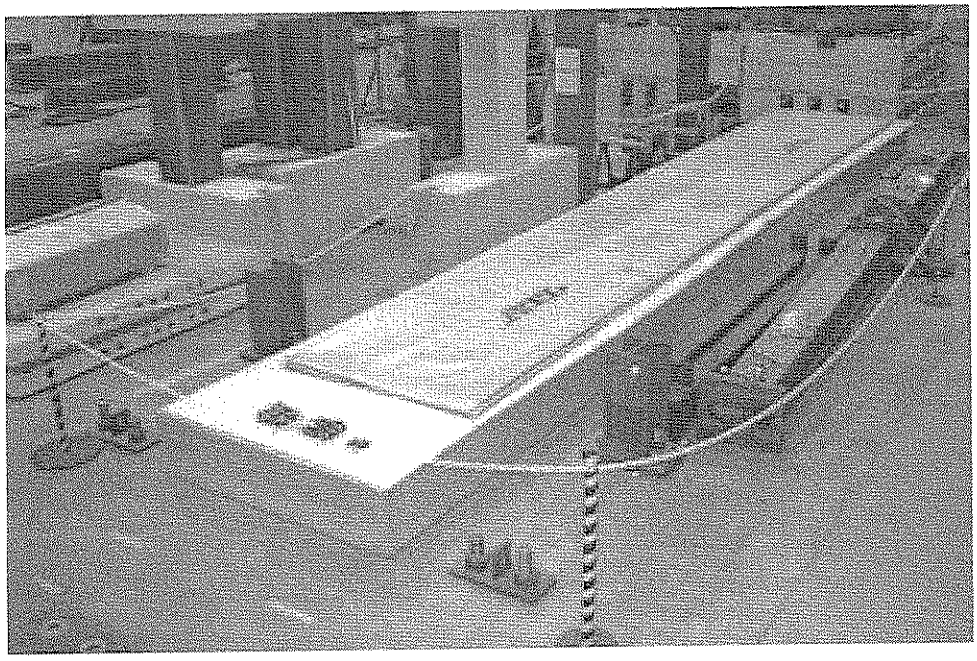

Figure 3.18 Air bladder shown in place on the concrete spacer blocks.

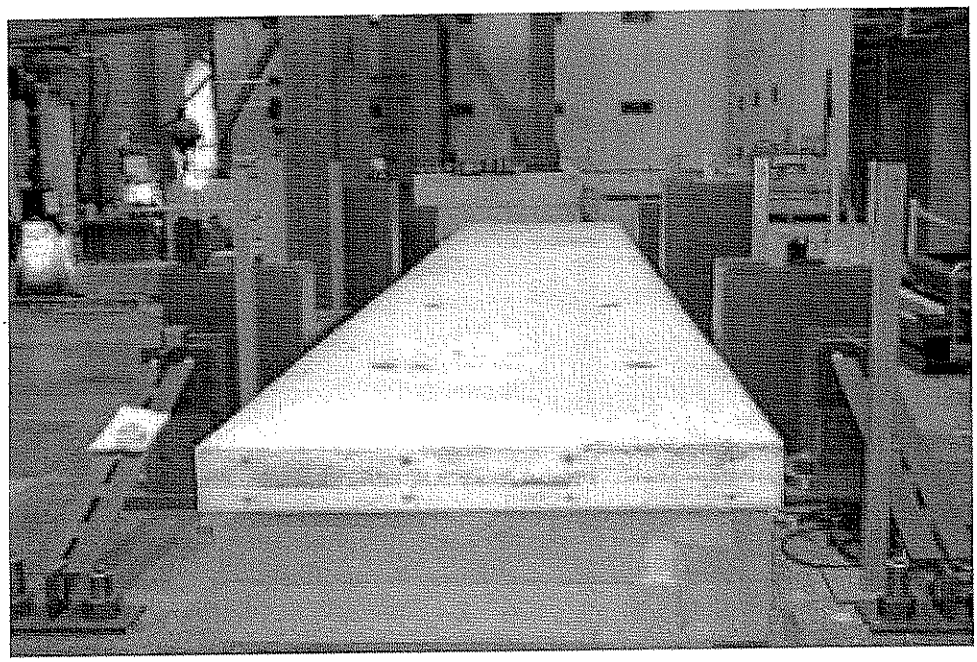

Figure 3.19 Test panel in place.

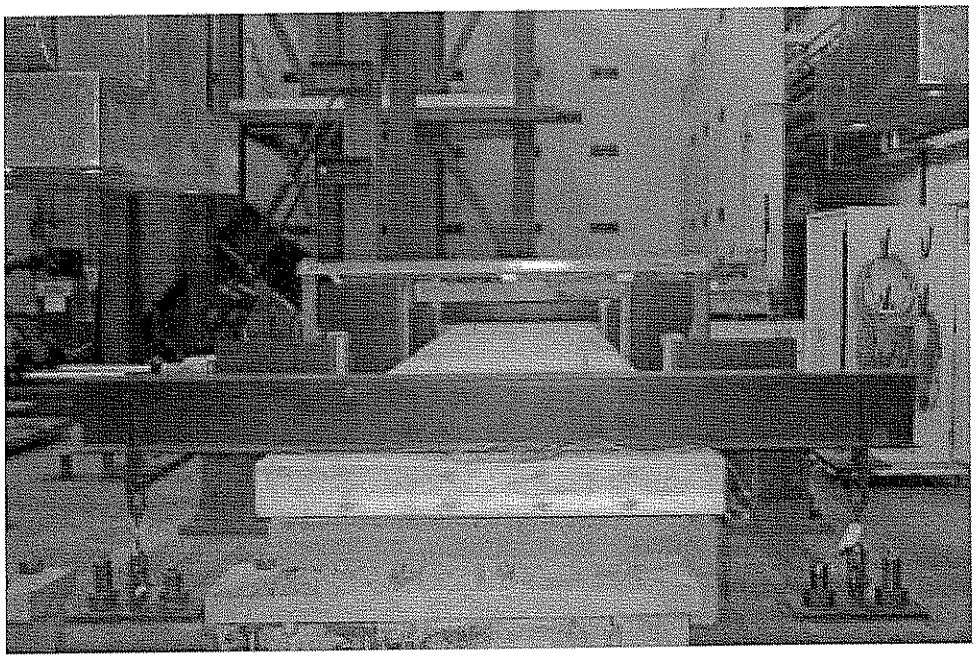

Figure 3.20 Test panel in place with test fixture fully assembled.

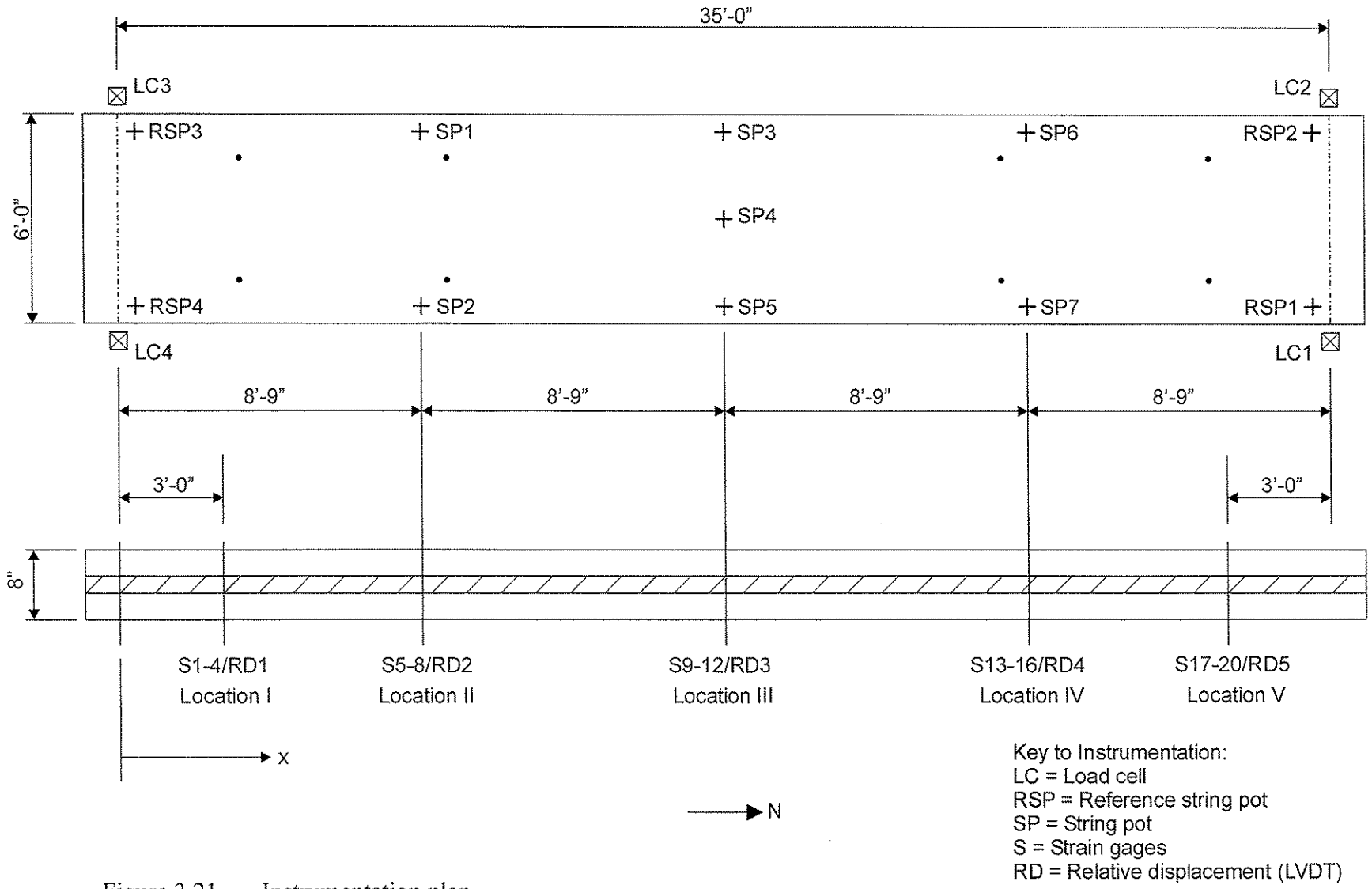


Figure 3.21 Instrumentation plan.

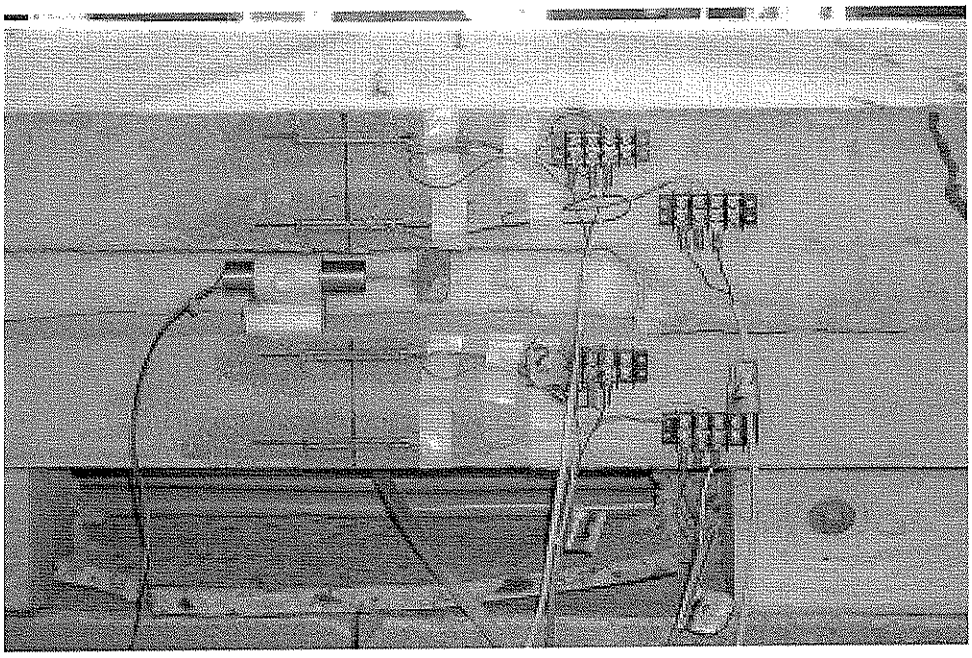

Figure 3.22 Strain gage and LVDT placement at one location along the span.

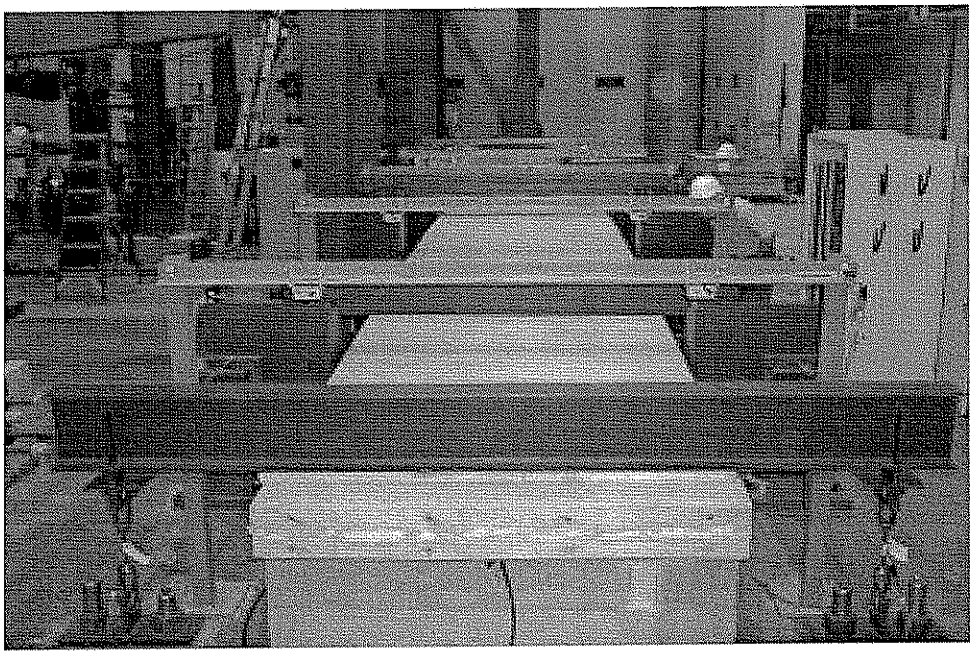

Figure 3.23 Steel frames used for mounting string pots.

# CHAPTER 4
# EXPERIMENTAL RESULTS

## 4.1 INTRODUCTION

This chapter presents a detailed description of the results of the experimental program. The loading procedure used to test the panels is described in Section 4.2. Individual summaries of the tests of each of the panels are presented using the same general format, which is outlined in Section 4.3. The test results for Panel 1, the Prototype panel, are summarized in Section 4.4. The test results for Panel 2, containing only M ties, are summarized in Section 4.5. The test results for Panel 3, containing only solid concrete regions, are summarized in Section 4.6. Finally, the test results for Panel 4, containing only bond between the concrete and the insulation, are summarized in Section 4.7.

## 4.2 GENERAL LOADING PROCEDURE

All panels were tested in a horizontal position with simply supported end conditions. The panels were subjected to a uniform pressure lateral load. No axial load was applied. The loading procedure for Panels 2 through 4 was modified slightly after Panel 1 was tested.

None of the four test panels exhibited failure by crushing of the concrete in the compression zone in flexure. Instead, all test panels became increasingly more flexible as the tests progressed to the point where midspan deflection continued to increase with relatively little increase in resistance. Loading was stopped when the maximum midspan deflection of the panels reached between approximately 9 and 9.5 in. Panels were then unloaded by evacuating the air from the air bladder. Data was recorded throughout the process of loading and unloading each panel.

Panel 1 was tested first. Early in the loading process, as panel self-weight was overcome by the upward pressure in the air bladder, the panel had to experience a small amount of lift-off from its wooden supports before engaging the tension links against the lab floor. During this lift-off, the panel was supported by the air bladder. Therefore, a state of equilibrium existed between the air bladder and the panel in which the total force exerted by the air bladder was equal to the self-weight of the panel. This state of equilibrium existed until the bladder inflated enough to cause the tension links to fully engage and resist further lift-off.

During lift-off, the panel was not subjected to a full uniformly distributed load along its entire length because the air bladder was only 32 ft. long, while the test panel was 37 ft. long. This created a total unsupported length of 2.5 ft. at each end of the panel. This unsupported self-weight, along with the weight of the reaction beams and other test fixture hardware, caused some initial bending of the panel as lift-off occurred.

In the data reduction for Panel 1, the values of load are adjusted to account for the additional load that was initially applied to the panel by the self-weight of the unsupported length of panel and the test fixture. In particular, the sum of the self-weight of the unsupported panel and the self-weight of the test fixture were added to the total applied lateral load. For Panel 1, the value

is 3250 lbs. Since the panel was still in the uncracked, linear elastic range the data was easily extrapolated back to the origin of the load deflection plot.

There was some concern that the remaining panels may not remain in the uncracked, linear elastic range during this lift-off part of the loading. Therefore, the test procedure was modified slightly for the remaining three panels. The initial moment created by the unsupported panel self-weight and the fixture self-weight was eliminated by applying an upward concentrated load at each end of the panel. The concentrated loads were applied using two 30-ton capacity hydraulic flat jacks placed at mid-width of the panel directly beneath the reaction beams. Figures 4.1 and 4.2 show the placement of a flat jack at one end of a test panel.

The point load to be applied to each panel was calculated individually based on the fixture self-weight and on the unsupported panel self-weight. Unsupported panel self-weight varied based on whether or not the panel had solid concrete end regions. These values were 3000, 3250, and 3000 lbs. for Panels 2, 3, and 4 respectively. All loading values presented in the remainder of this report include the adjustments for panel weight and test fixture weight as described above. In the modified test procedure, the hydraulic pump was turned on to apply the point loads to the ends of the panel, and then the lateral load was applied by filling the air bladder.

## 4.3 FORMAT OF TEST SUMMARIES

The individual test summary for each panel is presented using the same general format described below. For reference, the instrumentation plan was presented earlier in Figure 3.21.

1. A summary of the geometry and the material properties of the panel.
2. A description of the behavior of the panel during the test.
3. A table which shows the sequence of key events for the panel.
4. A plot of lateral load versus lateral deflection. Data is plotted for lateral deflection at midspan (x=0.5L) and at the quarter points (x=0.25L and x=0.75L).
5. A plot of lateral load versus lateral deflection at midspan, annotated to show where cracks were observed to occur in the tension wythe. Also included is a plan view drawing of the panel that shows the locations of the cracks. The cracks are numbered in the order in which they were observed to occur.
6. A plot of load versus relative displacement of the wythes. Positive relative displacement indicates that the tension wythe displaced to the south relative to the compression wythe. Negative relative displacement indicates that the tension wythe displaced to the north relative to the compression wythe. The load versus relative displacement plot is preceded by a plot of load versus deflection, annotated to show key points on the load versus relative displacement plot.
7. Plots of load versus strain. There are 5 plots, one for each location along the span (Locations I through V) at which there was a set of 4 strain gages. Positive strain indicates tension, while negative strain indicates compression. Load versus strain curves are not shown for gages where it is suspected that the gage failed. The load versus strain plots are preceded by a plot of load versus midspan deflection, annotated to show key points on the load versus strain plots.

8. Plots of strain distributions at various locations along the span (Locations I through V) at selected loads. The strain distribution plots are preceded by a plot of load versus deflection, annotated to show the values of load at which the strain distributions are plotted.
9. Photographs that show various details of the panel during the test.

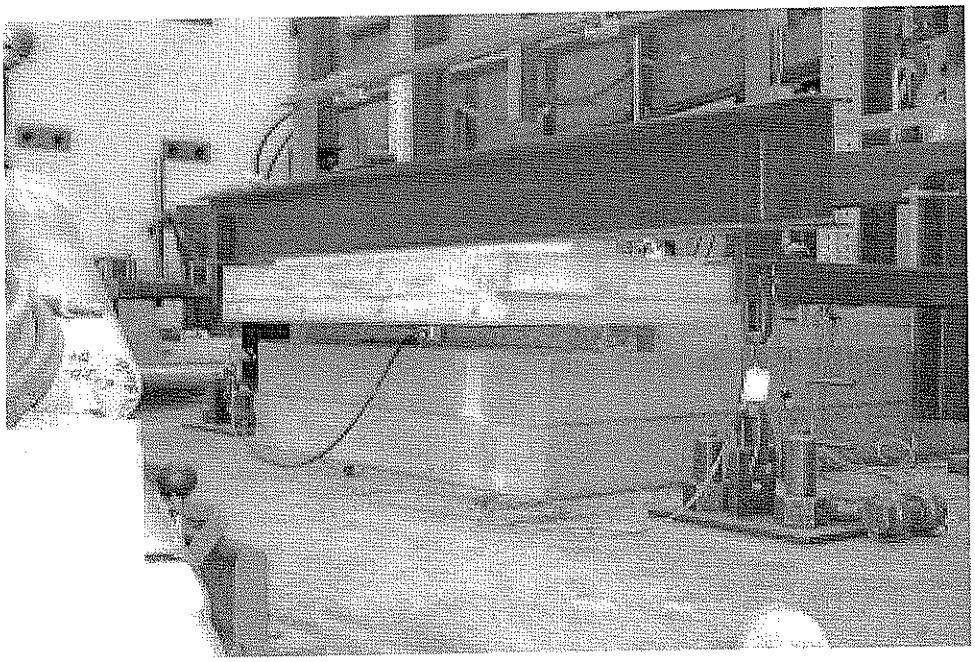

Figure 4.1 30-ton capacity hydraulic flat jack in place between the test panel and spacer blocks, and aligned beneath the reaction beam.

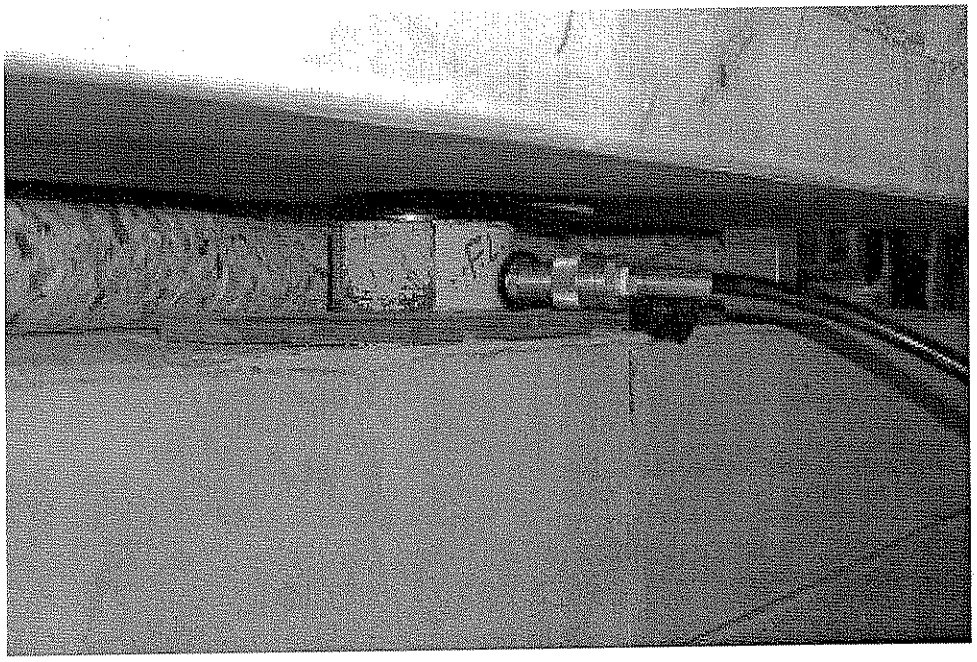

Figure 4.2 Close-up view of 30-ton capacity hydraulic flat jack in place between the test panel and reaction beam.

## 4.4 PANEL 1

The purpose of Panel 1 was to investigate the behavior of a typical sandwich wall panel. This panel was made with a 1 ft. wide solid band of concrete at each end of the panel, and eight 1 ft. square solid regions spaced in pairs along the span of the panel. This panel also contained steel M-tie connectors spaced at 2 ft. on center. No attempt was made to disrupt the bond between the concrete wythes and the insulation.

The unconfined concrete compressive strength of the concrete of the face (compression) wythe was 7050 psi and the unconfined concrete compressive strength for back (tension) wythe was 6820 psi. The average unconfined compressive strength of the concrete in both wythes was 6930 psi.

The lateral load versus deflection plot is shown in Figure 4.3. In terms of deflection, the panel behaved in a symmetric manner, with the values of deflection at the two quarter points remaining nearly identical throughout the test.

Figures 4.4 and 4.8 show the cracking behavior of Panel 1. The panel behaved in a linear elastic manner up to a load of P=8710 lbs. and a lateral deflection of $\Delta$=0.68 in. As shown in Figure 4.4, the first flexural crack was observed at this point. In general, the formation of each flexural crack was associated with a distinct drop in load in the load deflection plot. The panel shows a dramatic reduction in stiffness, upon formation of the second flexural crack, at a load of P=10490 lbs. and a lateral deflection of $\Delta$=1.16 in. Deflection increases much more rapidly for a given increase in load beyond this point. The panel was loaded up to a maximum load of P=16340 lbs. and a lateral deflection of $\Delta$=9.26 in. The test was terminated at this point and the panel was unloaded. Figures 4.9 and 4.10 show the deflected shape of Panel 1 at two different stages in the loading. Flexural failure of the test panel, by crushing of the concrete in the compression zone, was not reached.

Eight flexural cracks were observed in the tension wythe of the panel. The first cracks to occur formed near midspan. Successive flexural cracks formed along the span, generally progressively further from midspan. All cracks propagated across the full width of the panel. Several cracks formed along the edges of the 1 ft. square concrete regions. A close up view of a typical flexural crack is shown in Figure 4.11. The crack is marked with a felt-tipped marker in this photograph.

Figure 4.5 shows results of the measurements of relative displacements between wythes for Panel 1. Relative to the other panels, small values of relative displacements were observed for this panel throughout the entire test. At the formation of the second flexural crack, at a load of P=10490 lbs. (point A), relative displacement begins to increase more rapidly with load. At the peak load of P=16340 lbs., all values of relative displacement were less than 0.020 in.

Figure 4.6 shows the results of strain measurements for Panel 1. All load versus strain plots for this panel show dashed lines for values of strain up to a load of P=3250 lbs. The strain data was extrapolated back to the origin of each plot. This is due to the necessary load correction that was discussed in Section 4.2.

Figure 4.6 (b) shows the load-strain data at Location I. All values of strain increased linearly with increasing load until loading was stopped. The maximum values of strain in measured tension and compression were 0.00010 in./in. (gage S1) and –0.00012 in./in. (gage S4).

Figure 4.6 (c) shows the load-strain data at Location II. All values of strain increased linearly until the panel began to lose stiffness near the load where the second flexural crack formed. At a load of P=9860 lbs. (point b), the values of strain at gage S5 began to increase in tension much more rapidly with increasing load. At a load of P=10490 lbs. (point d), the values of strain at gage S6 also began to increase rapidly to very large values of strain in tension with increasing load. This point corresponds with the formation of the second flexural crack. At the same point in the loading, the values of strain at gage S8 began to increase in compression at a greater rate, up to a maximum strain of approximately –0.0004 in./in.

Figure 4.6 (d) shows the load-strain data at Location III. All values of strain increased linearly up to a load of P=8710 lbs. (point a), which corresponds with the formation of the first flexural crack. At this point, the strain at gage S9 decreased in tension, while the strain at gage S10 increased in tension. Also, the strain at gage S11 began to decrease in compression, until eventually going into tension at point c. Above point c, the strain in gages S9 and S10 remained relatively constant with increasing load.

Figure 4.6 (e) shows the load-strain data at Location IV. All values of strain increased linearly up to a load of approximately P=10000 lbs. At a load of P=10870 lbs. (point e), which corresponds with the formation of the fourth flexural crack, the values of strain at gages S13 and S14 began to decrease and increase in tension, respectively. At this point, the values of strain at gage S16 began to increase at a slightly greater rate, up to a strain of –0.00038 in./in.

Figure 4.6 (f) shows the load-strain data at Location V. All values of strain increased linearly with increasing load until loading was stopped. Gages S18 and S19 appeared to record almost no measurable strain. The maximum values of strain measured in tension and compression were 0.00011 in./in. (gage S17) and –0.00010 in./in. (gage S20).

Figure 4.7 shows plots of the strain distributions at Locations I through V for Panel 1. At all locations, the strain distributions do not seem to indicate plane section behavior throughout the entire depth of the panel. The strain distributions are discussed further in Section 5.6.

It was noted during the test that in some locations the concrete wythes began to separate from the insulation. Figure 4.12 shows one example of the separation of the tension wythe from the insulation near midspan.

| Load (lbs.) | Deflection (in.) | Event | | |
|---|---|---|---|---|
| | | Crack | Relative Displacement | Strain |
| 8710 | 0.68 | 1 | | a |
| 9860 | 0.93 | | | b |
| 10150 | 0.97 | | | c |
| 10490 | 1.16 | 2 | A | d |
| 10260 | 1.27 | 3 | | |
| 10870 | 1.69 | 4 | | e |
| 11630 | 2.18 | 5 | | |
| 11700 | 2.46 | 6 | | |
| 12800 | 3.34 | 7 | | |
| 13640 | 4.31 | 8 | | |
| 15190 | 6.92 | | | f |

Table 4.1 Sequence of key events for Panel 1.

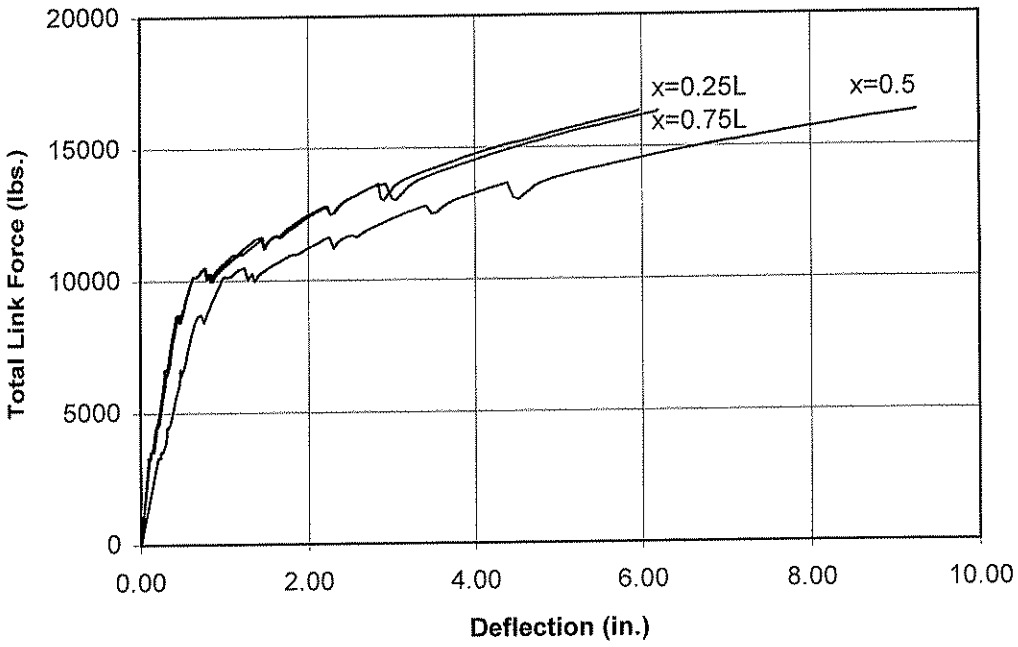


Figure 4.3 Plot of lateral load versus lateral deflection for Panel 1.

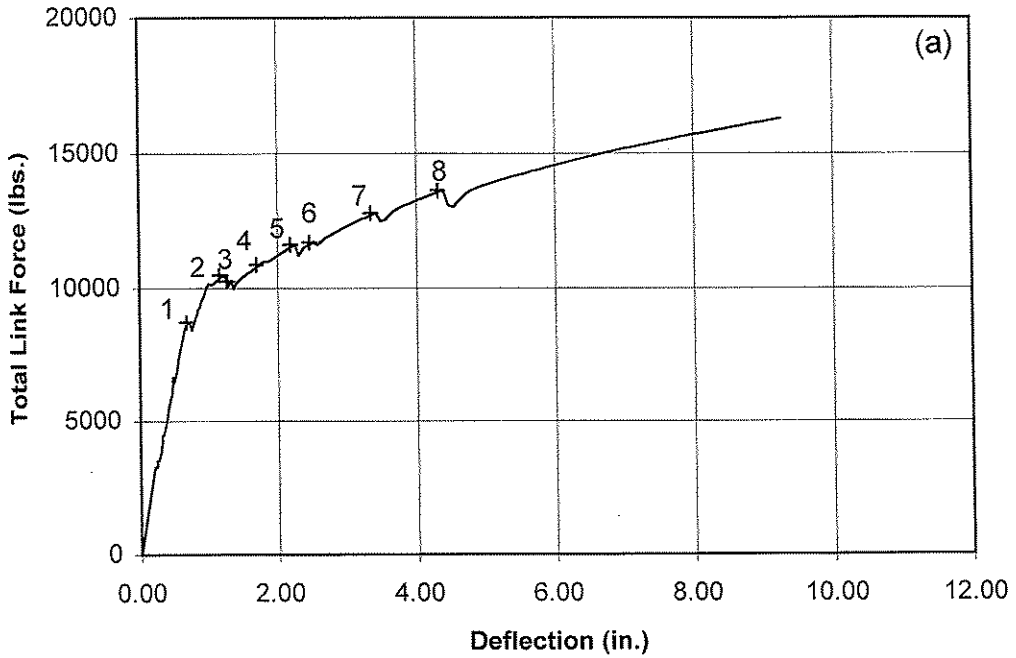


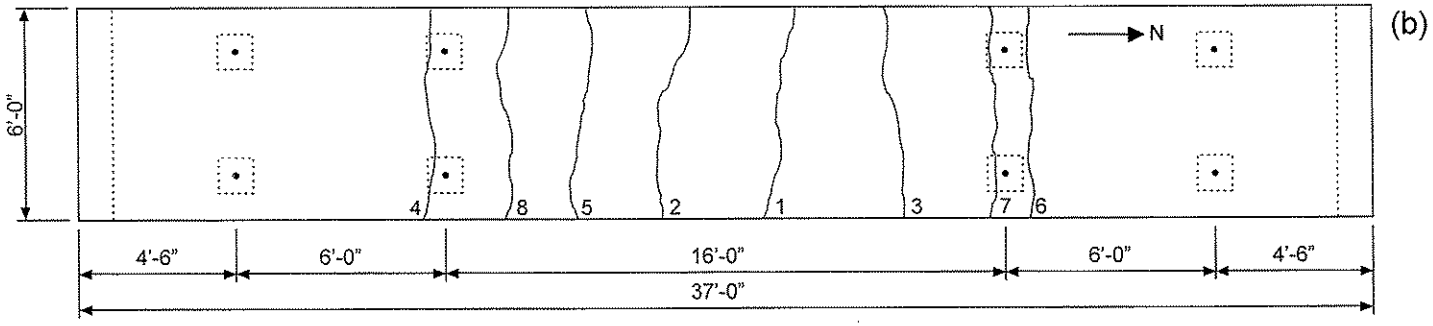


Figure 4.4 Cracking behavior of Panel 1: (a) key points on load-deflection plot; and (b) plan view of Panel 1 showing crack locations.

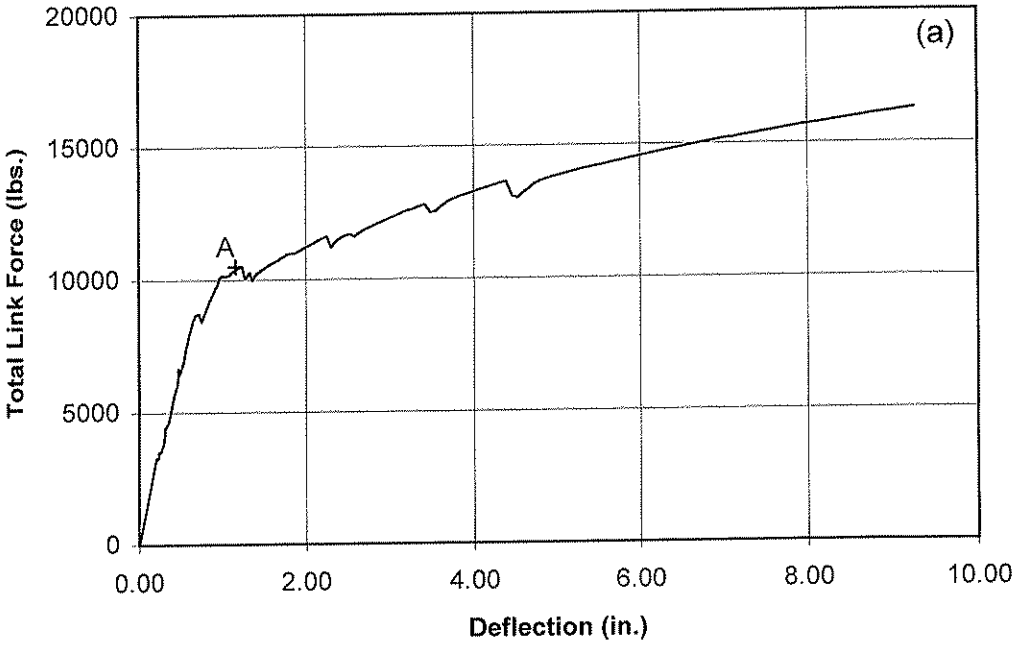


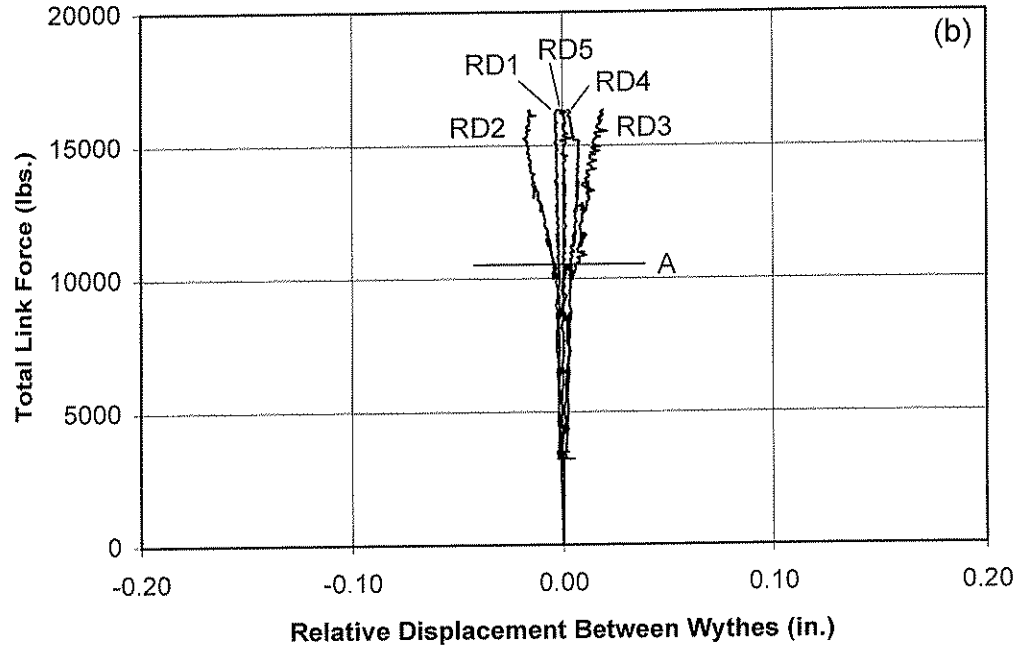


Figure 4.5 Relative displacement between wythes for Panel 1: (a) key point on load-deflection plot; and (b) total link force versus relative displacement between wythes.

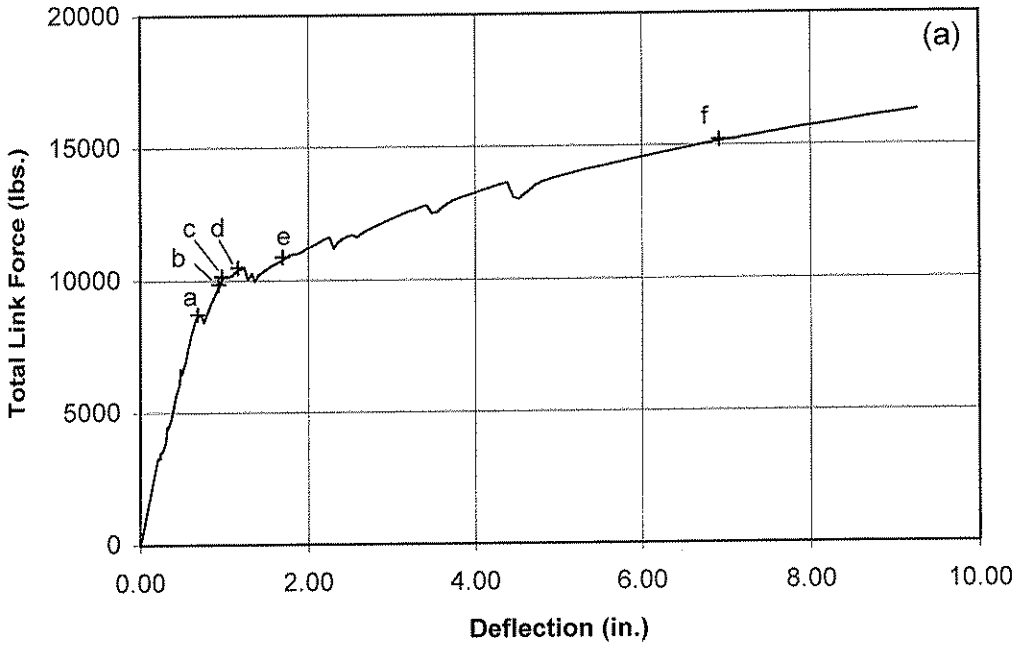


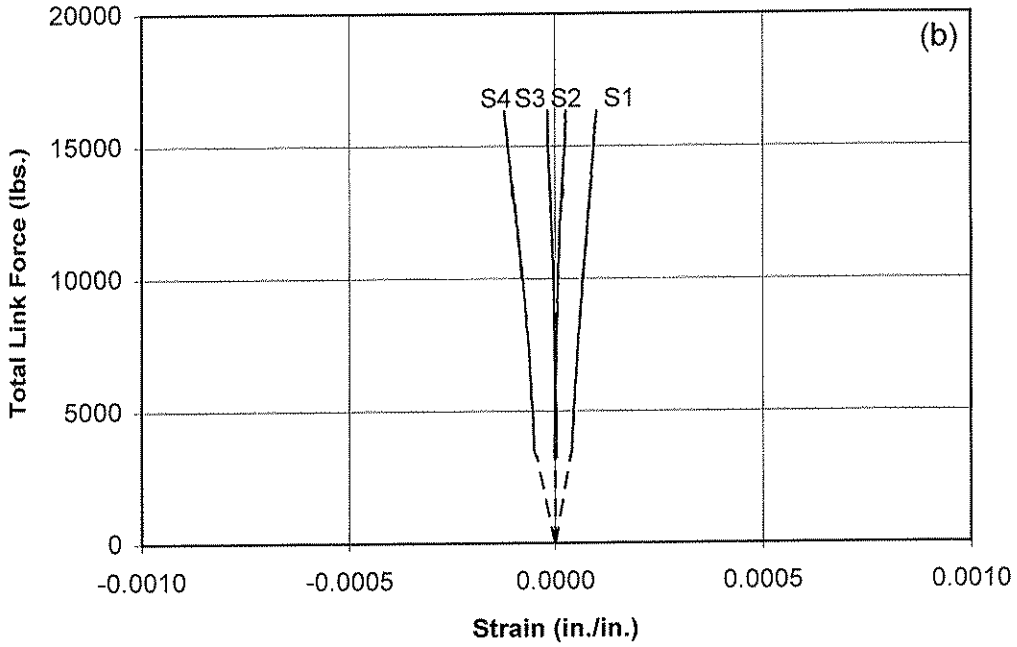


Figure 4.6 Strain measurement results for Panel 1: (a) key points on load-deflection plot; (b) total link force versus strain at Location I (gages S1 through S4).

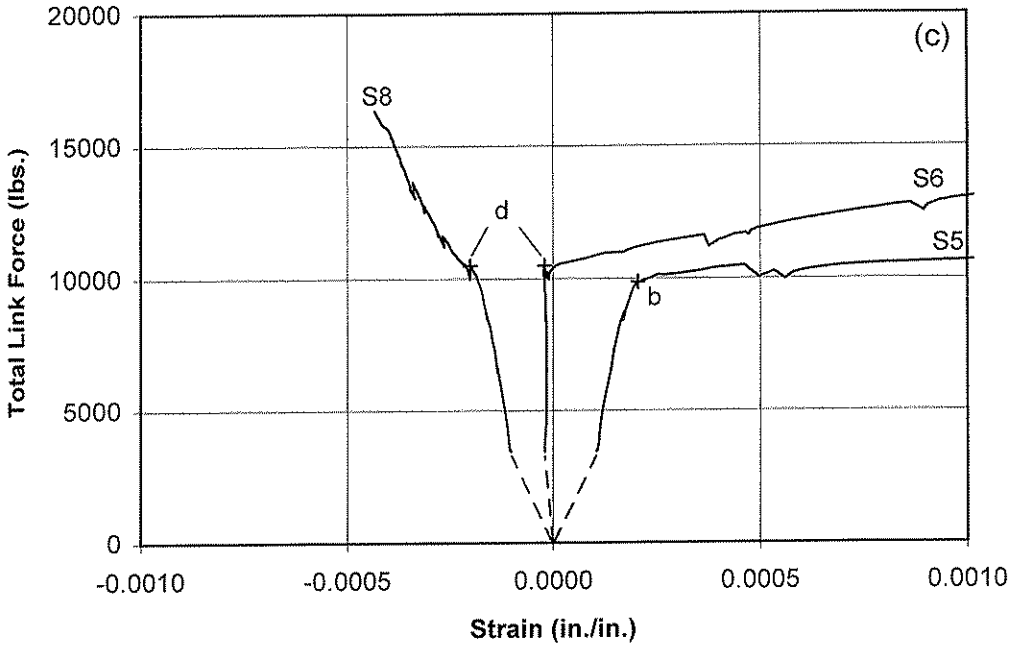


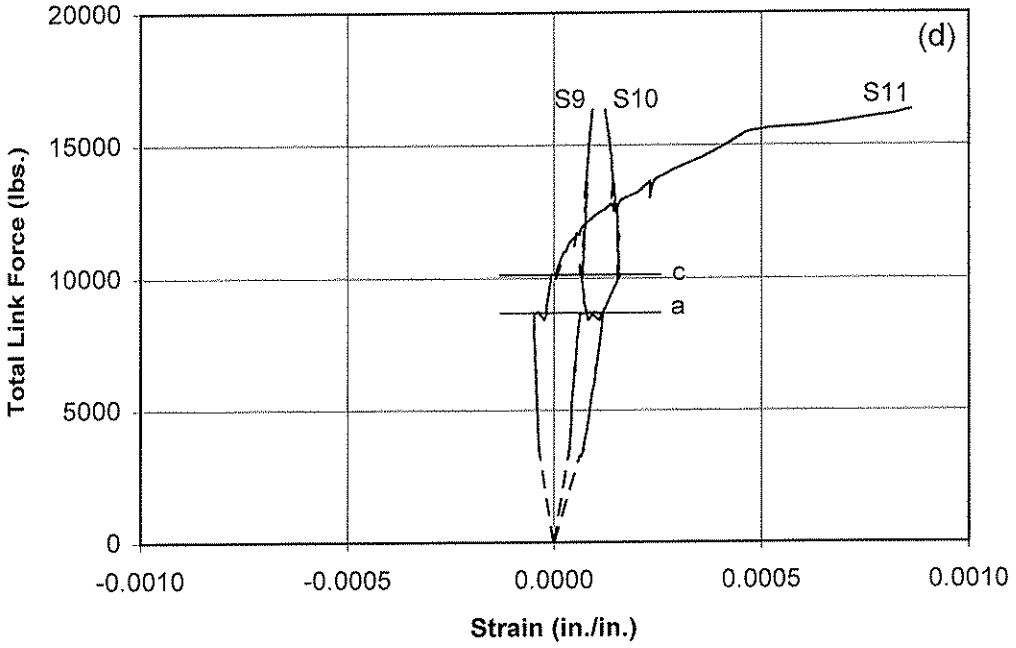


Figure 4.6 (c) total link force versus strain at Location II (gages S5 through S8);
(d) total link force versus strain at Location III (gages S9 through S12);

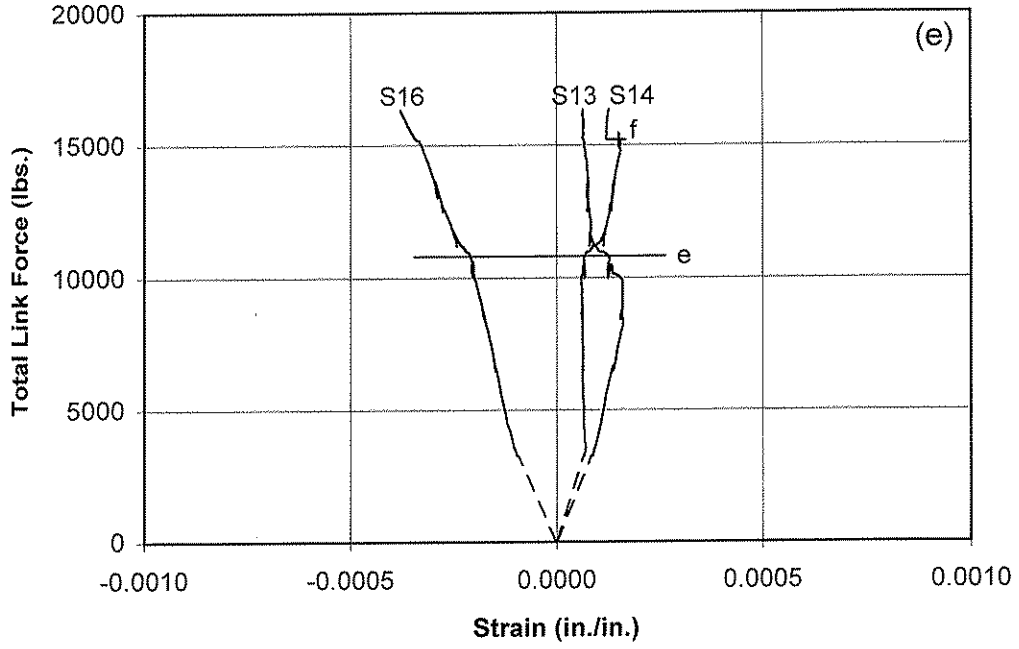


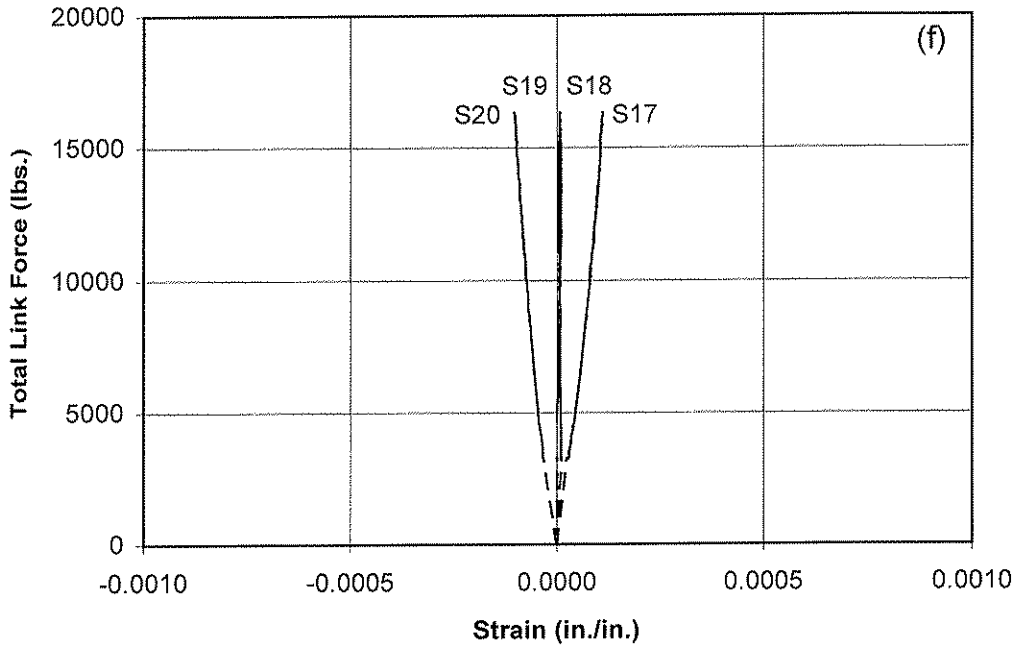


Figure 4.6 (e) total link force versus strain at Location IV (gages S13 through S16);
(f) total link force versus strain at Location V (gages S17 through S20);

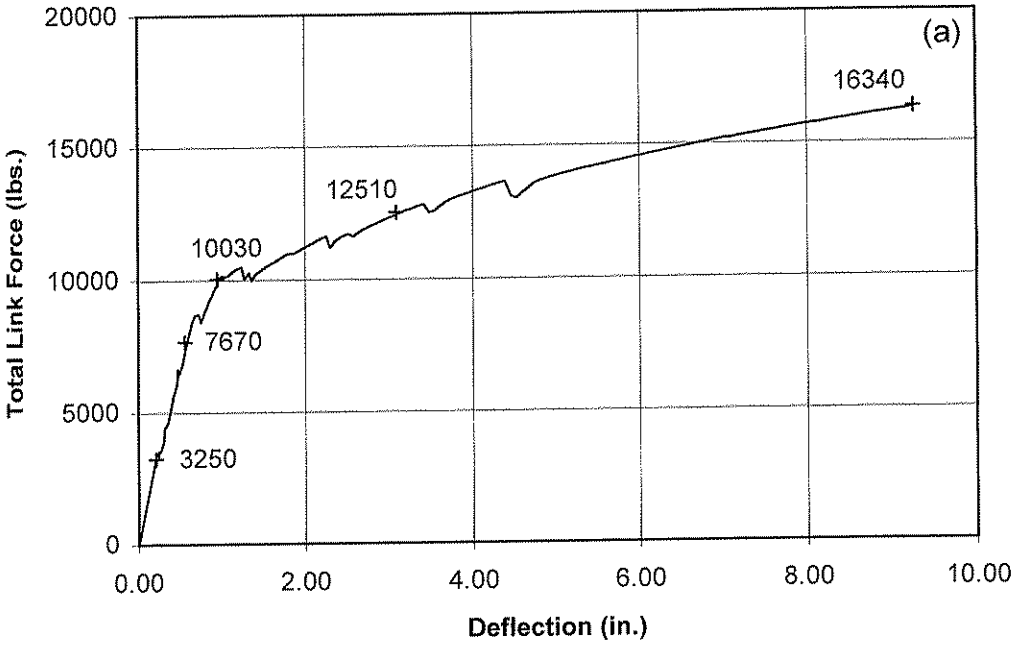


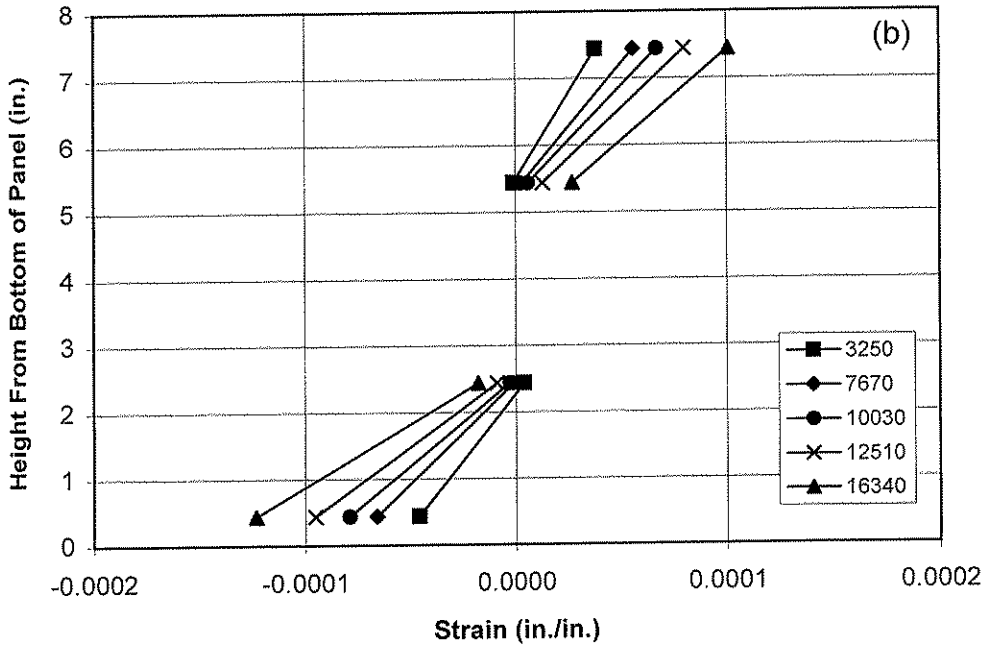


Figure 4.7 Strain distributions for Panel 1: (a) load-deflection plot showing points at which strain distributions are plotted; (b) strain distributions at Location I.

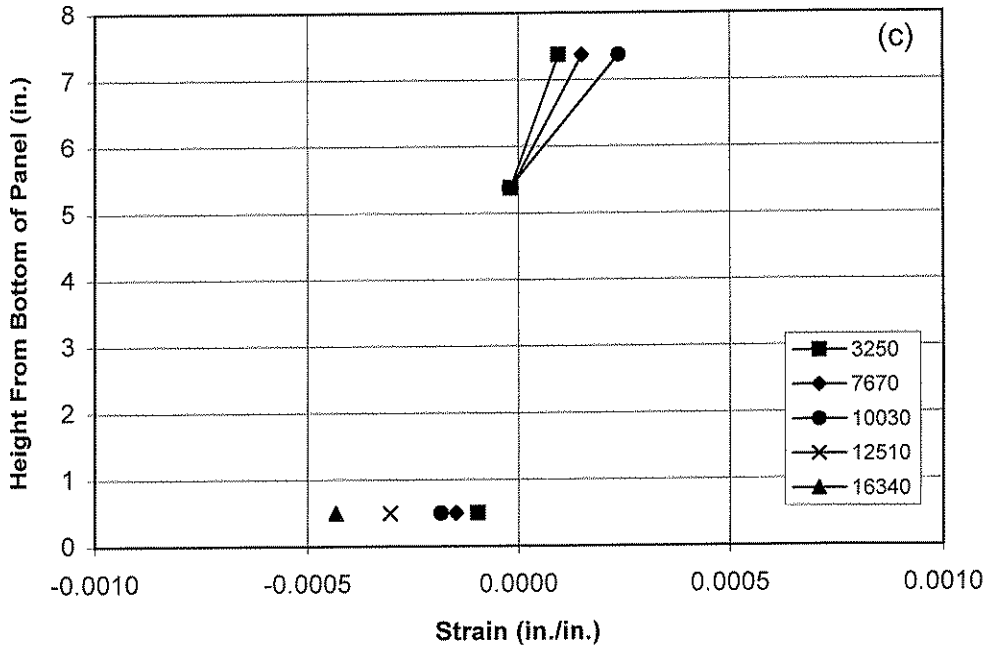


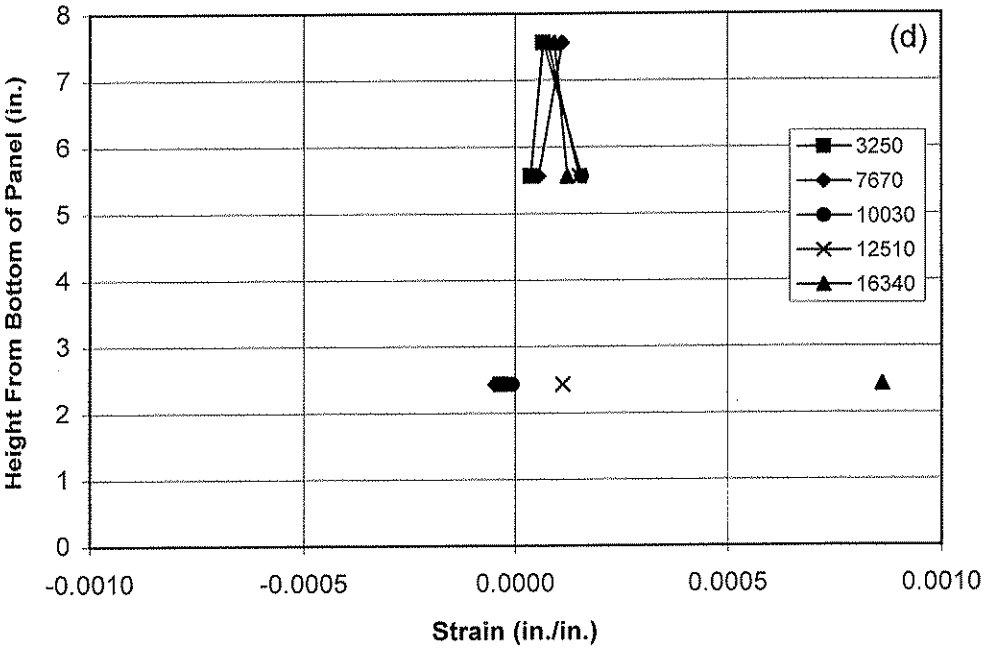


Figure 4.7 (c) strain distributions at Location II;
(d) strain distributions at Location III;

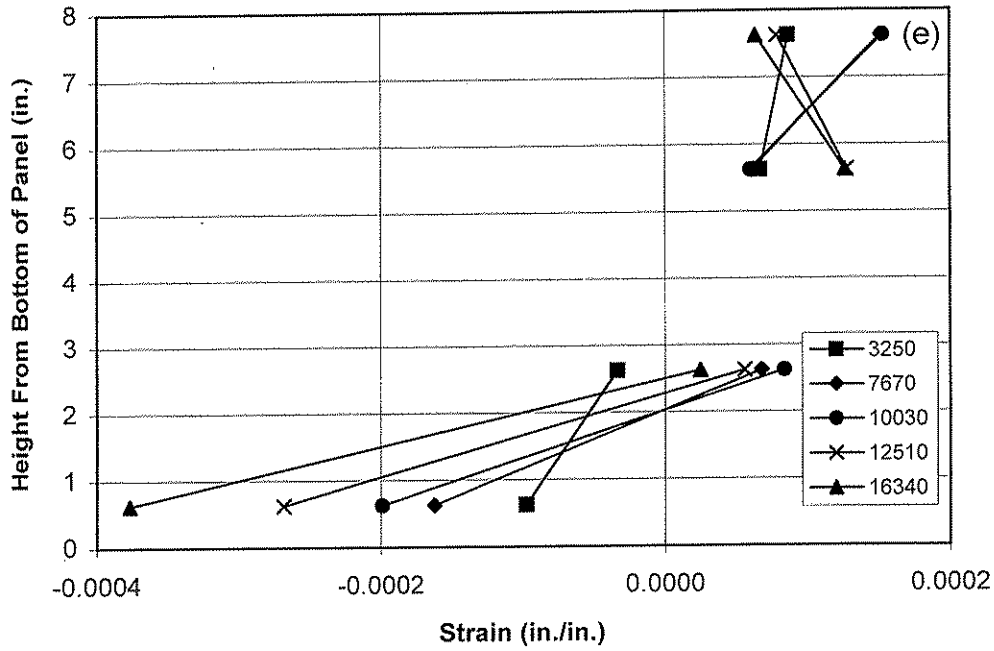


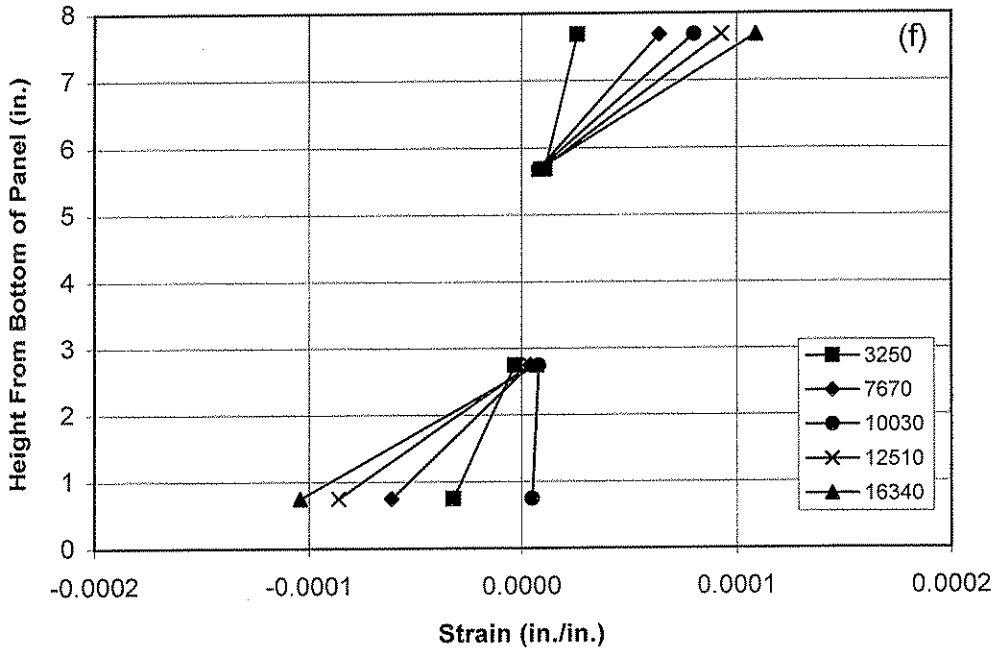


Figure 4.7 (e) strain distributions at Location IV;
(f) strain distributions at Location V;

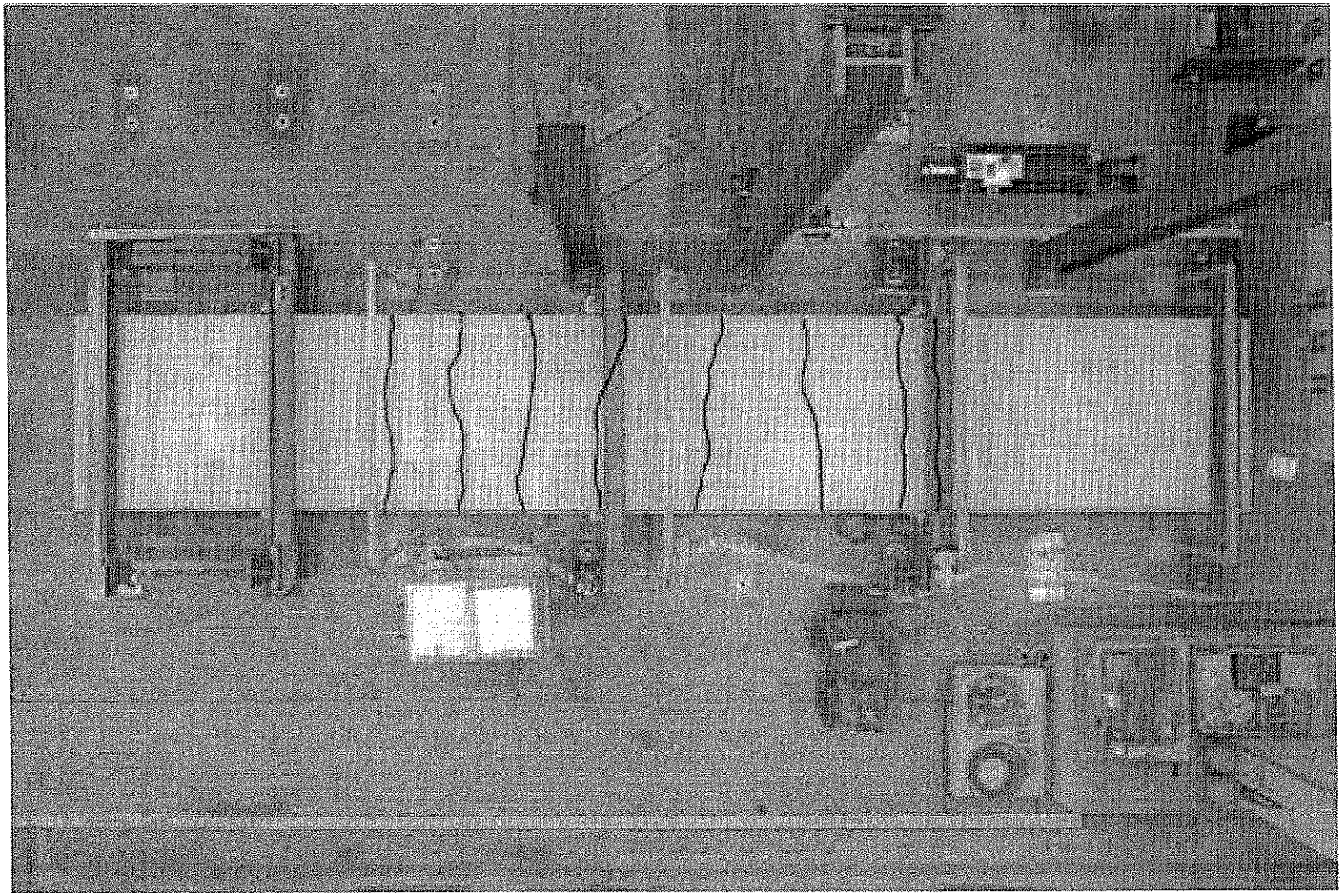

Figure 4.8 Post test photograph of Panel 1 showing crack locations.

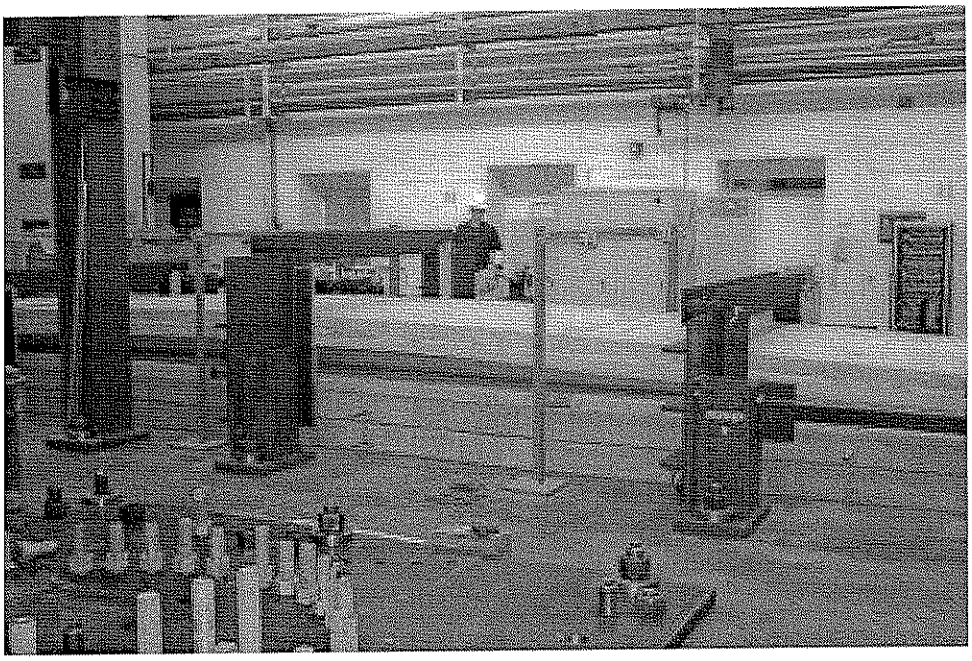

Figure 4.9 Deflected shape of Panel 1 at P=15280 lbs. and midspan deflection Δ=7.11 in.

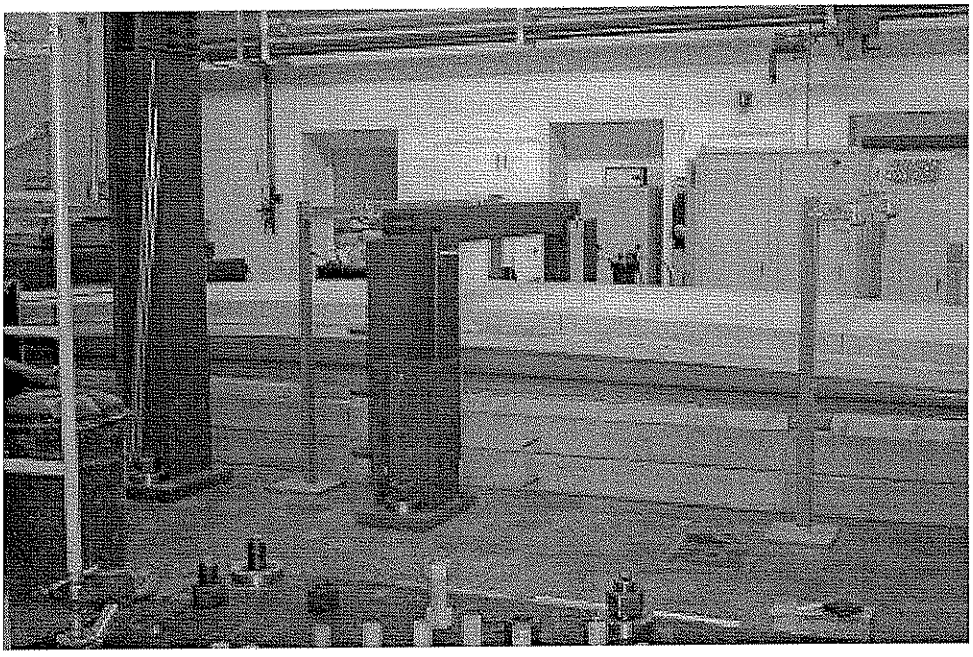

Figure 4.10 Deflected shape of Panel 1 at maximum load P=16340 lbs. and midspan deflection Δ=9.26 in.

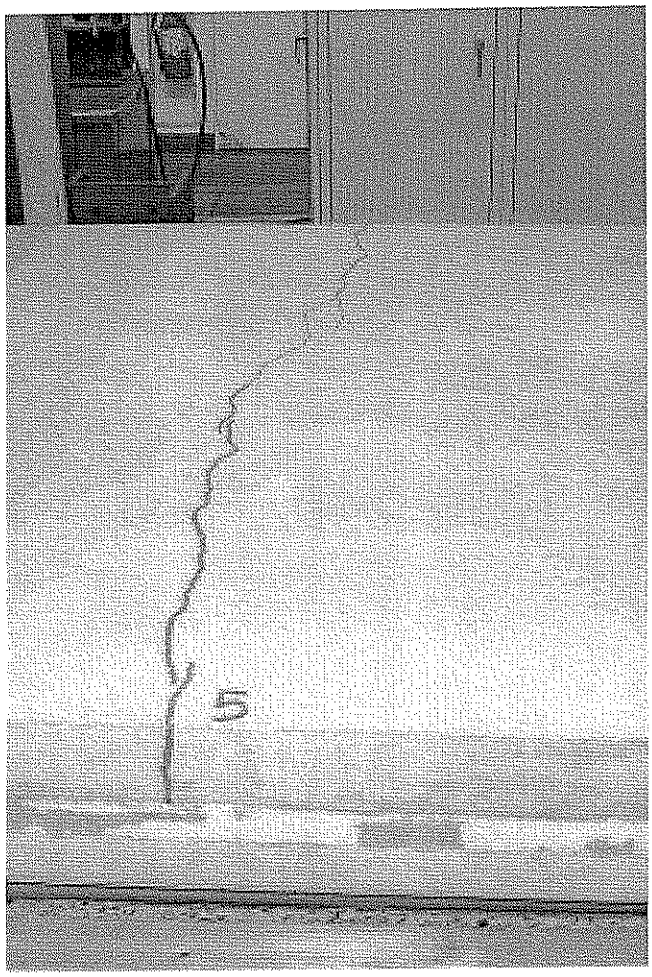

Figure 4.11 Typical flexural crack in the tension wythe of Panel 1.

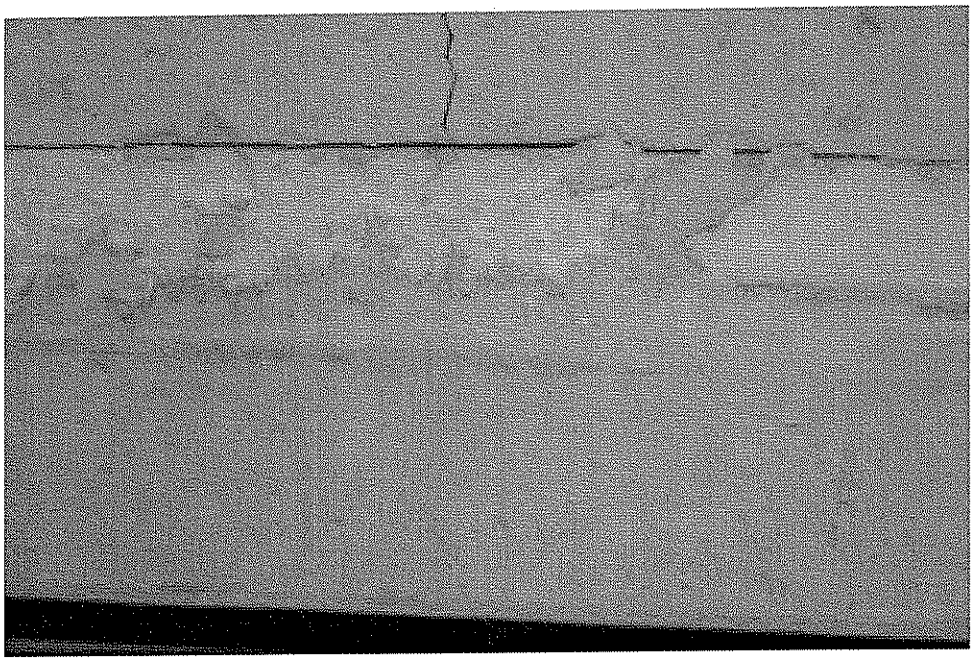

Figure 4.12 Separation of the tension wythe from insulation near midspan in Panel 1.

## 4.5 PANEL 2

The purpose of Panel 2 was to investigate the fraction of composite action provided by the steel M-tie connectors. This panel contained M-tie connectors spaced at 2 ft. on center, but contained no solid regions and the bond between the concrete wythes and the insulation was destroyed using a plastic bond breaker. Therefore, the steel M-ties provided the only intended mechanism of shear transfer.

The unconfined concrete compressive strength of the concrete of the face (compression) wythe was 8340 psi and the unconfined concrete compressive strength for back (tension) wythe was 9170 psi. The average unconfined compressive strength of the concrete in both wythes was 8760 psi.

The lateral load versus deflection plot is shown in Figure 4.13. In terms of deflection, the panel behaved in a symmetric manner, with the values of deflection at the two quarter points remaining nearly identical throughout the test.

Figures 4.14 and 4.18 show the cracking behavior of Panel 2. The panel behaved in a linear elastic manner up to a load of P=2890 lbs. and a lateral deflection of $\Delta$=0.98 in. As shown in Figure 4.14, the first flexural crack was observed at this point. In general, the formation of each flexural crack was not associated with a distinct drop in load in the load deflection plot. Instead the panel exhibited a continual degradation of flexural stiffness. After the first flexural crack formed, there was a gradual decrease in flexural stiffness of the panel throughout the rest of the test. The panel was loaded up to a maximum load of P=7850 lbs. and a lateral deflection of $\Delta$=9.25 in. The test was terminated at this point and the panel was unloaded. Figures 4.19 and 4.20 show the deflected shape of Panel 2 at two different stages in the loading. Flexural failure of the test panel, by crushing of the concrete in the compression zone, was not reached.

Thirteen flexural cracks were observed in the tension wythe of the panel. The first cracks to occur formed near midspan. Successive cracks formed along the span, generally progressively further from midspan. Away from midspan, not all cracks propagated across the full width of the panel.

Figure 4.15 shows the results of the measurements of relative displacements between wythes for Panel 2. Large values of relative displacements were observed for this panel. At a load of P=3740 lbs. (point A), the values of relative displacement for instruments RD1, RD2, RD4, and RD5 began to increase more rapidly with increasing load. At the peak load of P=7850 lbs., instrument RD1 recorded a relative displacement of –0.242 in. and instrument RD5 recorded a relative displacement of 0.365 in. The largest relative displacements occurred near the ends of the panel. Figures 4.21 and 4.22 depict the relative displacements between wythes at the north and south ends of the panel respectively.

Figure 4.16 shows the results of the strain measurements for Panel 2.

Figure 4.16 (b) shows the load-strain data at Location I. Values of strain increased linearly for gages S1, S2, and S4 up to a load of approximately 5000 lbs., while the value of strain for gage S3 increased somewhat erratically. At a load of P=5490 lbs. (point c), which corresponds with the fourth flexural crack, the values of strain at gage S2 began to increase more rapidly with increasing load. At a load of P=6370 lbs. (point e), which corresponds with the seventh flexural crack, the values of strain at gage S3 increased abruptly with little increase in load.

Figure 4.16 (c) shows the load-strain data at Location II. All values of strain increased linearly up to a load of approximately 5000 lbs. At a load of P=4870 lbs. (point b) the values of strain for gage S7 began to increase more rapidly with increasing load. At a load of P=5490 lbs. (point c), which corresponds with the formation of the fourth flexural crack, the values of strain for gage S5 began to increase more rapidly with increasing load. The maximum values of strain measured in tension and compression were 0.00022 in./in. (gage S5) and –0.00016 in./in. (gage S8).

Figure 4.16 (d) shows the load-strain data at Location III. Values of strain for gages S10 and S11 increased linearly up to a load of approximately 5000 lbs. Values of strain for gages S9 and S12 initially increased linearly up to a load of approximately 3000 lbs., but then gradually began to increase more rapidly. At a load of P=4870 lbs. (point b), values of strain for gage S10 stopped increasing and remained relatively constant with increasing load, while values of strain in gage S9 decreased in tension before continuing to increase. At a load of P=6080 lbs. (point d), which corresponds with the sixth flexural crack, strain at gage S11 began to decrease in tension. The maximum values of strain measured in tension and compression were 0.00020 in./in. (gage S9) and –0.00024 in./in. (gage S12).

Figure 4.16 (e) shows the load-strain data at Location IV. Values of strain for gages S13 and S15 increased linearly up to a load of P=4210 lbs. (point a), which corresponds with the formation of the second flexural crack, while values of strain at gage S16 increased linearly for almost the entire test. Values of strain for gage S14 initially remained relatively constant, but began to increase rapidly in compression at point a.

Figure 4.16 (f) shows the load-strain data at Location V. All values of strain increased linearly with increasing load until loading was stopped. The maximum values of strain in measured tension and compression were 0.00005 in./in. (gage S17) and –0.00004 in./in. (gage S20).

Figure 4.17 shows plots of the strain distributions at Locations I through V for Panel 2. At all locations, the strain distributions do not seem to indicate plane section behavior throughout the entire depth of the panel. The strain distributions are discussed further in Section 5.6.

| Load (lbs.) | Deflection (in.) | Event | | |
|---|---|---|---|---|
| | | Crack | Relative Displacement | Strain |
| 2890 | 0.98 | 1 | | |
| 3740 | 1.35 | | A | |
| 4210 | 1.57 | 2 | | a |
| 4870 | 1.96 | | | b |
| 4980 | 2.05 | 3 | | |
| 5490 | 2.56 | 4 | | c |
| 5650 | 2.72 | 5 | | |
| 6080 | 3.25 | 6 | | d |
| 6370 | 3.65 | 7 | | e |
| 6670 | 4.26 | 8 | | |
| 7080 | 5.58 | 9 | | g |
| 7130 | 5.84 | | | h |
| 7140 | 5.82 | 10 | | |
| 7490 | 7.21 | 11 | | |
| 7800 | 8.73 | 12 | | |

Table 4.2 Sequence of key events for Panel 2.

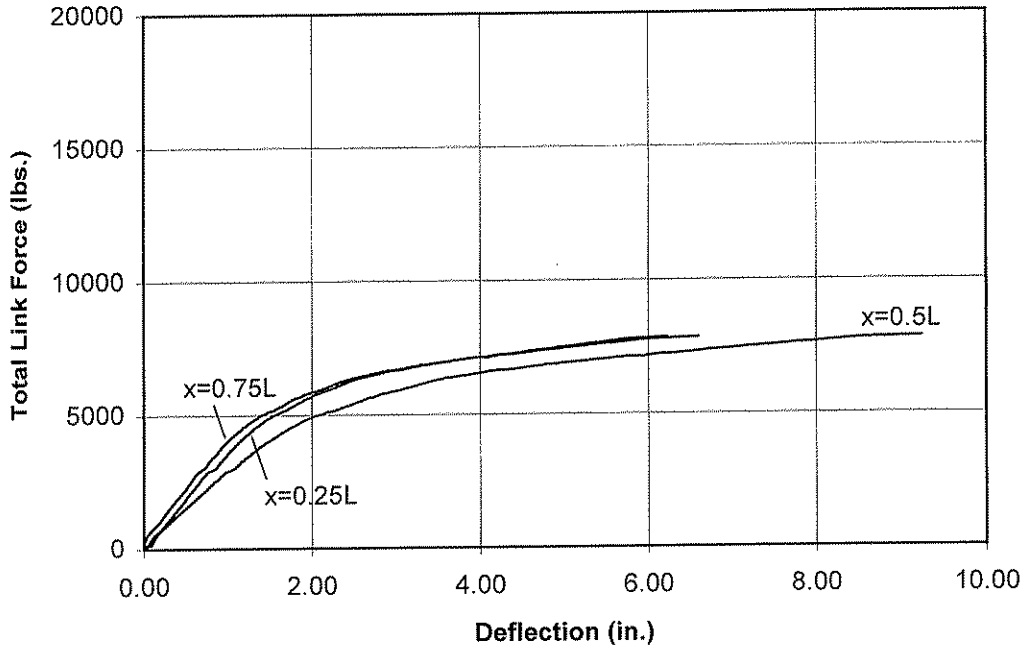


Figure 4.13 Plot of lateral load versus lateral deflection for Panel 2.

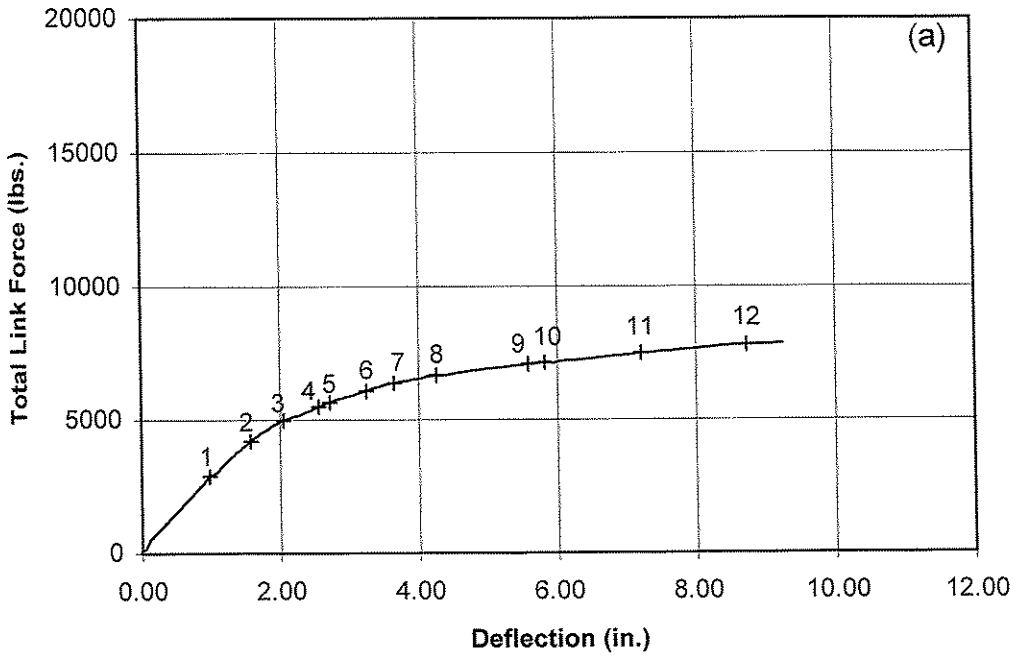


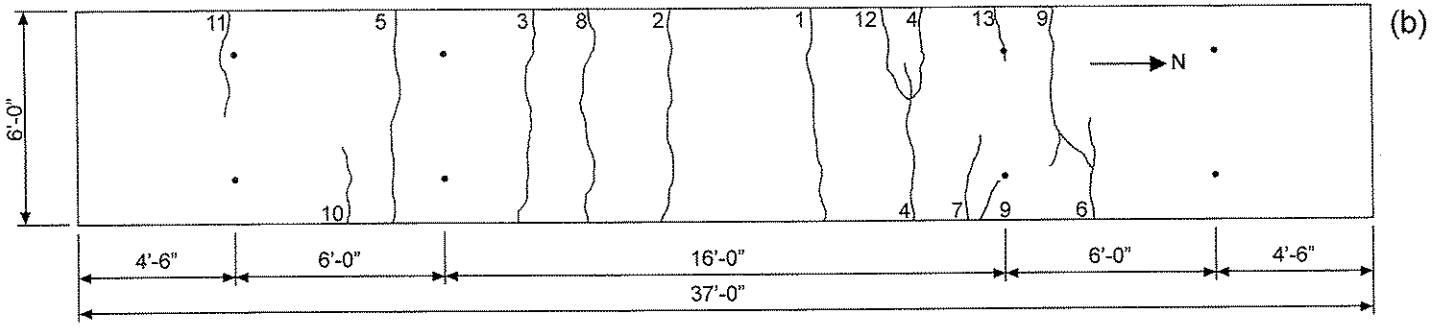


Figure 4.14 Cracking behavior of Panel 2: (a) key points on load-deflection plot; and (b) plan view of Panel 2 showing crack locations.

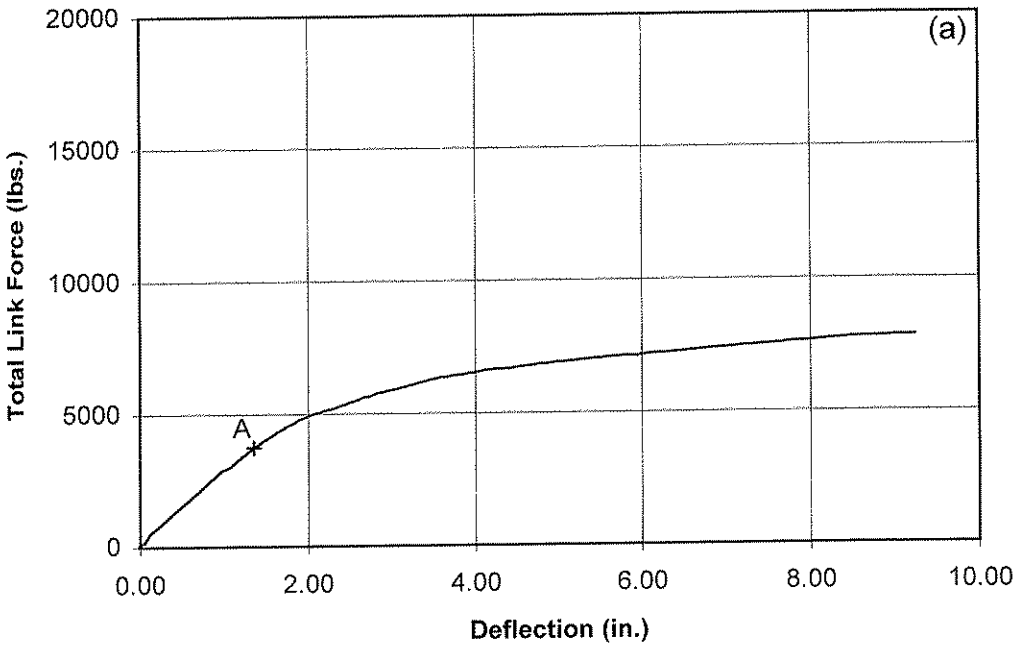


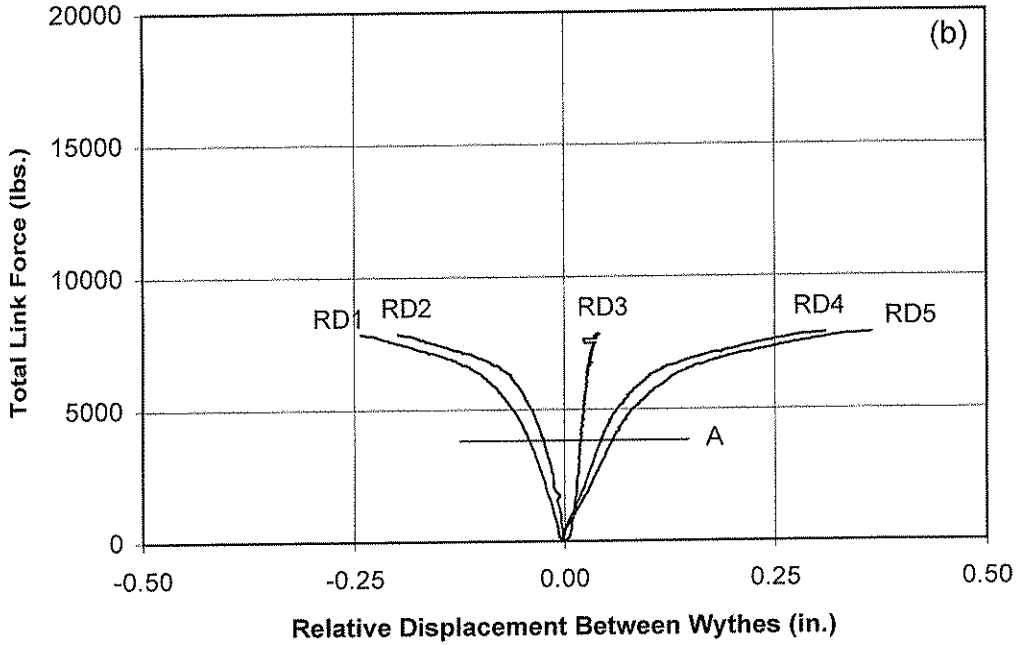


Figure 4.15 Relative displacement between wythes for Panel 2: (a) key point on load-deflection plot; and (b) total link force versus relative displacement between wythes.

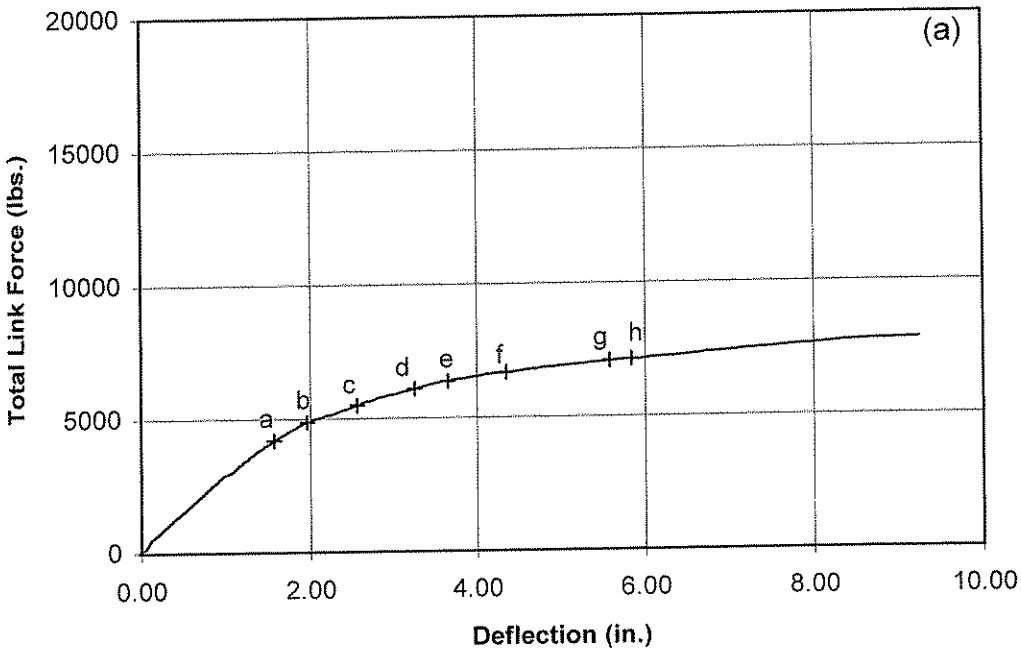


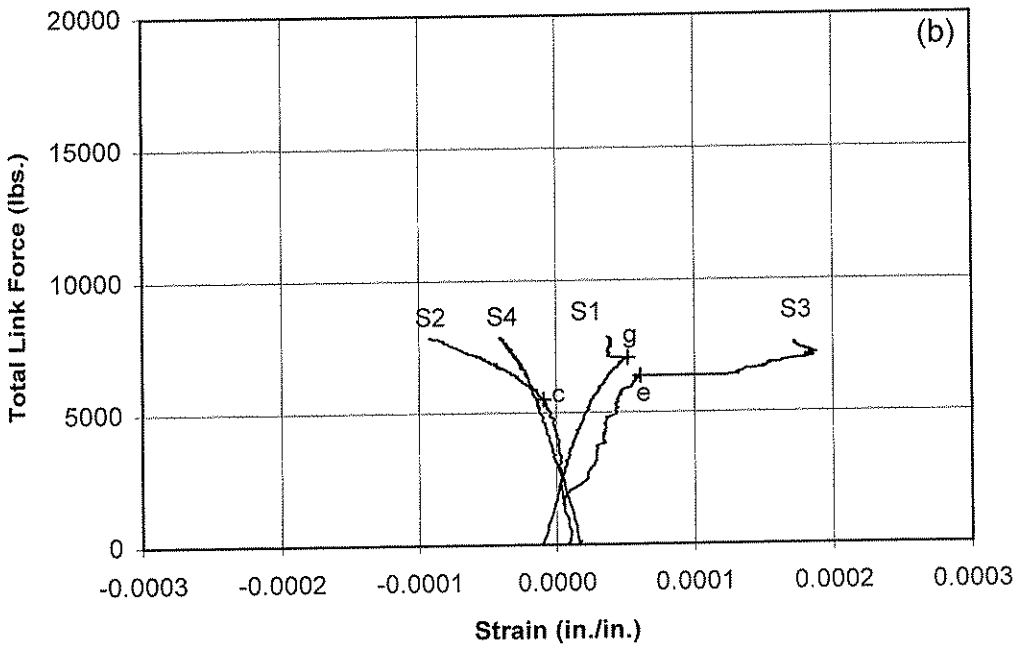


Figure 4.16 Strain measurement results for Panel 2: (a) key points on load-deflection plot; (b) total link force versus strain at Location I (gages S1 through S4).

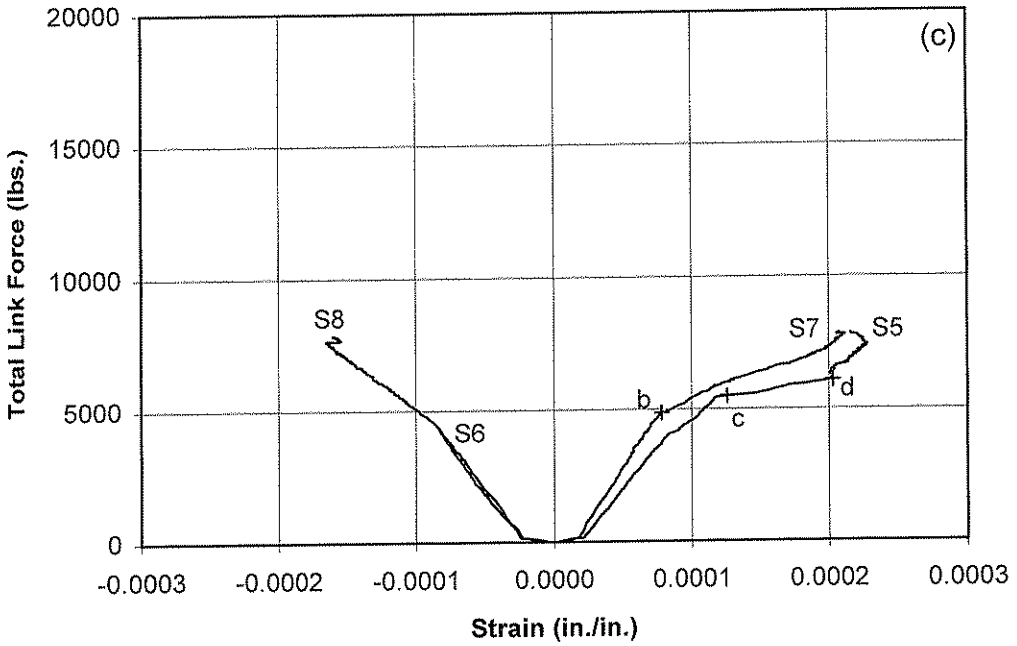


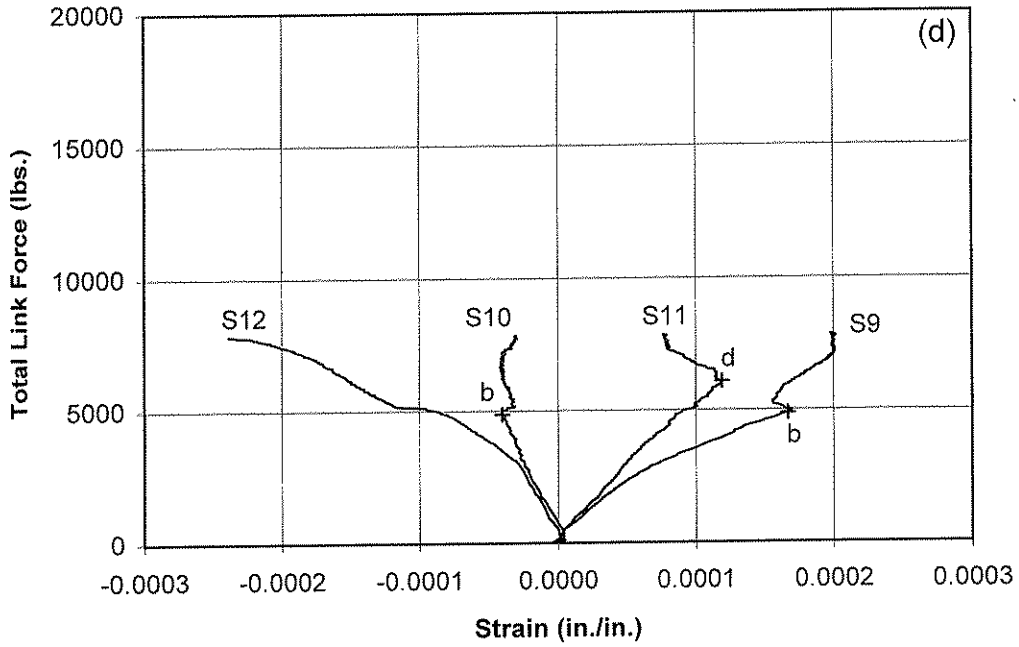


Figure 4.16 (c) total link force versus strain at Location II (gages S5 through S8);
(d) total link force versus strain at Location III (gages S9 through S12);

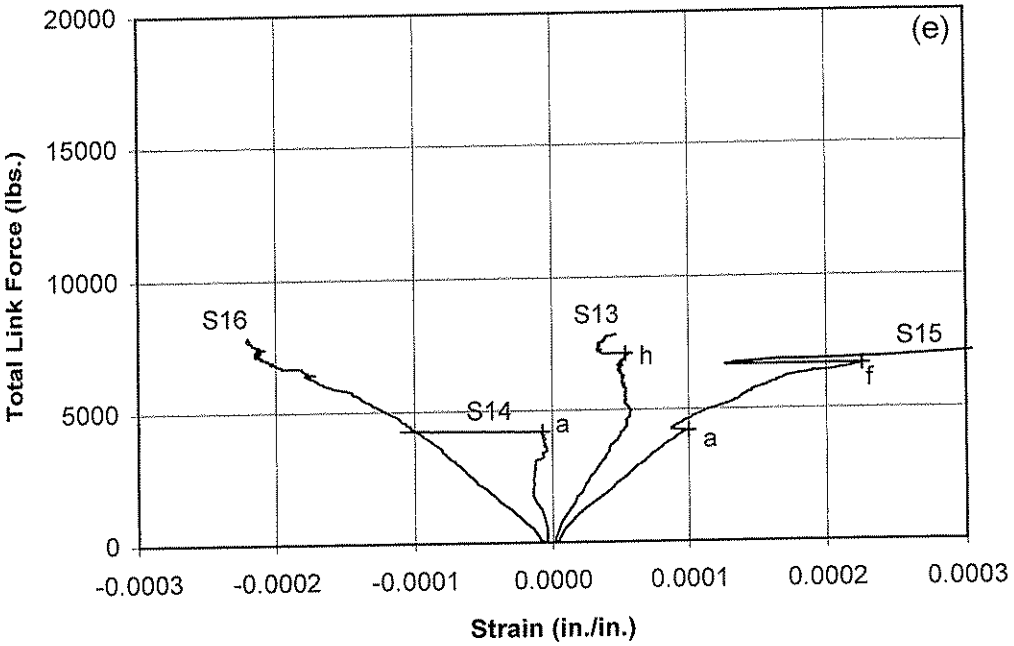


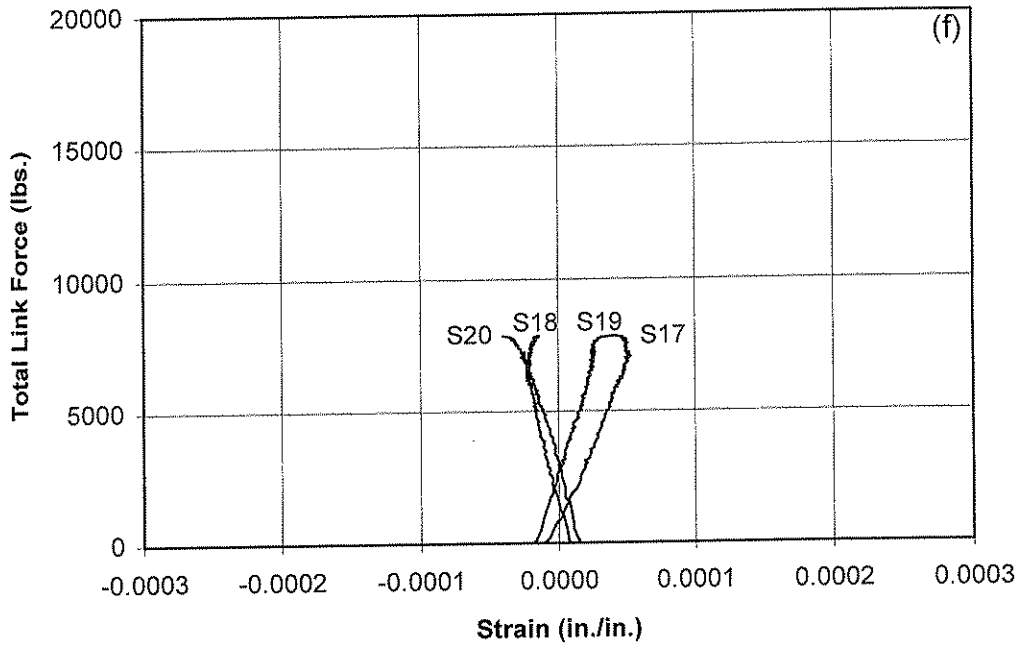


Figure 4.16 (e) total link force versus strain at Location IV (gages S13 through S16);
(f) total link force versus strain at Location V (gages S17 through S20);

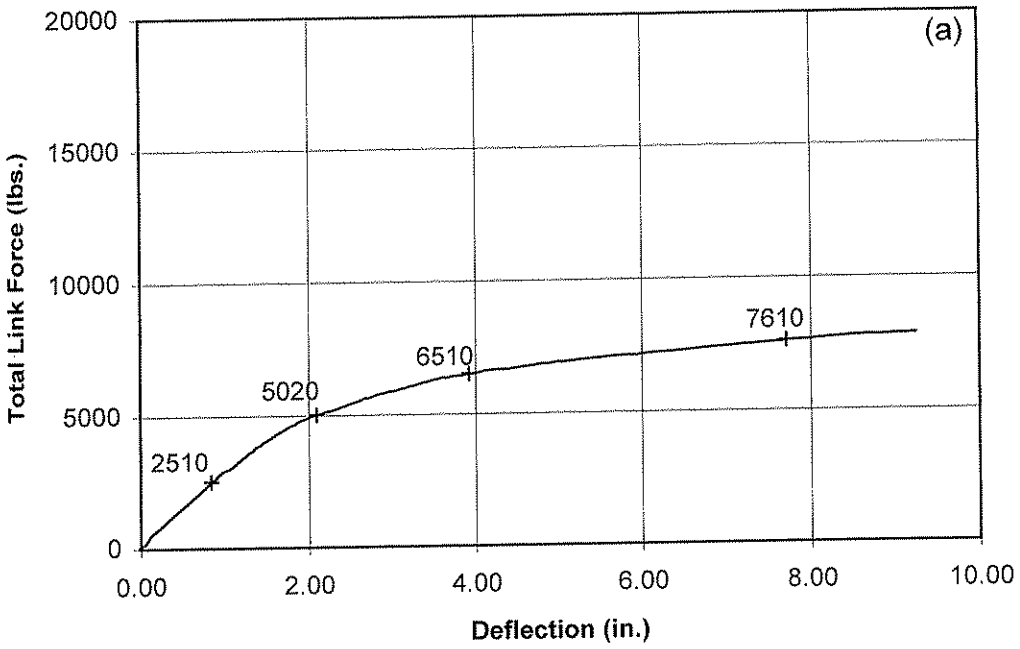


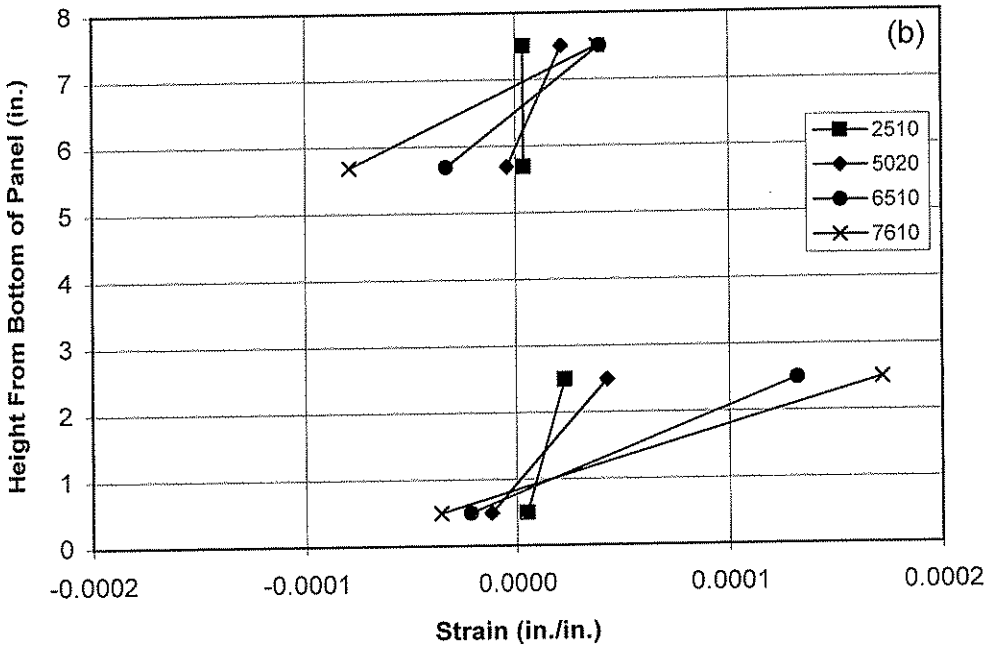


Figure 4.17 Strain distributions for Panel 2: (a) load-deflection plot showing points at which strain distributions are plotted; (b) strain distributions at Location I.

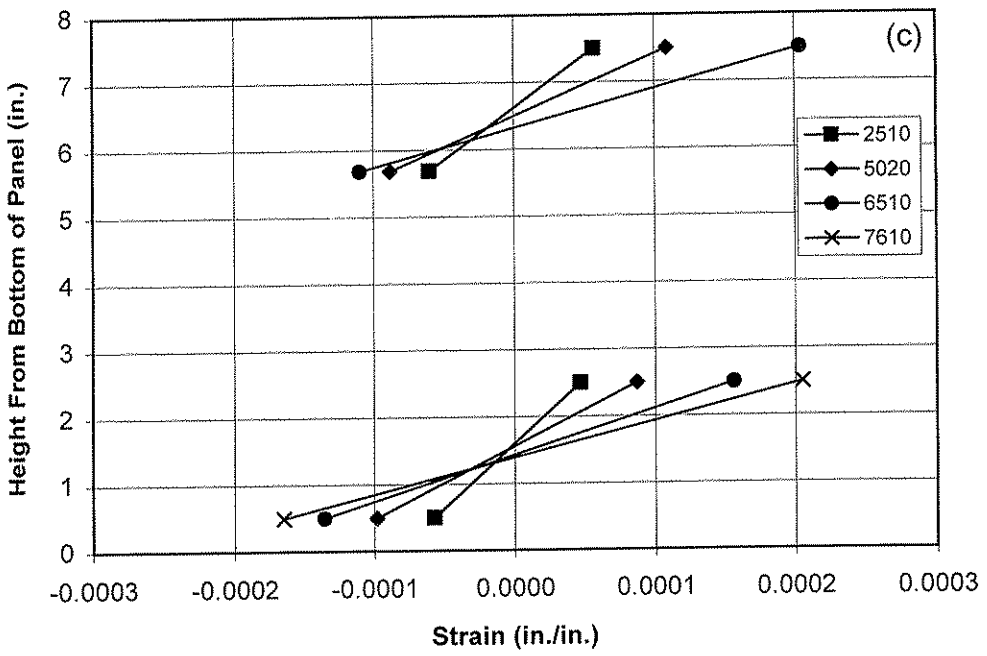


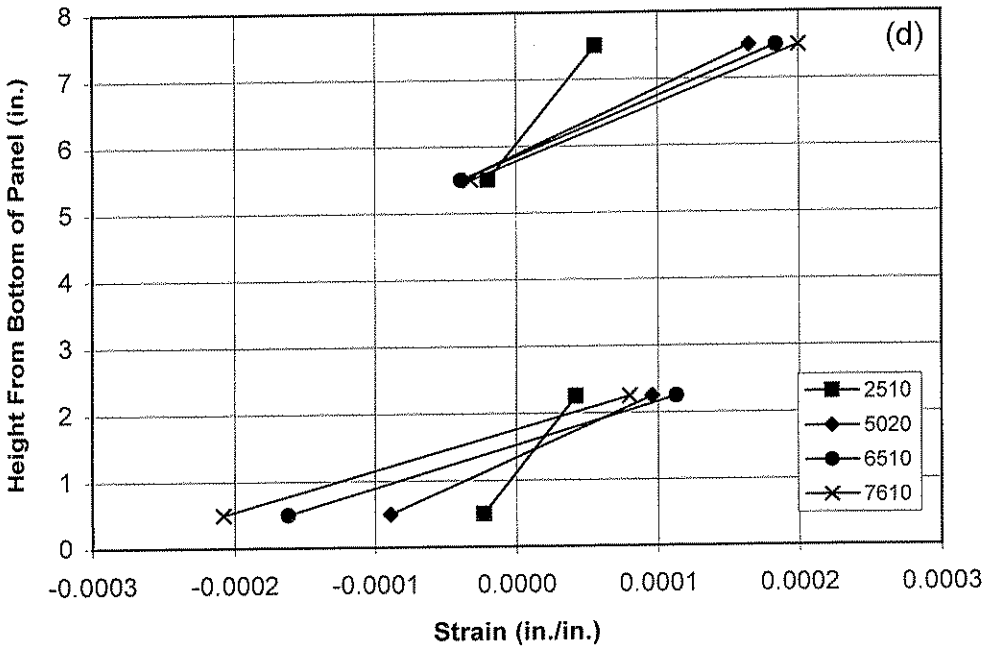


Figure 4.17 (c) strain distributions at Location II;
(d) strain distributions at Location III;

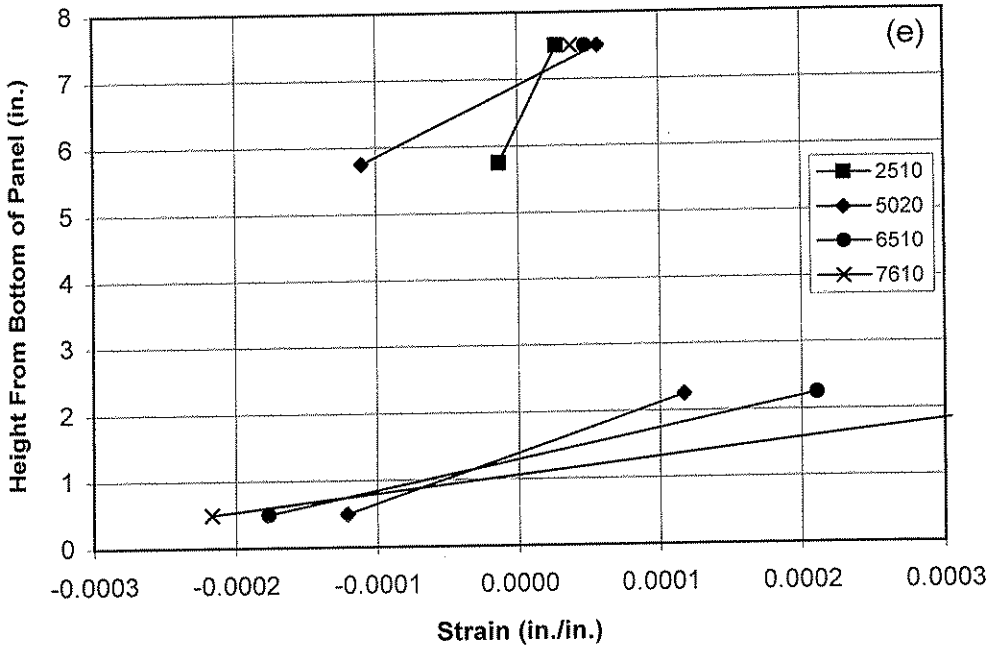


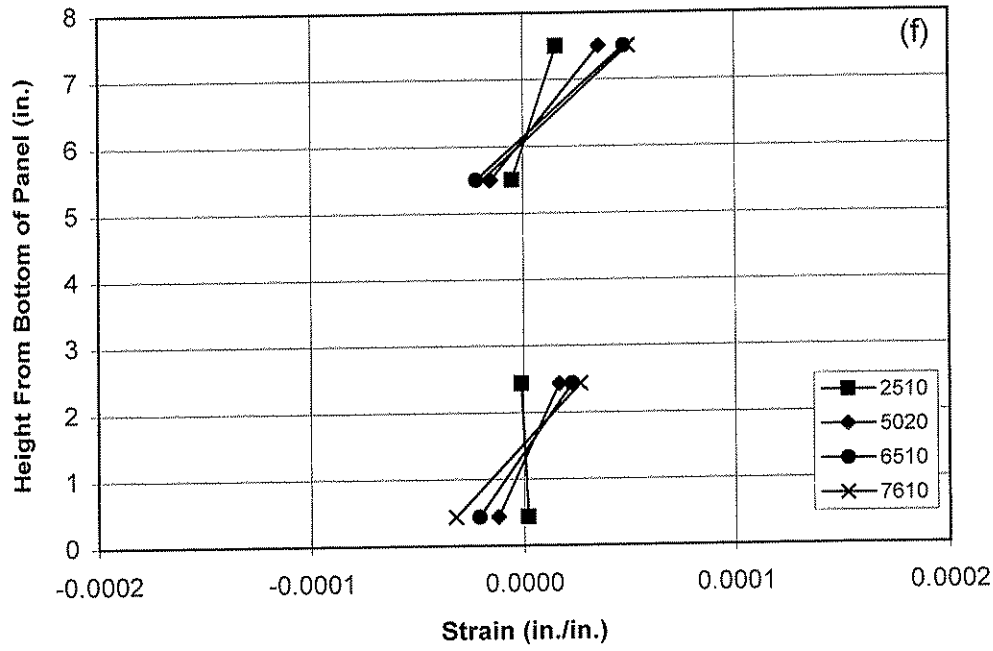


Figure 4.17 (e) strain distributions at Location IV;
(f) strain distributions at Location V;

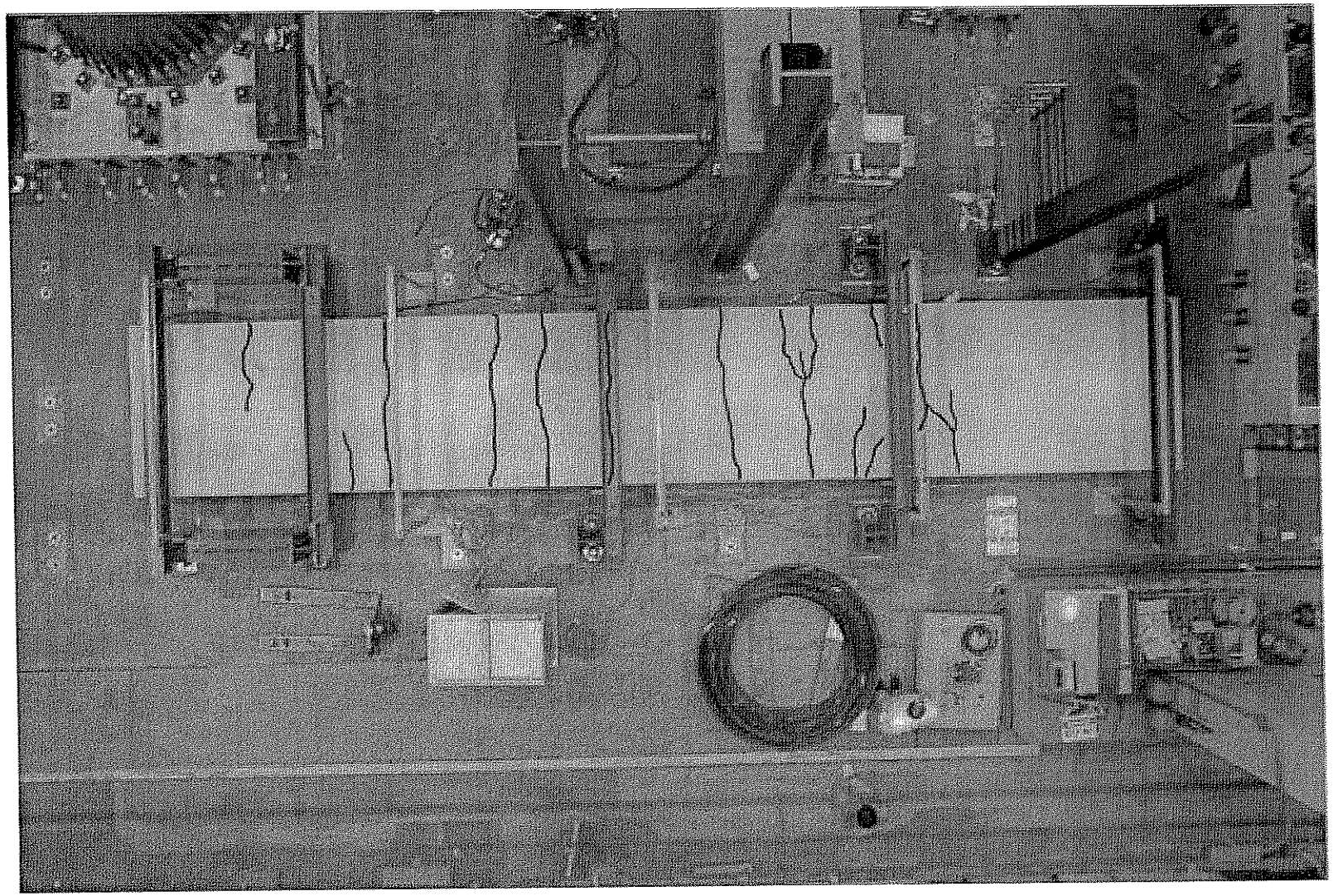

Figure 4.18 Post test photograph of Panel 2 showing crack locations.

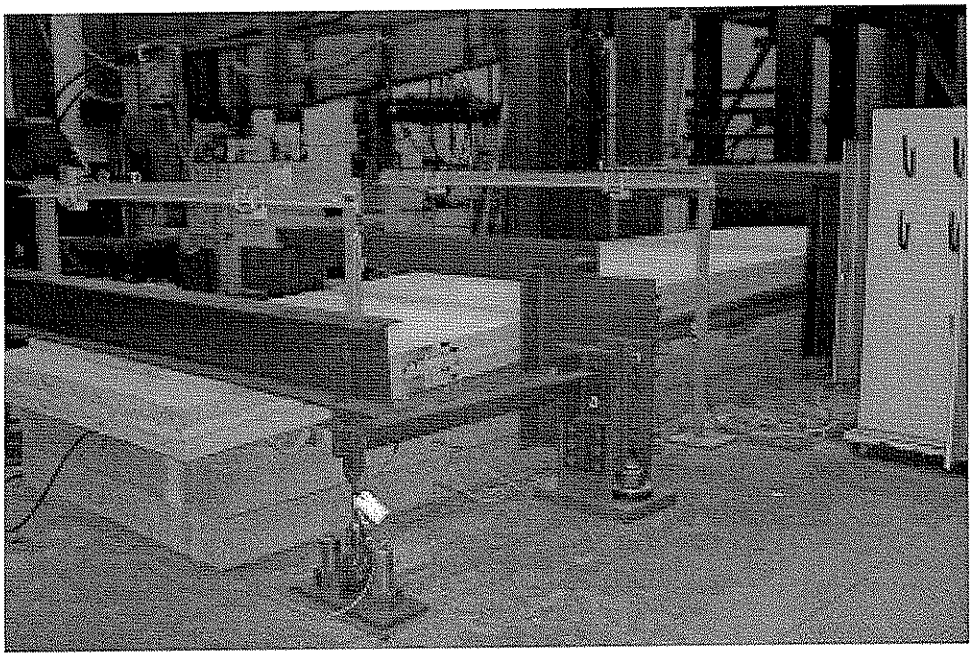

Figure 4.19 Deflected shape of Panel 2 at P=7220 lbs. and midspan deflection Δ=6.24 in.

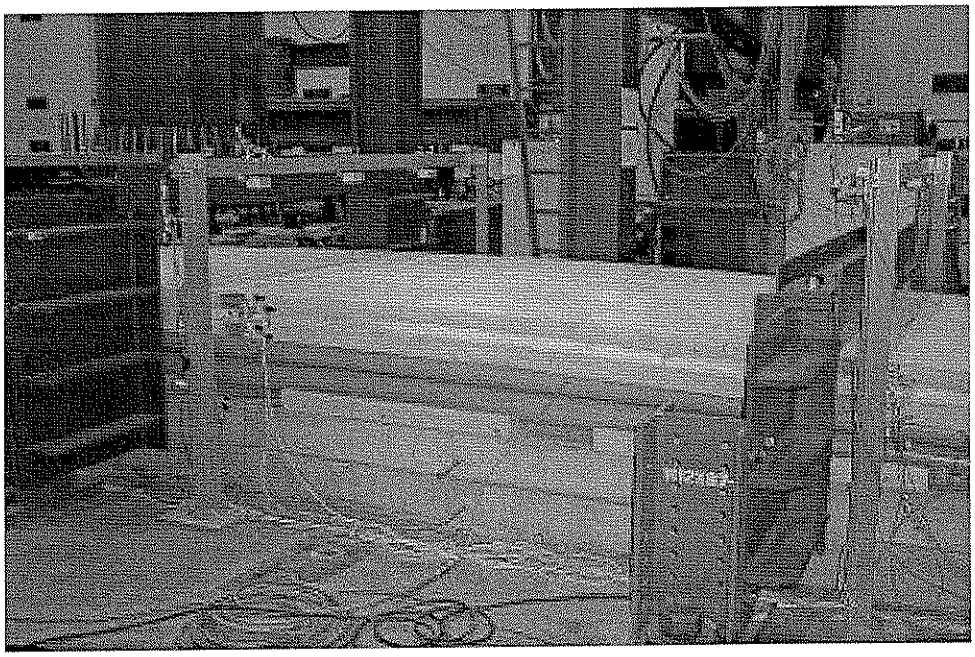

Figure 4.20 Deflected shape of Panel 2 at maximum load P=7850 lbs. and midspan deflection Δ=9.25 in.

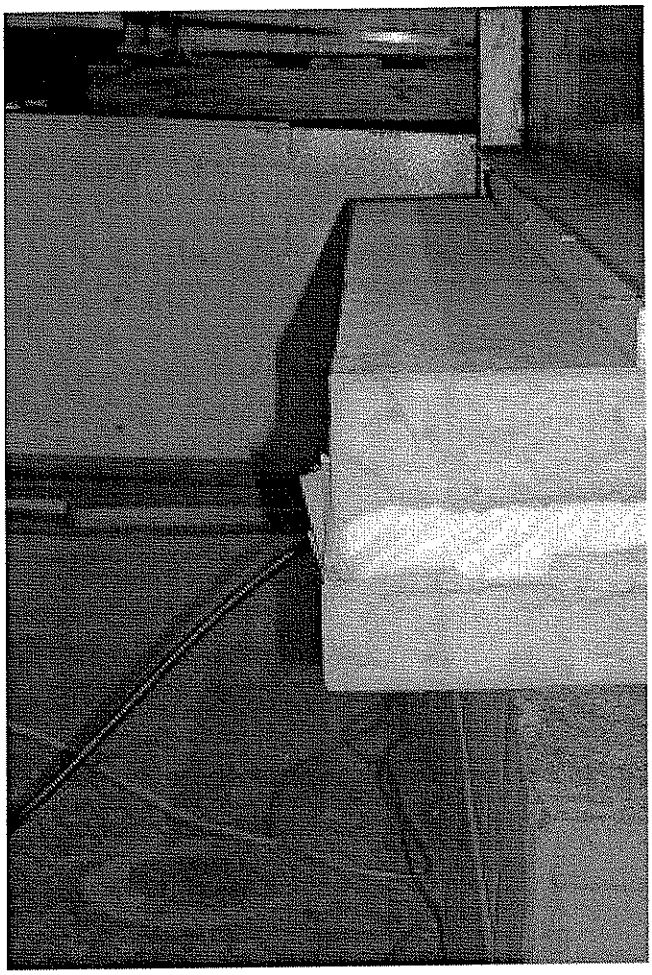

Figure 4.21 Relative displacement of wythes at the north end of Panel 2.

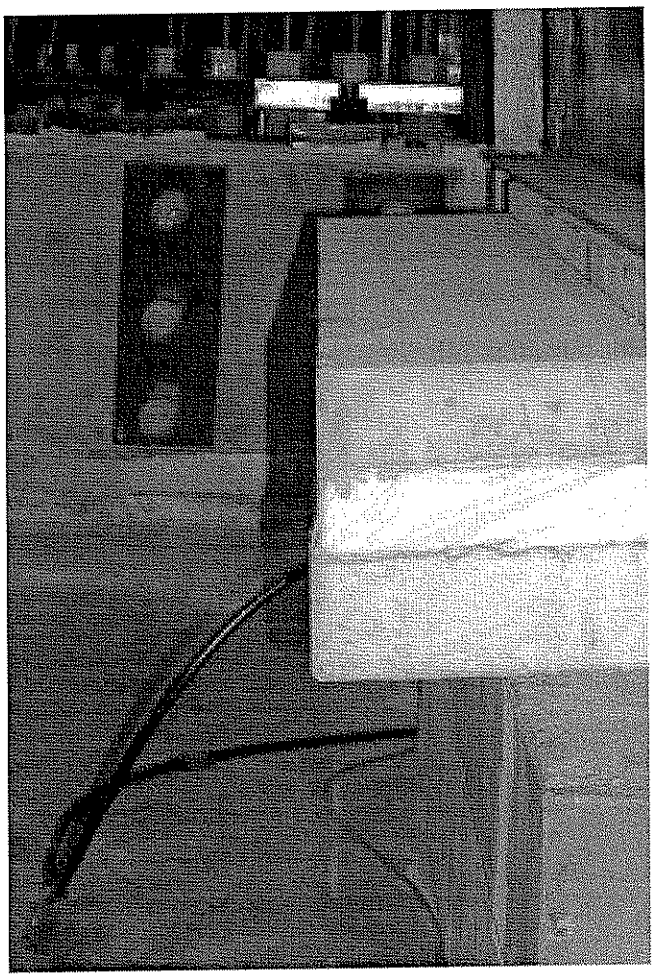

Figure 4.22 Relative displacement of wythes at the south end of Panel 2.

## 4.6 PANEL 3

The purpose of Panel 3 was to investigate the fraction of composite action provided by the solid concrete regions. This panel was made with a 1 ft. wide solid band of concrete at each end of the panel, and eight 1 ft. square solid regions spaced in pairs along the span of the panel. This panel contained no M-tie connectors and the bond between the concrete wythes and the insulation was destroyed using a plastic bond breaker. Therefore, the solid concrete regions provided the only intended mechanism of shear transfer.

The unconfined concrete compressive strength of the concrete of the face (compression) wythe was 8000 psi and the unconfined concrete compressive strength for back (tension) wythe was 4480 psi. The average unconfined compressive strength of the concrete in both wythes was 6240 psi.

The lateral load versus deflection plot is shown in Figure 4.23. In terms of deflection, the panel did not behave in a symmetric manner, with the values of deflection at x=0.75L being somewhat larger than those at x=0.25L throughout the test.

Figures 4.24 and 4.28 show the cracking behavior for Panel 3. The panel behaved in a linear elastic manner up to a load of P=7080 lbs. and a lateral deflection of $\Delta$=0.59 in. As shown in Figure 4.24, the first flexural crack was observed at this point. In general, the formation of each flexural crack was associated with a distinct drop in load in the load deflection plot. The panel shows a dramatic reduction in stiffness upon formation of the third flexural crack, at a load of P=10140 lbs. and a lateral deflection of $\Delta$=1.36 in. Deflection increases much more rapidly for a given increase in load beyond this point. The panel was loaded up to a maximum load of P=16090 lbs. and a lateral deflection of $\Delta$=8.99 in. The test was terminated at this point and the panel was unloaded. Figures 4.29 and 4.30 show the deflected shape of Panel 3 at two different stages in the loading. Flexural failure of the test panel, by crushing of the concrete in the compression zone, was not reached.

Ten flexural cracks were observed in the tension wythe of the panel. Figure 4.31 depicts some typical flexural cracks that were observed during testing. All cracks propagated across the full width of the panel, except for cracks 6 and 7, which joined together with crack 2. Figure 4.32 shows a detail of cracks 2, 6, and 7, which formed around a 1 ft. square solid concrete region. Several cracks formed along the edges of the 1 ft. square solid concrete regions.

Figure 4.25 shows results of the measurements of relative displacements between wythes for Panel 3. Small values of relative displacements were observed for this panel throughout the test. However, at a load of P=7080 lbs. (point A), the values of relative displacement for instruments RD2 and RD4 began to increase more rapidly with increasing load. At a load of P=11400 lbs. (point C), the value of relative displacement for instrument RD4, makes a short, sharp increase before becoming relatively constant for the rest of the test. At a load of P=13600 lbs. (point D), the values of relative displacement for instruments RD2 and RD3 increase sharply. At the peak load of P=16090 lbs., instrument RD2 recorded a relative displacement of –0.153 in. and

instrument RD3 recorded a relative displacement of –0.058 in. Therefore, the larger relative displacements occurred near midspan.

Figure 4.26 shows the results of the strain measurements for Panel 3.

Figure 4.26 (b) shows the load-strain data at Location I. Values of strain in gages S1 and S4 increased linearly up to a load of P=9060 lbs. (point d), after which the strains remain relatively constant with increasing load, up to point i. Values of strain in gages in S2 and S3 changed little with increasing load. At a load of P=13600 lbs. (point i), strains in gages S1, S2, and S4 increase abruptly in compression.

Figure 4.26 (c) shows the load-strain data at Location II. Values of strain in gages S5 and S8 increased linearly up to a load of P=8490 lbs. (point c). Values of strain in gages in S6 and S7 changed little with increasing load.

Figure 4.26 (d) shows the load-strain data at Location III. Values of strain only increased linearly in gage S12. At a load of P=7080 lbs. (point b), which corresponds with the first flexural crack, all gages experienced a rapid increase or decrease in strain with little change in load. Similarly, at a load of P=10140 lbs. (point e), which corresponds with the third flexural crack, all gages experienced a rapid increase or decrease in strain with little change in load.

Figure 4.26 (e) shows the load-strain data at Location IV. Values of strain in gage S16 increased linearly up to a load of approximately 7000 lbs. Values of strain in gage S13 increased in a relatively linear manner up to a load of P=6050 lbs. (point a), after which the strain began to decrease. All gages experienced rapid increases or decreases in strain at a load of P=10140 lbs. (point e), which corresponds to the third flexural crack.

Figure 4.26 (f) shows the load-strain data at Location V. Values of strain in gage S17 increased linearly up to a load of approximately 10000 lbs. and values of strain in gage S20 increased linearly up to a load of approximately 11000 lbs. At a load of P=12710 lbs. (point h), values of strain in gage S20 begin to decrease in tension, and then remain relatively constant with increasing load. Values of strain in gages S18 and S19 remain relatively constant up to a load of approximately 11000 lbs., after which the strains increase slightly in tension and compression respectively. The maximum values of strain in measured tension and compression were 0.00011 in./in. (gage S17) and –0.00005 in./in. (gage S20).

Figure 4.27 shows plots of the strain distributions at Locations I through V for Panel 3. At all locations, the strain distributions do not seem to indicate plane section behavior throughout the entire depth of the panel. The strain distributions are discussed further in Section 5.6.

| Load (lbs.) | Deflection (in.) | Event | | |
|---|---|---|---|---|
| | | Crack | Relative Displacement | Strain |
| 6050 | 0.49 | | | a |
| 7080 | 0.59 | 1 | A | b |
| 8490 | 0.93 | | | c |
| 9060 | 1.05 | | | d |
| 10000 | 1.28 | 2 | | |
| 10140 | 1.36 | 3 | B | e |
| 9650 | 1.49 | 4 | | |
| 11400 | 2.55 | | C | f |
| 11850 | 2.88 | | | g |
| 12710 | 3.43 | | | h |
| 13600 | 4.13 | 5 | D | i |
| 12960 | 4.30 | 6 | | |
| 13410 | 4.84 | 7 | | |
| 14030 | 5.36 | 8 | | |
| 14300 | 6.50 | 9 | | |
| 14510 | 6.82 | 10 | | |

Table 4.3 Sequence of key events for Panel 3.

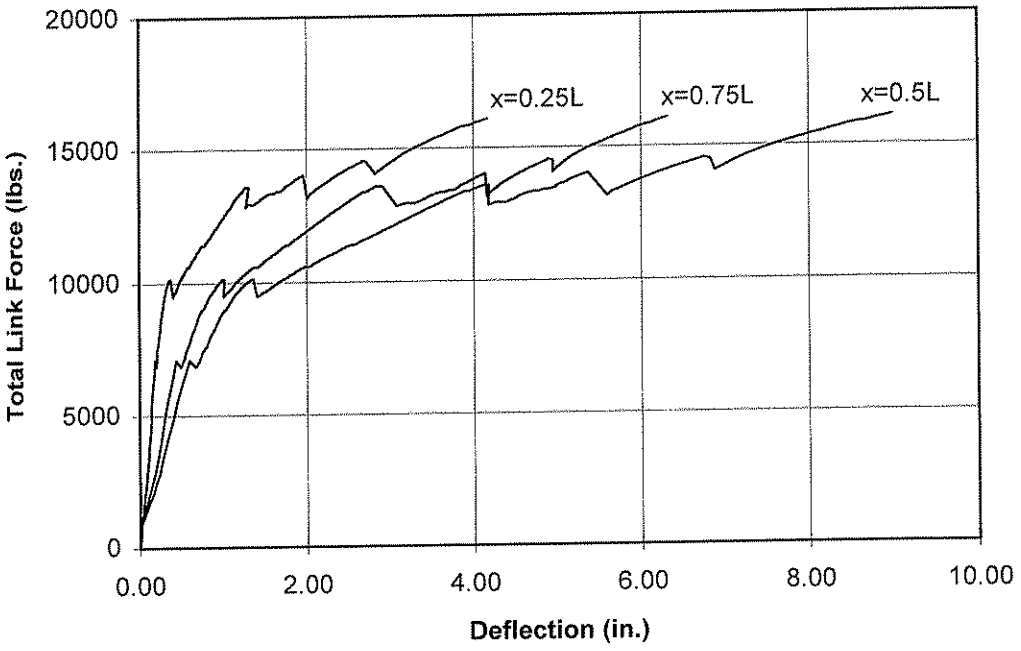


Figure 4.23 Plot of lateral load versus lateral deflection for Panel 3.

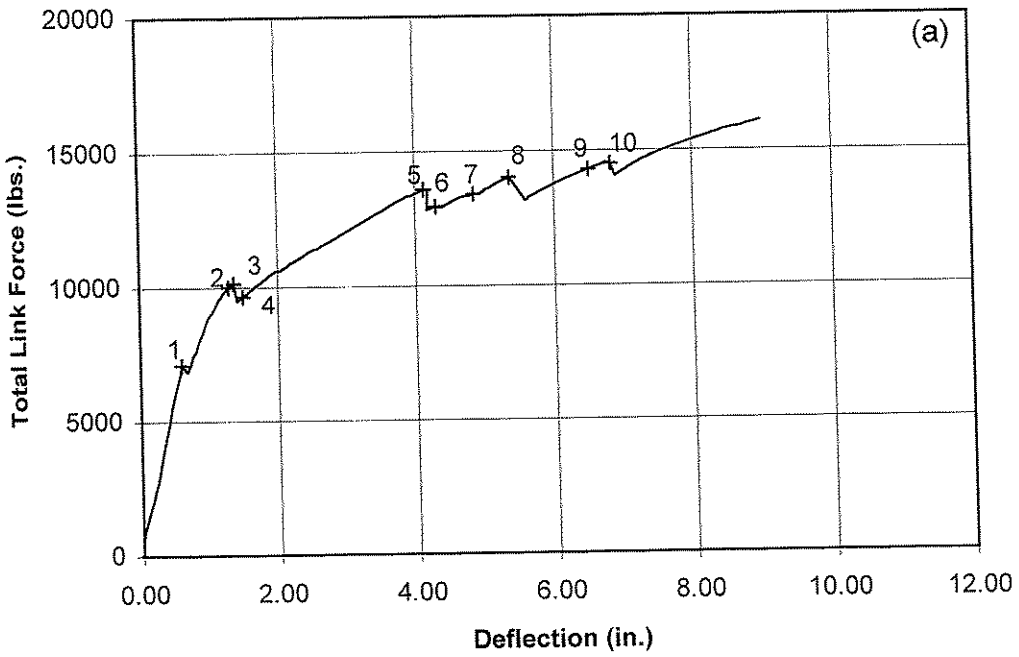


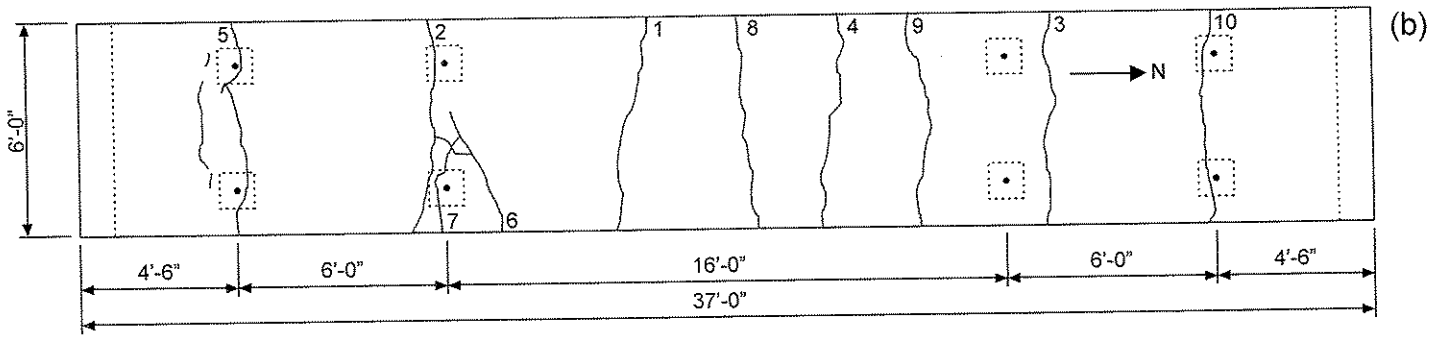


Figure 4.24 Cracking behavior of Panel 3: (a) key points on load-deflection plot; and (b) plan view of Panel 3 showing crack locations.

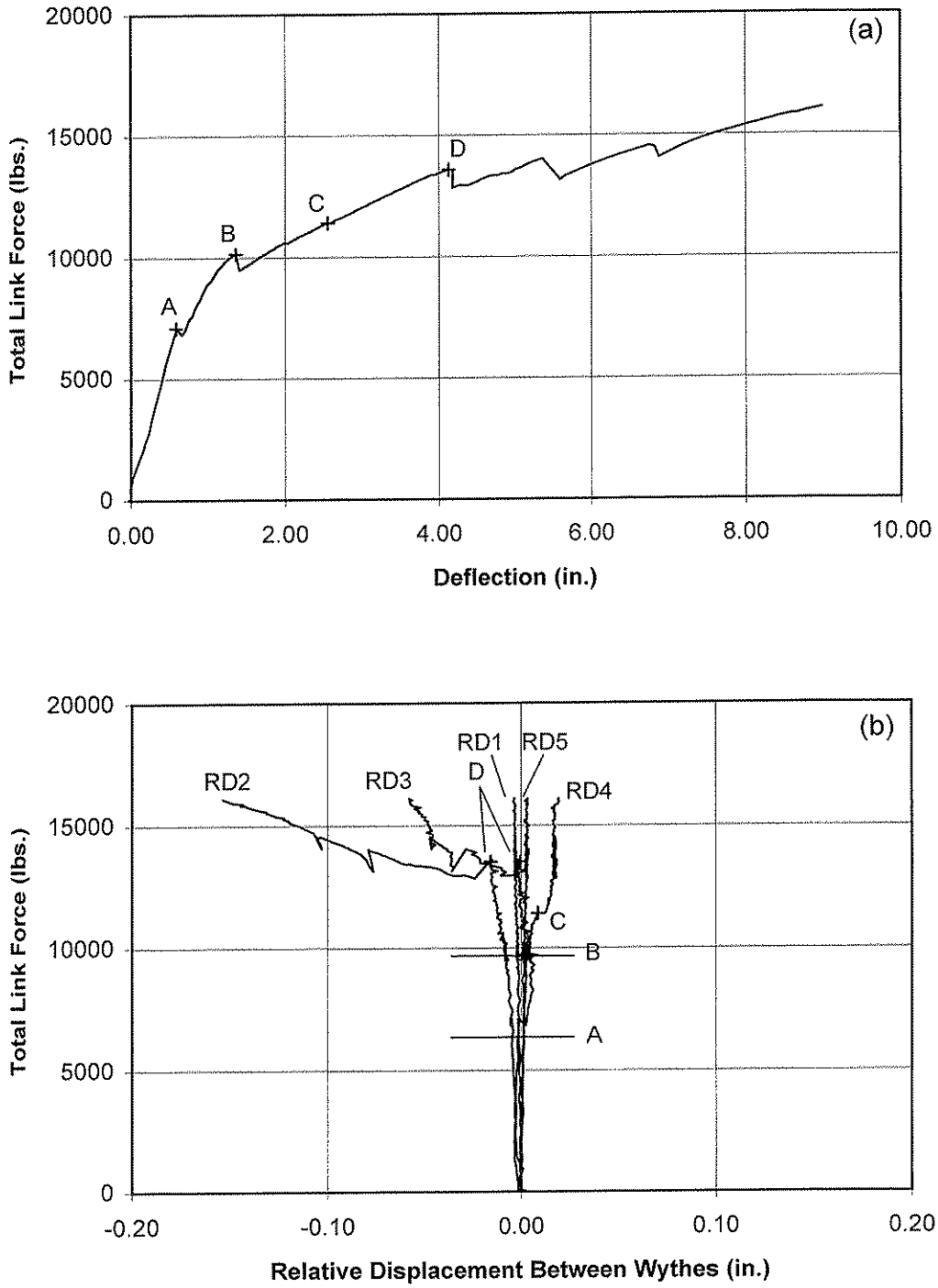


Figure 4.25 Relative displacement between wythes for Panel 3: (a) key points on load-deflection plot; and (b) total link force versus relative displacement between wythes.

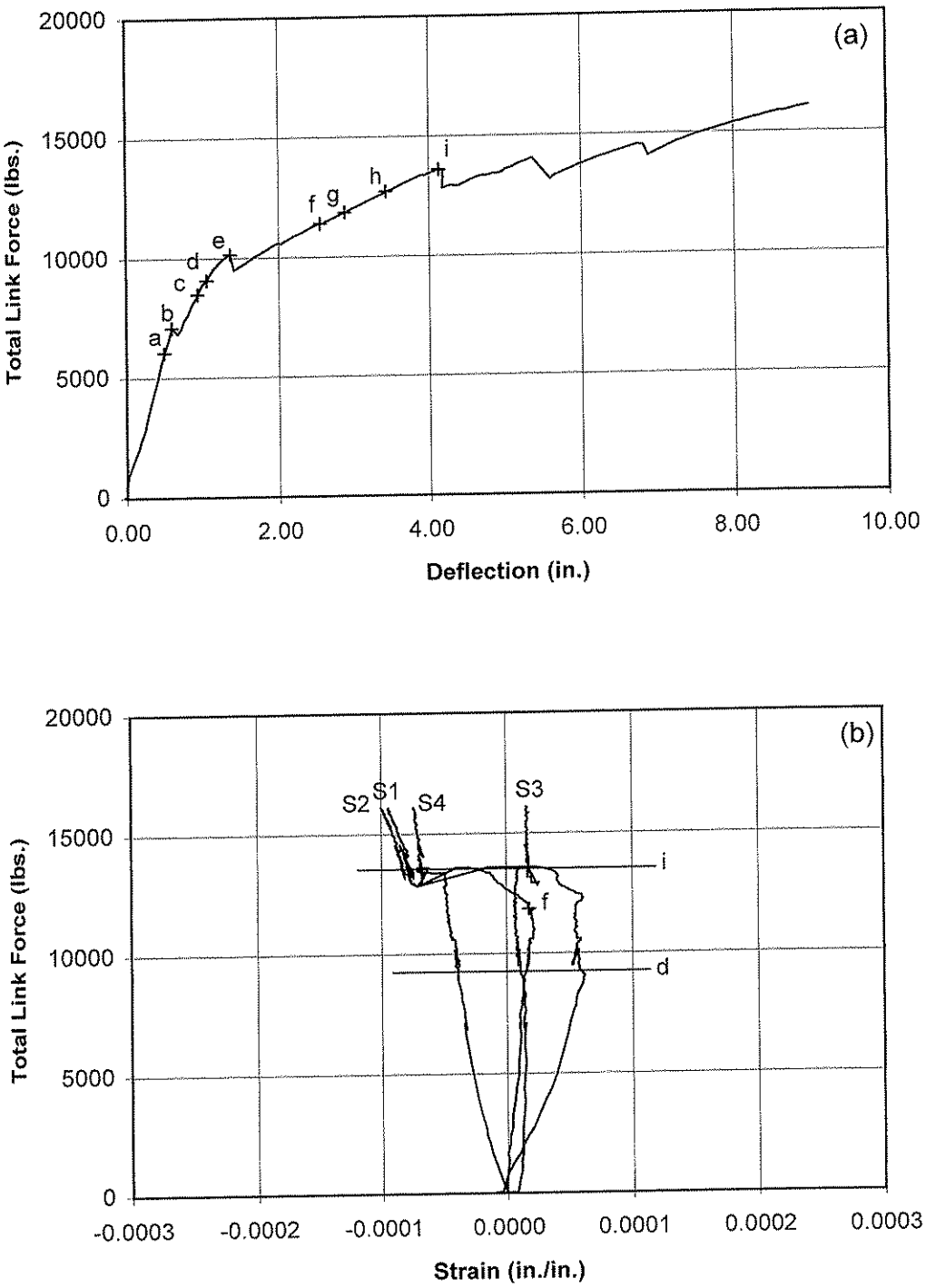


Figure 4.26 Strain measurement results for Panel 3: (a) key points on load-deflection plot; (b) total link force versus strain at Location I (gages S1 through S4).

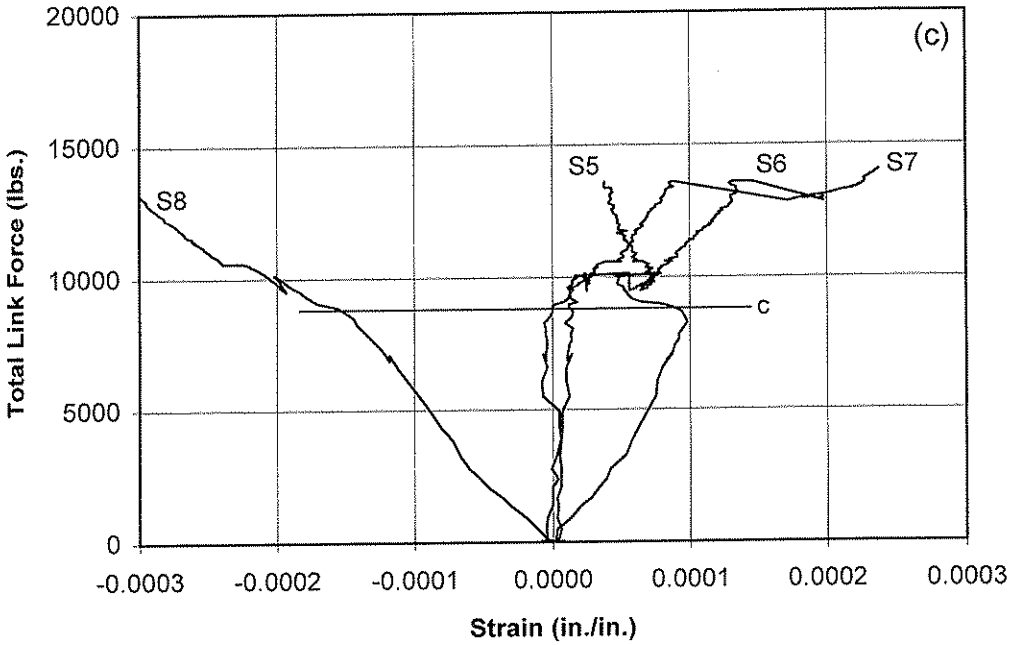


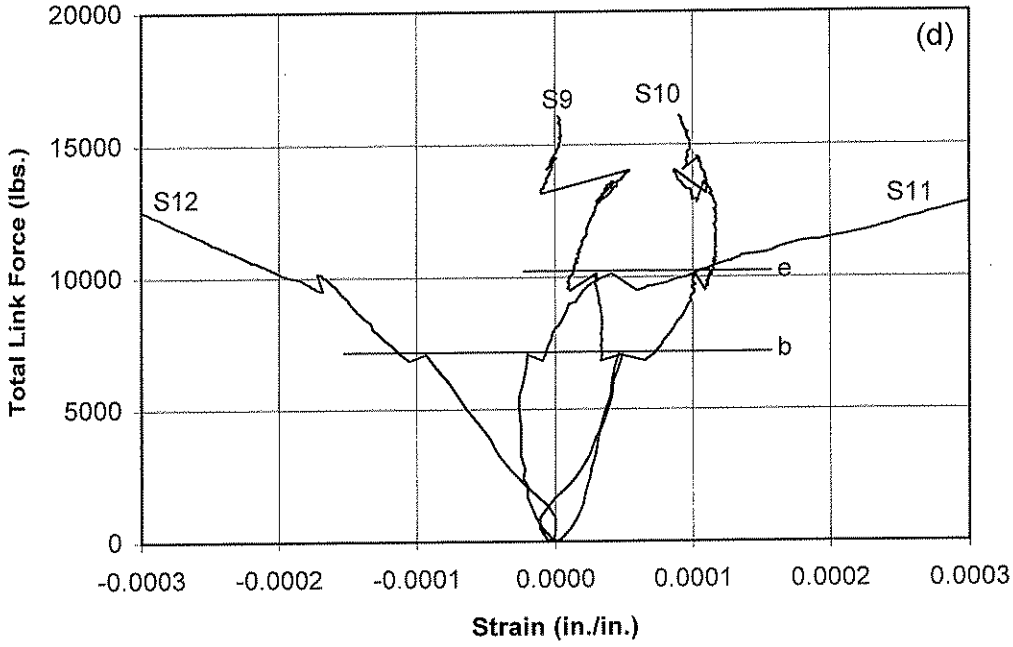


Figure 4.26 (c) total link force versus strain at Location II (gages S5 through S8);
(d) total link force versus strain at Location III (gages S9 through S12);

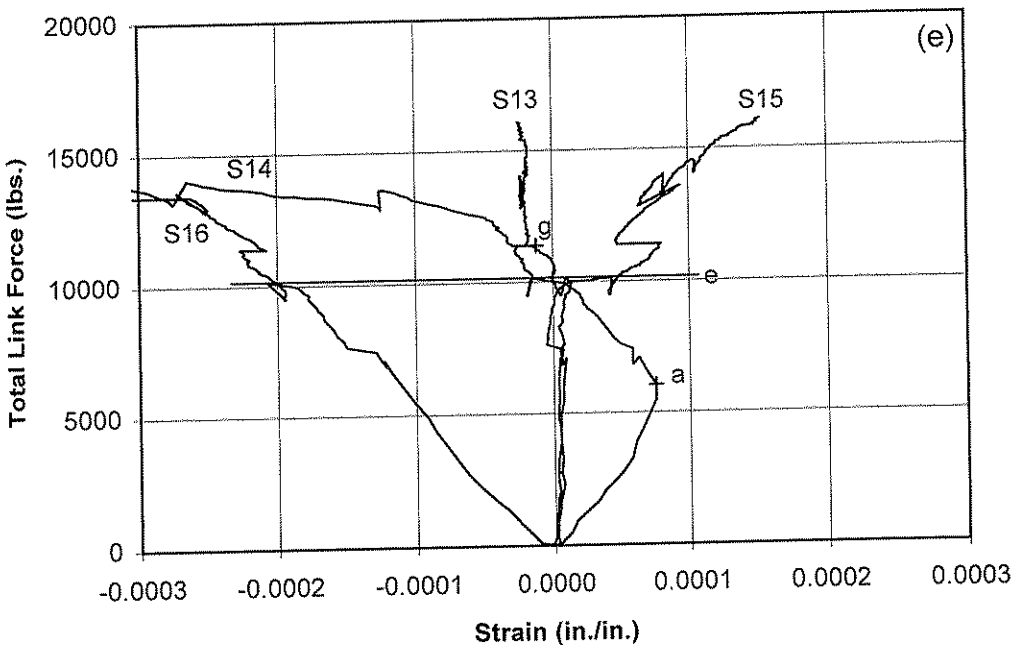


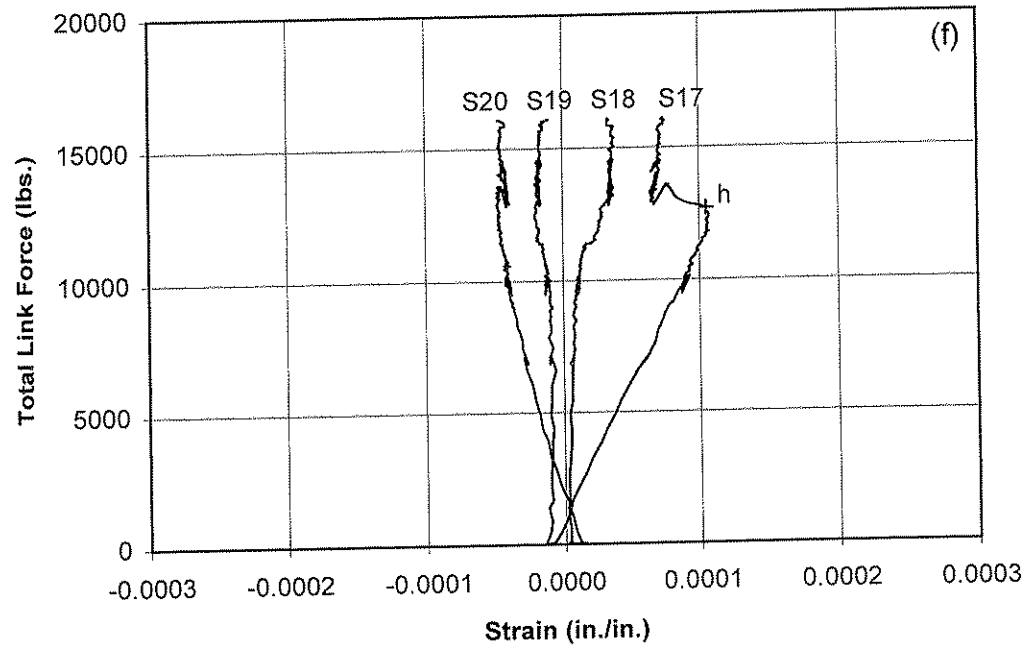


Figure 4.26 (e) total link force versus strain at Location IV (gages S13 through S16); (f) total link force versus strain at Location V (gages S17 through S20);

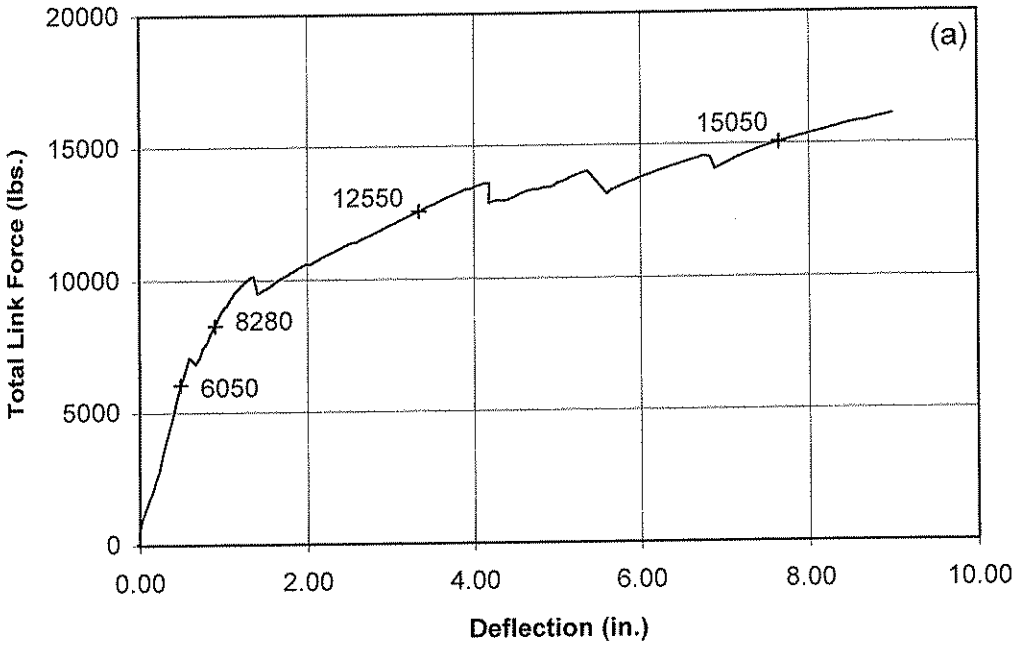


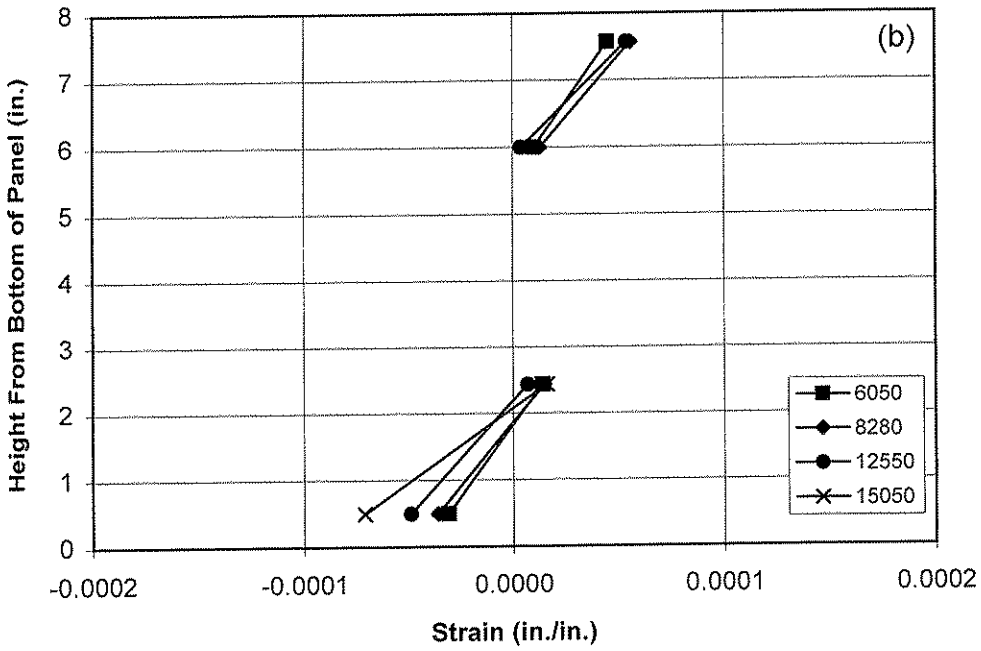


Figure 4.27 Strain distributions for Panel 3: (a) load-deflection plot showing points at which strain distributions are plotted; (b) strain distributions at Location I.

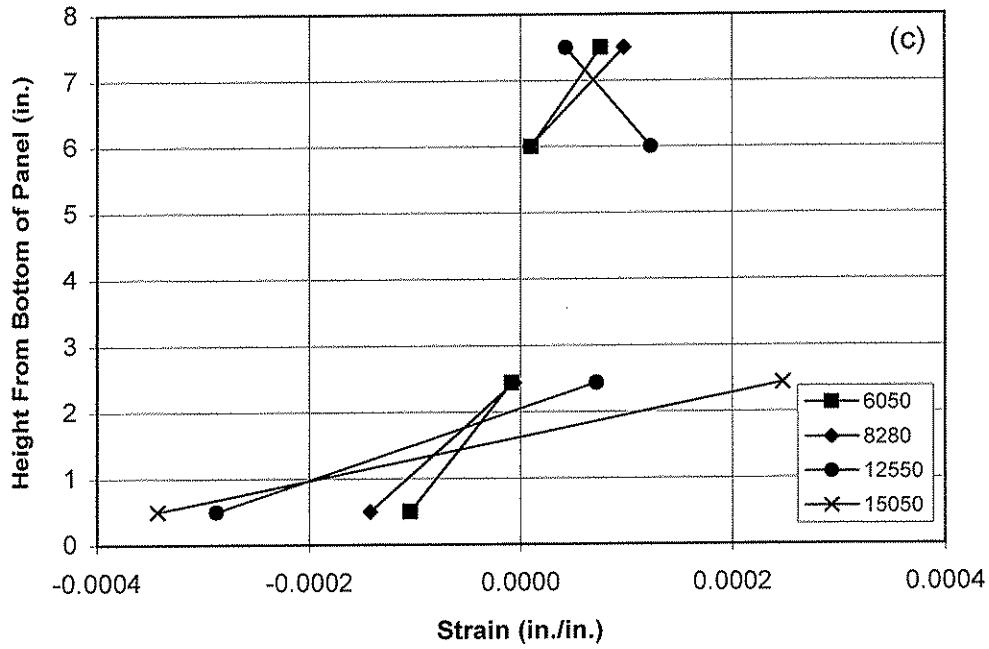


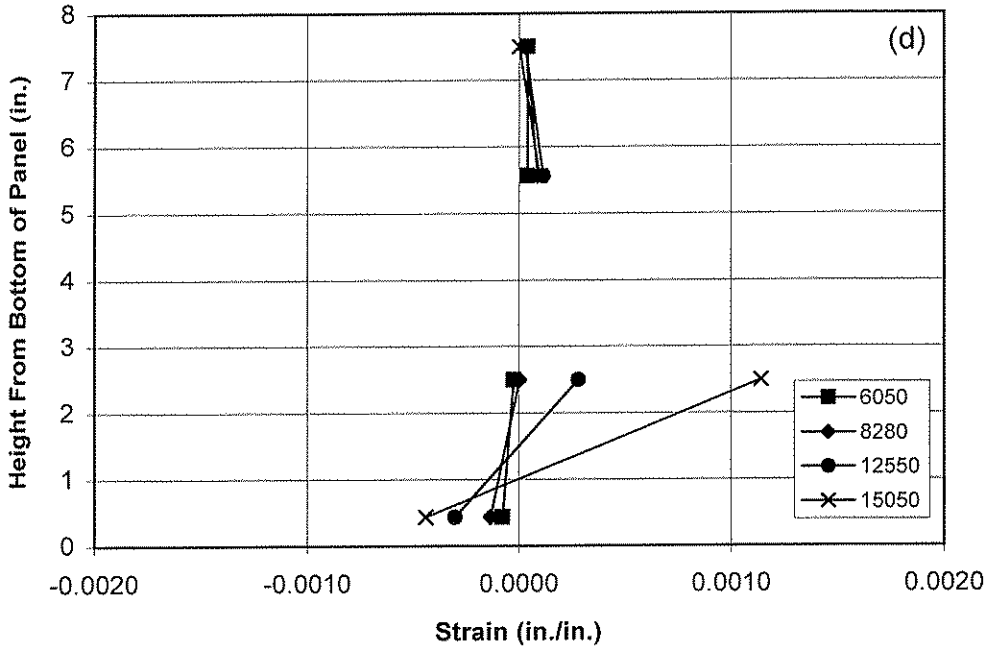


Figure 4.27 (c) strain distributions at Location II;
(d) strain distributions at Location III;

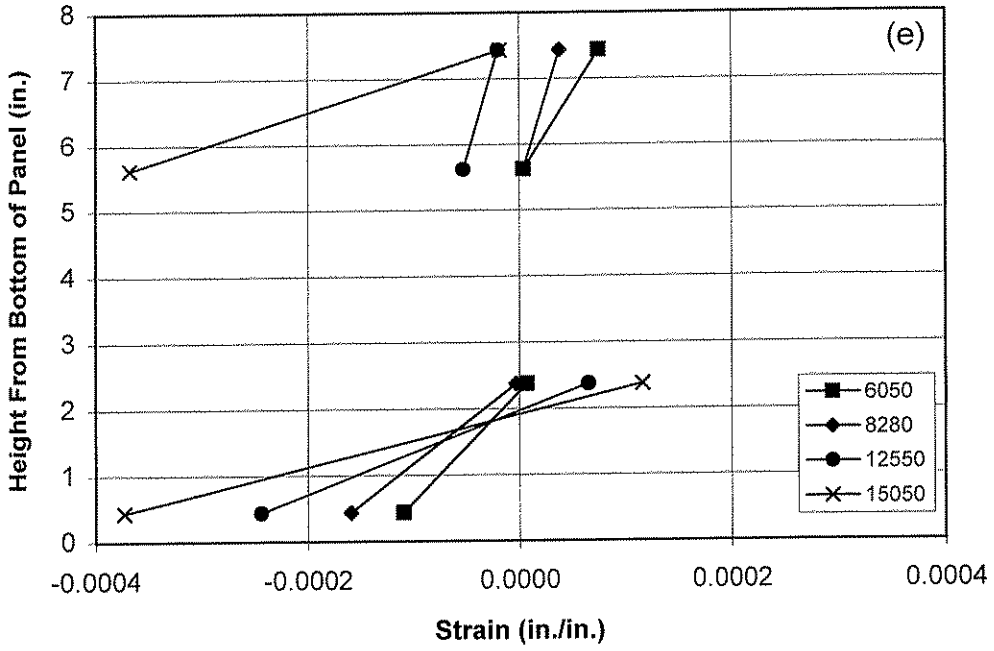


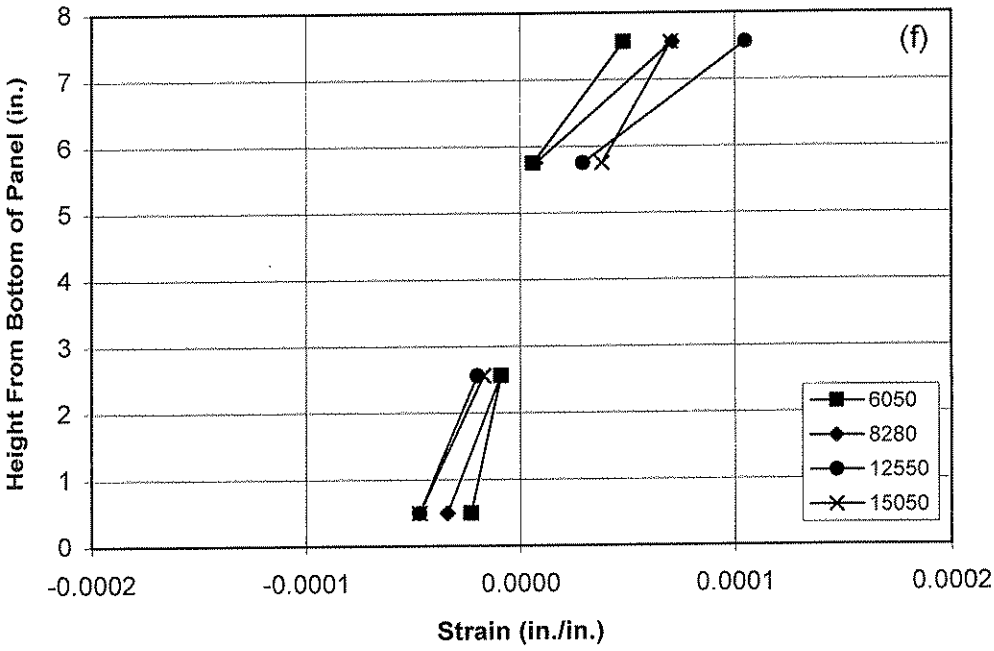


Figure 4.27 (e) strain distributions at Location IV;
(f) strain distributions at Location V;

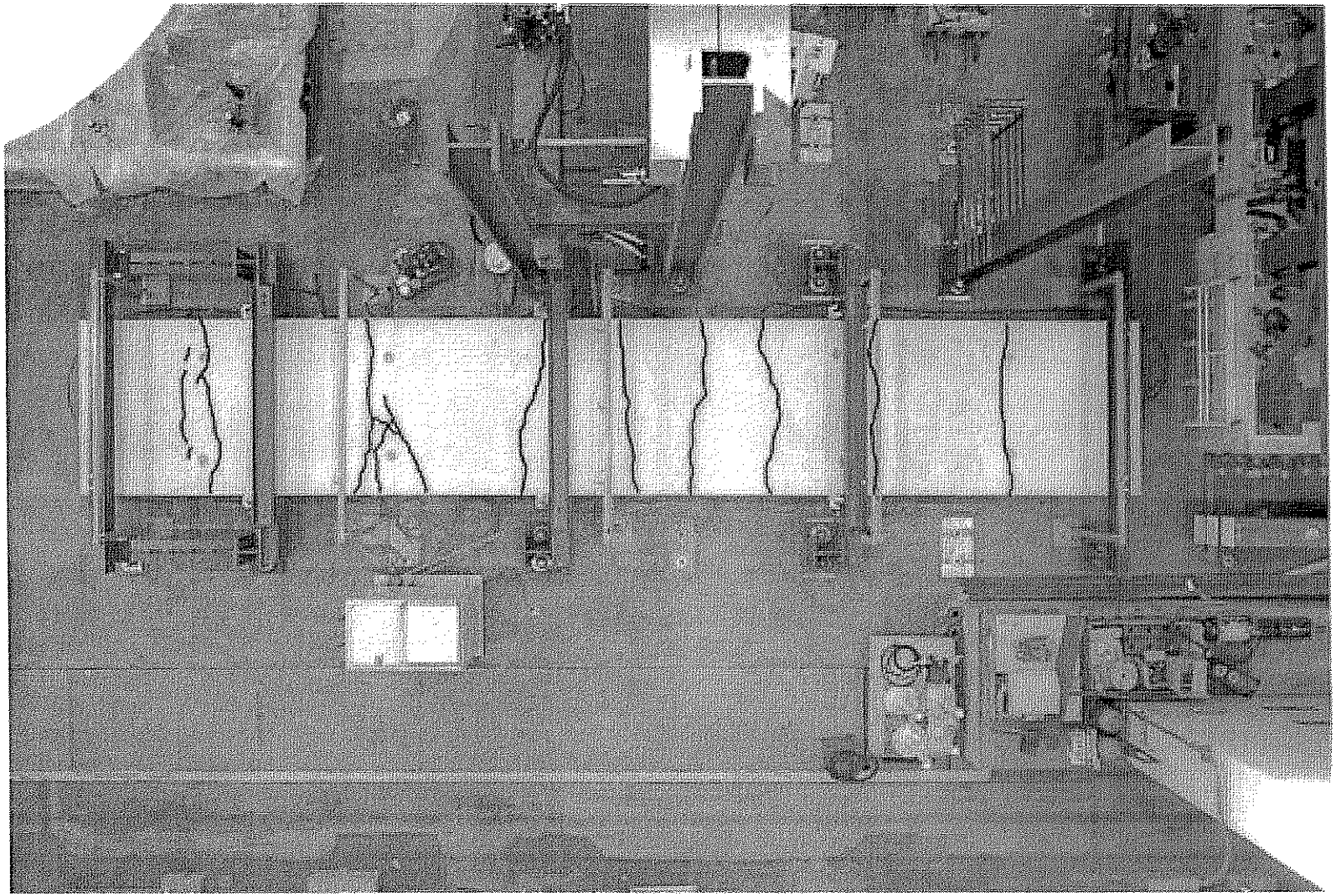

Figure 4.28 Post test photograph of Panel 3 showing crack locations.

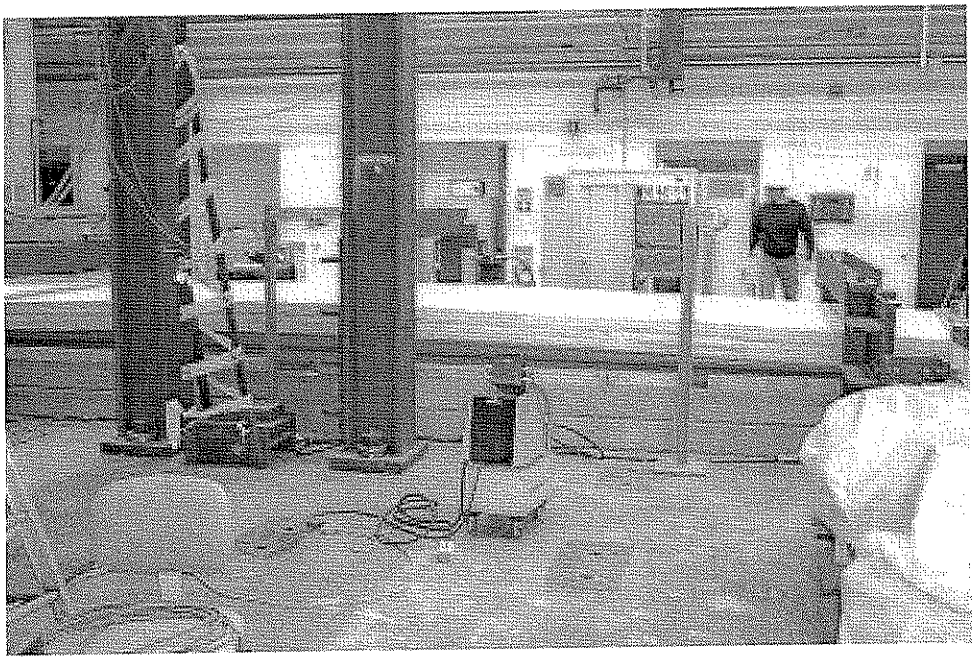

Figure 4.29 Deflected shape of Panel 3 at P=14040 lbs. and midspan deflection Δ=6.24 in.

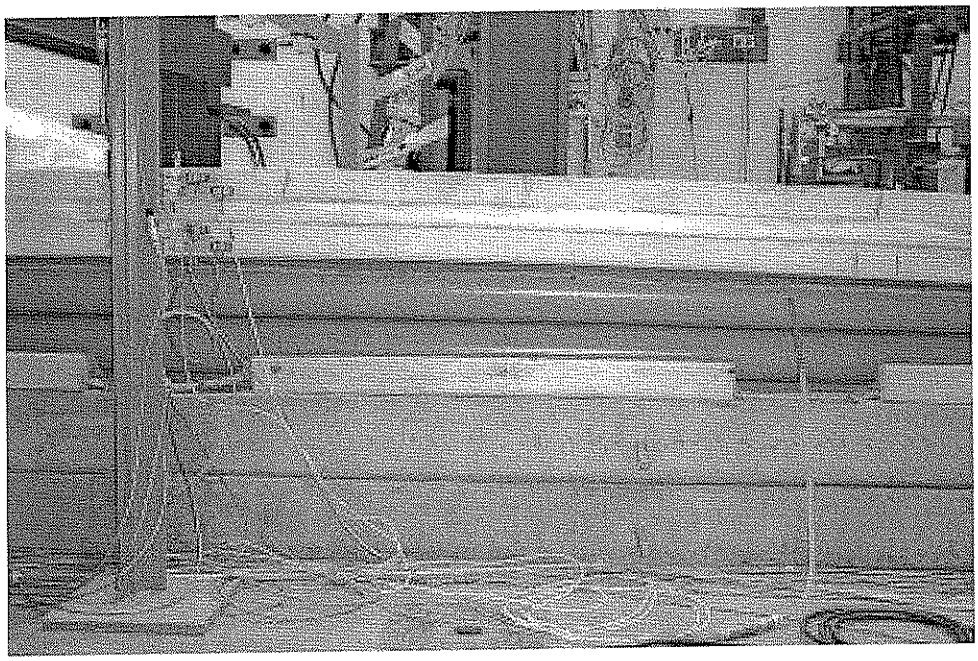

Figure 4.30 Deflected shape of Panel 3 at maximum load P=16090 lbs. and midspan deflection Δ=8.99 in.

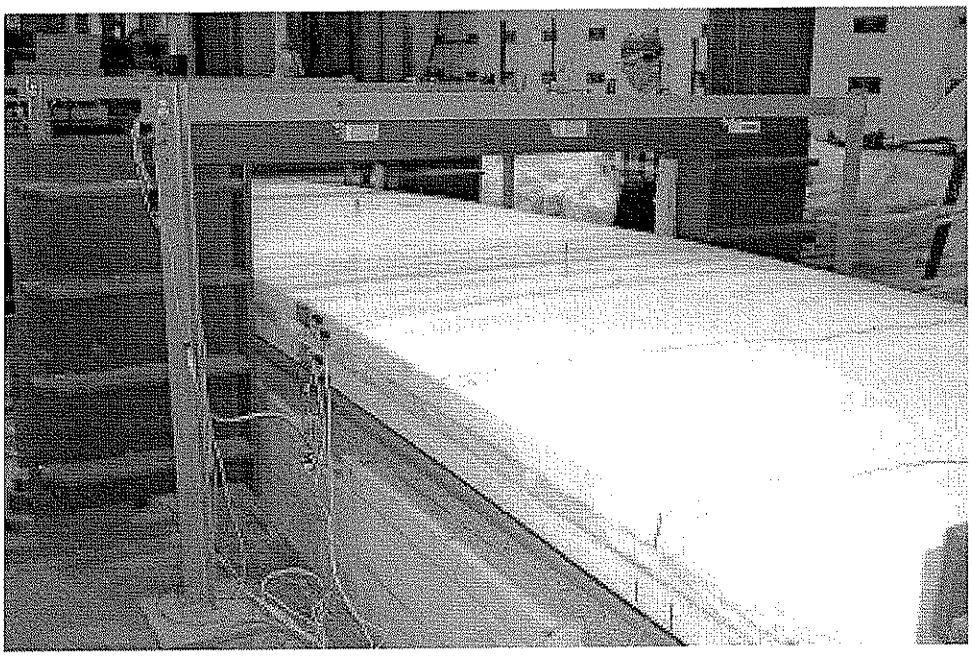

Figure 4.31 Flexural cracks in the tension wythe of Panel 3.

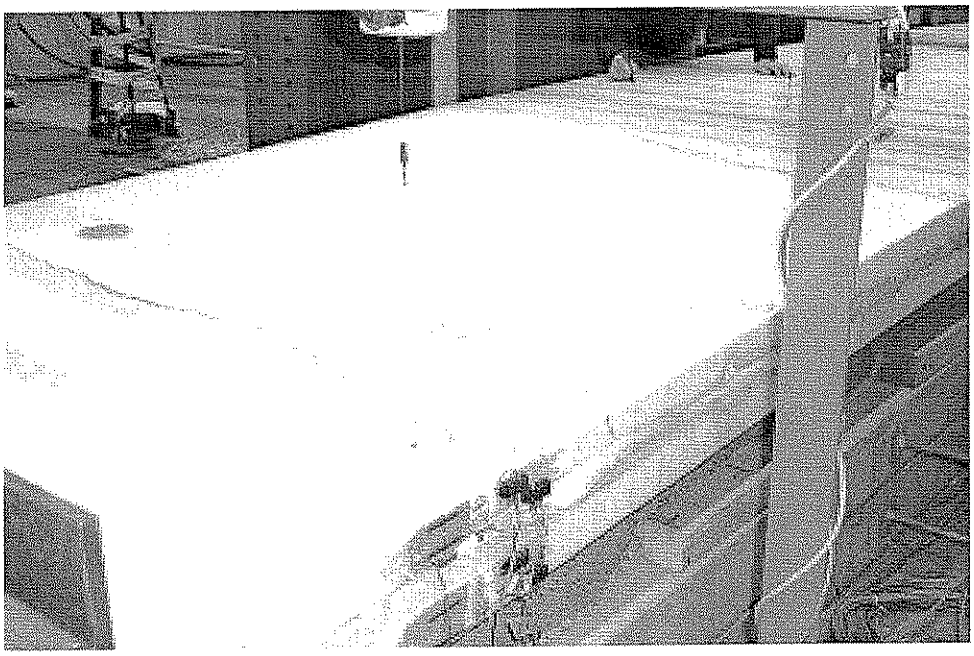

Figure 4.32 Cracks 2, 6, and 7, which formed around a 1 ft. square solid concrete region.

## 4.7 PANEL 4

The purpose of Panel 4 was to investigate the fraction of composite action provided by the bond between the concrete wythes and the insulation. This panel contained no M-ties or solid concrete regions, and no attempt was made to disrupt the bond between the concrete wythes and the insulation. Therefore, bond provided the only intended mechanism of shear transfer.

The unconfined concrete compressive strength of the concrete of the face (compression) wythe was 7480 psi and the unconfined concrete compressive strength for back (tension) wythe was 6510 psi. The average unconfined compressive strength of the concrete in both wythes was 7000 psi.

The lateral load versus deflection plot is shown in Figure 4.33. In terms of deflection, the panel did not behave in a symmetric manner, with the values of deflection at x=0.75L being somewhat larger than those at x=0.25L throughout the test.

Figures 4.34 and 4.38 show the cracking behavior of Panel 4. The panel behaved in a linear elastic manner up to a load of P=820 lbs. and a lateral deflection of $\Delta$=0.33 in. As shown in Figure 4.34, the first flexural crack was observed at this point. In general, the formation of each flexural crack was not associated with a distinct drop in load in the load deflection plot. Instead the panel exhibited a continual degradation of flexural stiffness. After the first flexural crack formed, there was a gradual decrease in flexural stiffness of the panel throughout the rest of the test. The panel was loaded up to a maximum load of P=6160 lbs. and a lateral deflection of $\Delta$=9.39 in. The test was terminated at this point and the panel was unloaded. Figure 4.39 shows the deflected shape of Panel 4. Flexural failure of the test panel, by crushing of the concrete in the compression zone, was not reached.

Four flexural cracks were observed in the tension wythe of the panel. All cracks propagated across the full width of the panel.

Figure 4.35 shows the results of the measurements of relative displacements between wythes for Panel 4. Large values of relative displacements were observed for this panel. At a load of P=4050 lbs. (point B), the values of relative displacement for instruments RD1 and RD2 began to increase more rapidly with increasing load. At the peak load of P=6160 lbs., instrument RD1 recorded a relative displacement of –0.488 in. and instrument RD5 recorded a relative displacement of 0.076 in. Therefore, the larger relative displacements occurred at the south end of the panel. Figure 4.40 depicts the relative displacement between wythes at the south end of the panel.

Figures 4.36 shows the results of the strain measurements for Panel 4.

Figure 4.36 (b) shows the load-strain data at Location I. Values of strain in gages S1, S3, and S4 increased linearly. The values of strain in gage S2 increased relatively linearly until a load of P=2400 lbs (point a), where the strain decreased in compression slightly at before continuing to increase. At a load of P=4530 lbs. (point d), the values of strain in gage S3 increased rapidly in

tension with little increase in load. Similarly, at a load of P=4930 lbs. (point f), the values of strain in gage S2 increased rapidly in compression with little increase in load. The maximum values of strain measured in tension and compression at Location I were 0.00012 in./in. (gage S3) and -0.000131 in./in. (gage S2).

Figure 4.36 (c) shows the load-strain data at Location II. Early in the loading, values of strains in all gages increased slowly. Values of strain in gages S5, S7, and S8 increased relatively linearly until a load of approximately 4500 lbs. At a load of P=4500 lbs., strains in gages S5 and S6 decreased before continuing to increase. The maximum values of strain in measured tension and compression were 0.00024 in./in. (gage S5) and –0.00019 in./in. (gage S8).

Figure 4.36 (d) shows the load-strain data at Location III. Early in the loading, gages S9 and S11 recorded strains in compression. At a load of approximately 500 lbs., strains in gages S9 and S11 began to increase linearly in tension. Similarly, gages S10 and S12 initially recorded strains in tension, before beginning to increase linearly in compression. At a load of P=2400 lbs. (point a), the values of strain in gages S9 and S10 decreased in tension and compression, respectively. The maximum values of strain in measured tension and compression were 0.00016 in./in. (gage S11) and –0.00025 in./in. (gage S12).

Figure 4.36 (e) shows the load-strain data at Location IV. Values of strain in gages S13, S14, and S15 increased linearly up to a load of approximately 3000 lbs. At a load of P=3640 lbs. (point b), strain in gage S13 stopped increasing and began to remain constant with increasing load. At a load of P=4650 lbs. (point e), the strain in gage S13 decreased rapidly with little increase in load, before continuing to remain relatively constant for the rest of the loading. The maximum values of strain in measured tension and compression were 0.00008 in./in. (gage S15) and –0.00007 in./in. (gage S14).

Figure 4.36 (f) shows the load-strain data at Location V. In general, values of strain in all gages increased linearly throughout the entire test. The maximum values of strain in measured tension and compression were 0.00007 in./in. (gage S19) and –0.00005 in./in. (gage S20).

Figure 4.37 shows plots of the strain distributions at Locations I through V for Panel 4. At all locations, the strain distributions do not seem to indicate plane section behavior throughout the entire depth of the panel. The strain distributions are discussed further in Section 5.6.

| Load (lbs.) | Deflection (in.) | Event | | |
|---|---|---|---|---|
| | | Crack | Relative Displacement | Strain |
| 820 | 0.33 | 1 | A | |
| 2400 | 1.16 | | | a |
| 3640 | 2.17 | | | b |
| 4050 | 2.61 | 2 | B | |
| 4500 | 3.25 | | | c |
| 4530 | 3.57 | | | d |
| 4650 | 3.89 | | | e |
| 4930 | 4.79 | | | f |
| 5000 | 5.01 | 3 | | |
| 4950 | 5.58 | 4 | | |

Table 4.4 Sequence of key events for Panel 4.

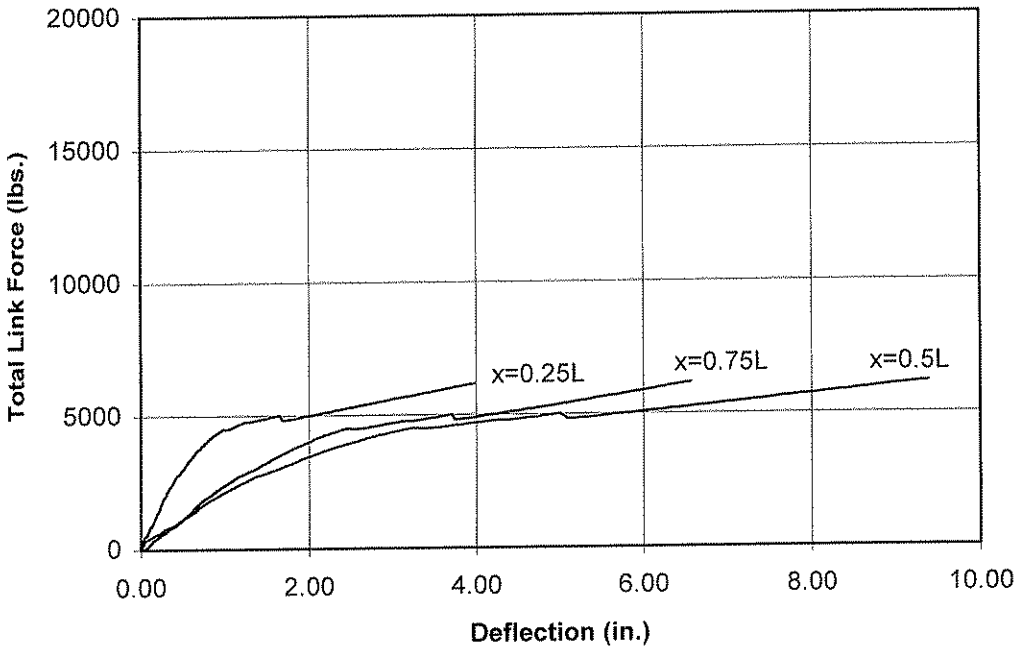


Figure 4.33 Plot of lateral load versus lateral deflection for Panel 4.

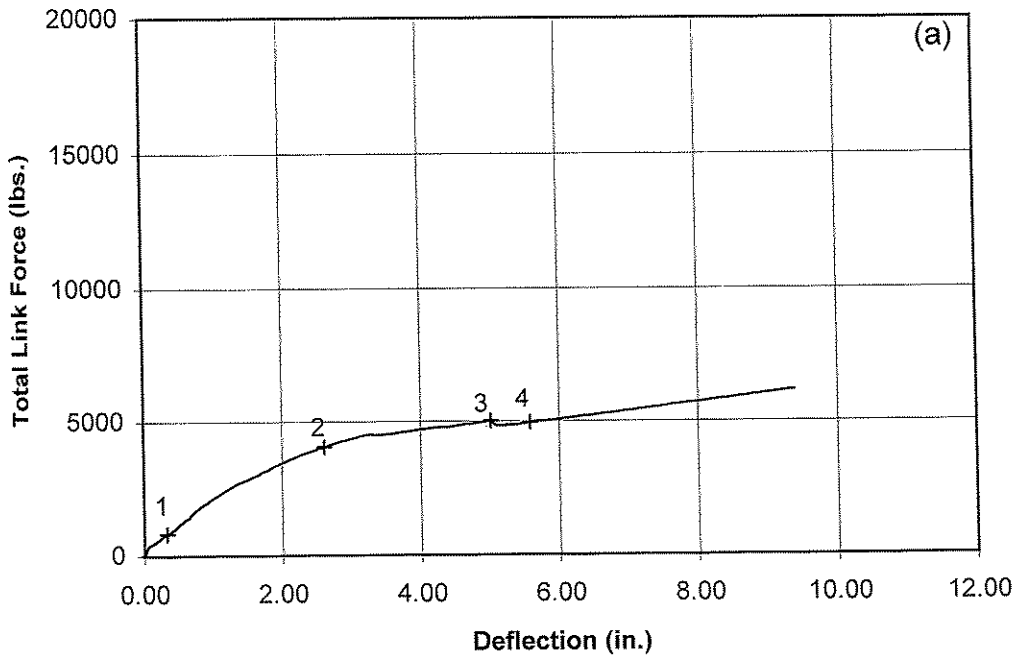


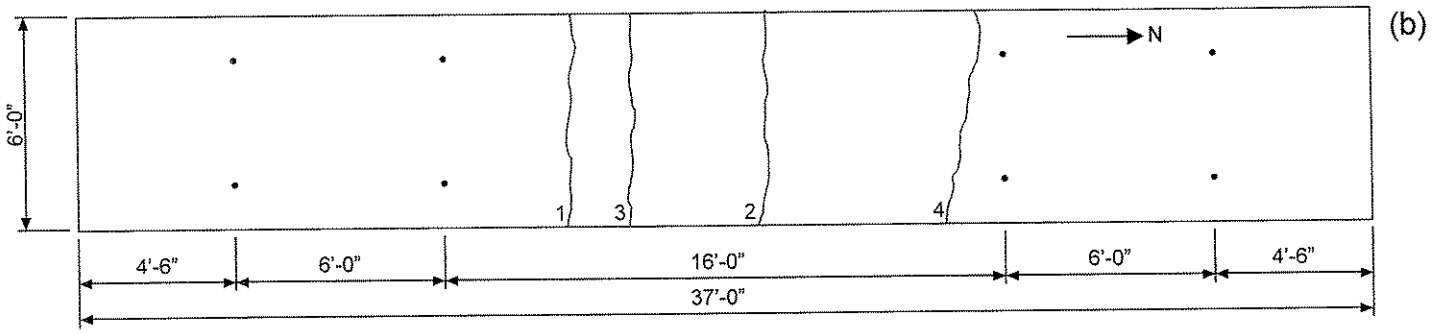


Figure 4.34 Cracking behavior of Panel 4: (a) key points on load-deflection plot; and (b) plan view of Panel 4 showing crack locations.

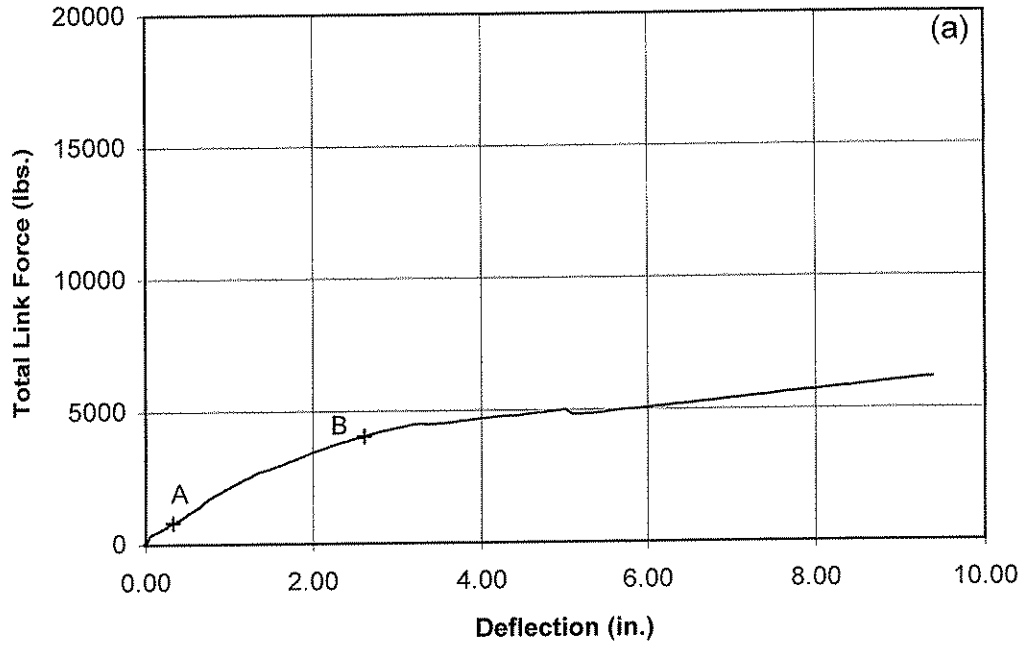


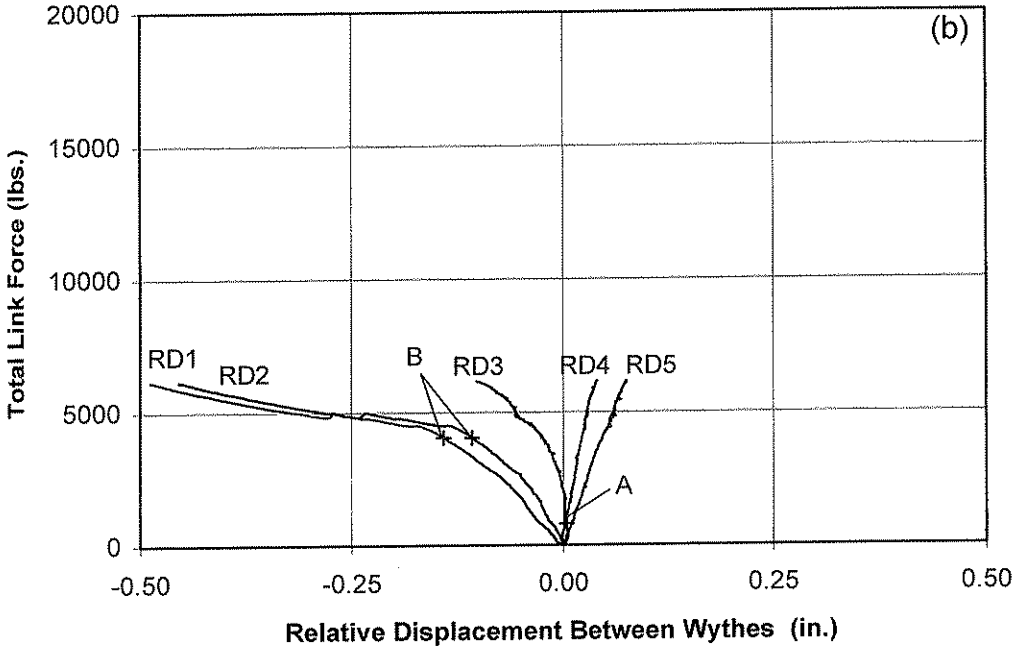


Figure 4.35 Relative displacement between wythes for Panel 4: (a) key points on load-deflection plot; and (b) total link force versus relative displacement between wythes.

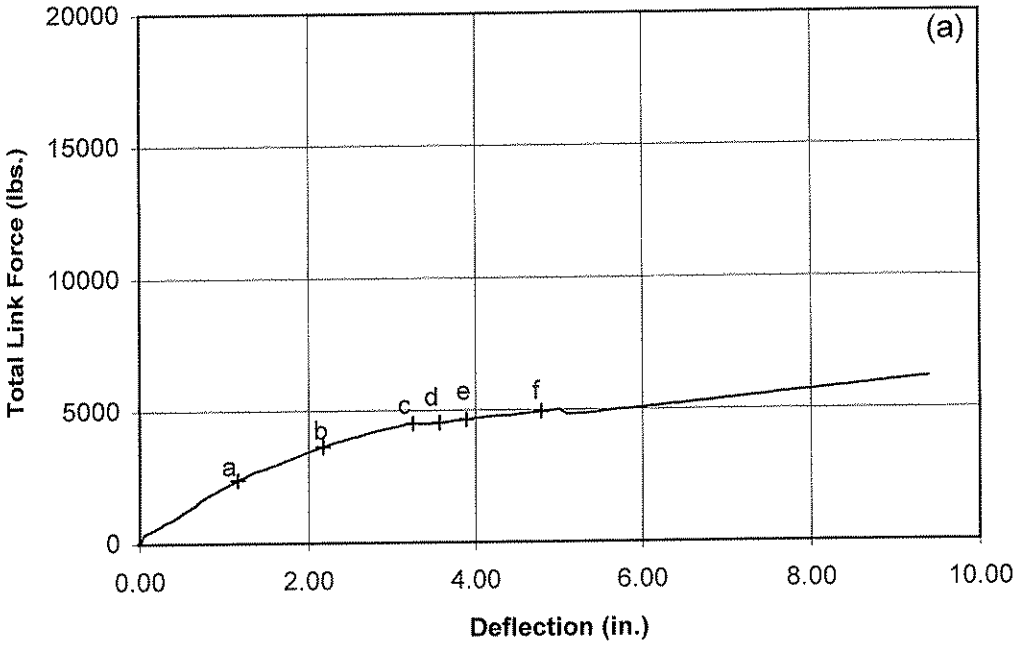


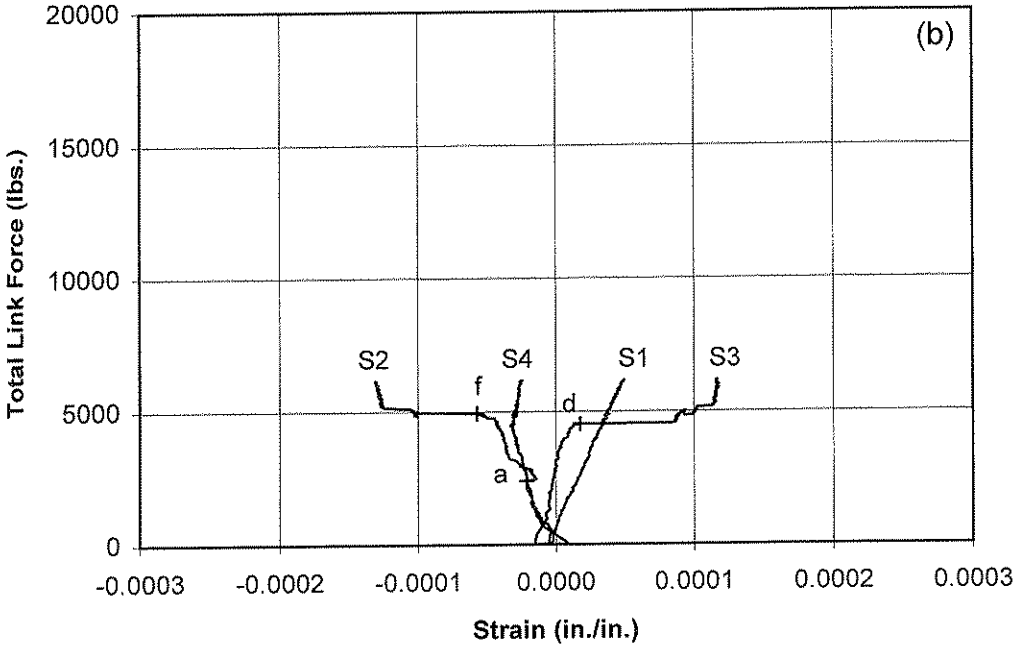


Figure 4.36 Strain measurement results for Panel 4: (a) key points on load-deflection plot; (b) total link force versus strain at Location I (gages S1 through S4).

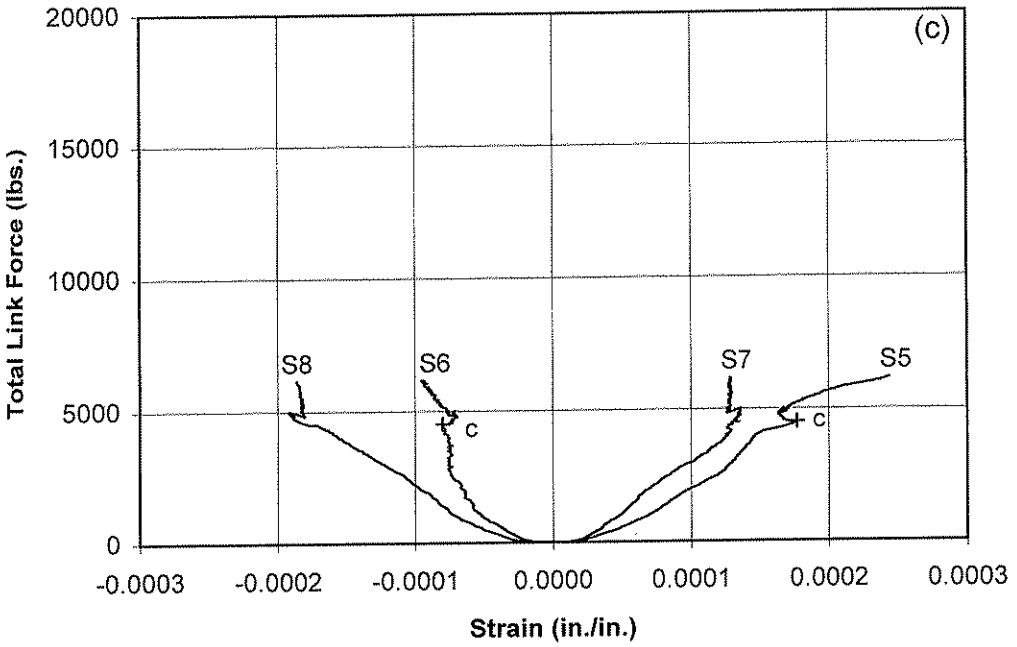


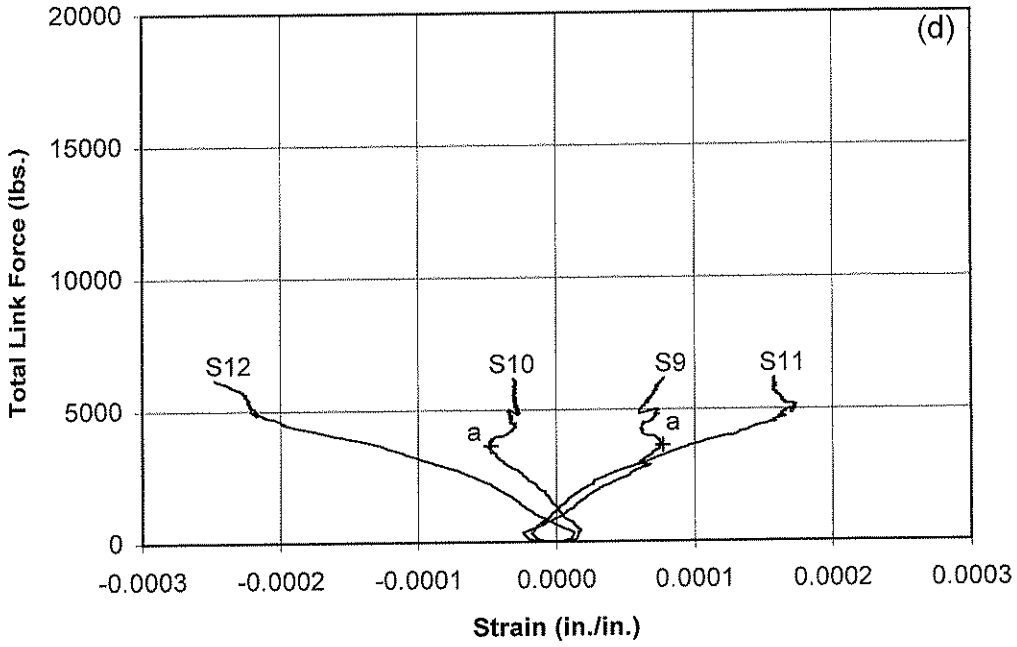


Figure 4.36 (c) total link force versus strain at Location II (gages S5 through S8);
(d) total link force versus strain at Location III (gages S9 through S12);

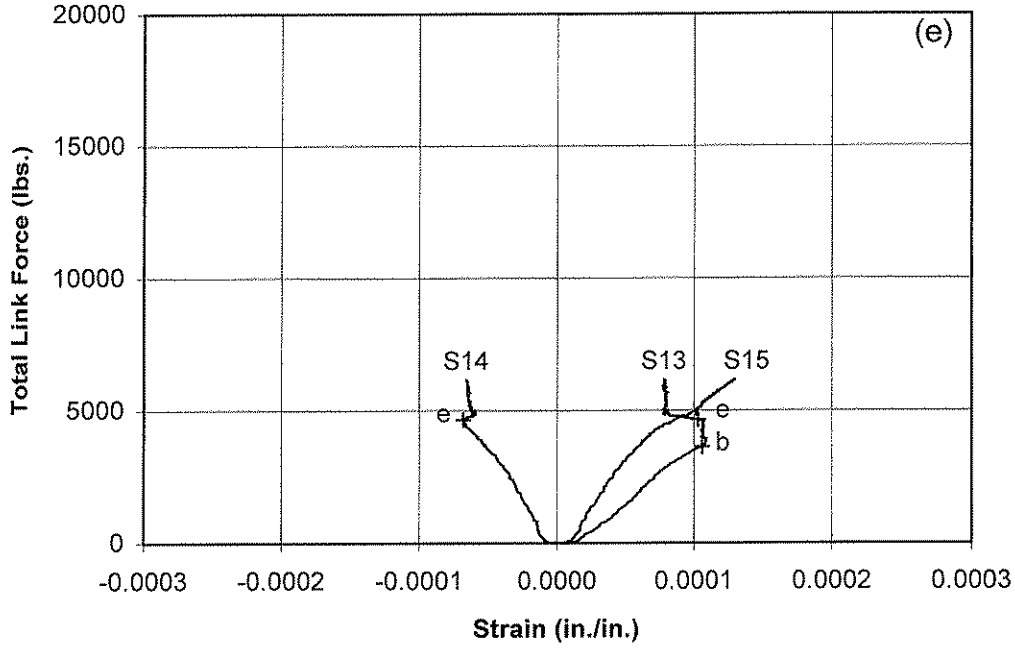


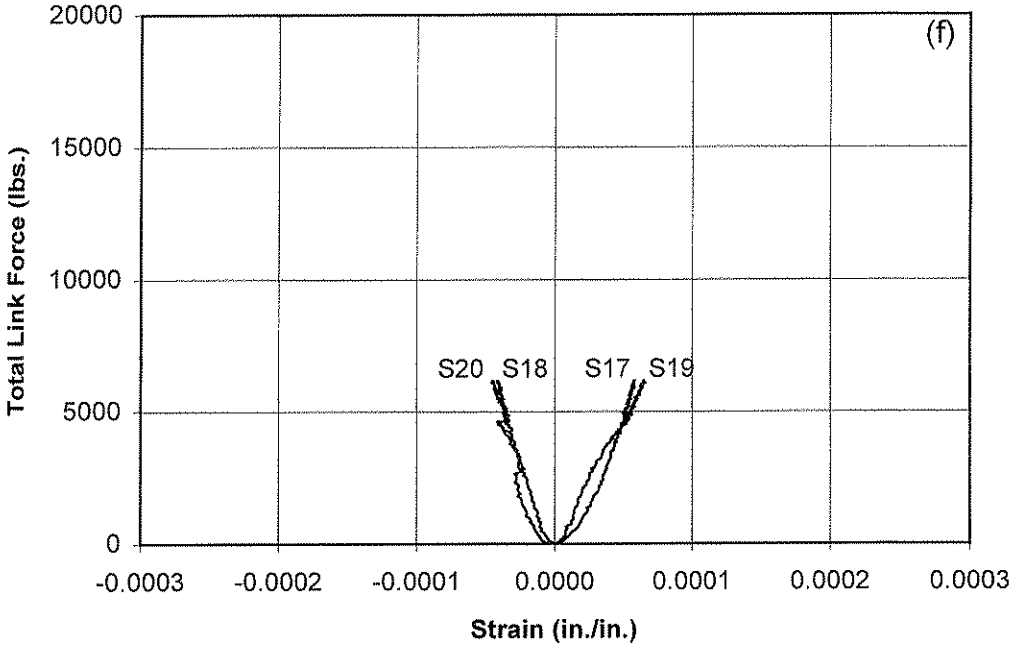


Figure 4.36 (e) total link force versus strain at Location IV (gages S13 through S16); (f) total link force versus strain at Location V (gages S17 through S20);

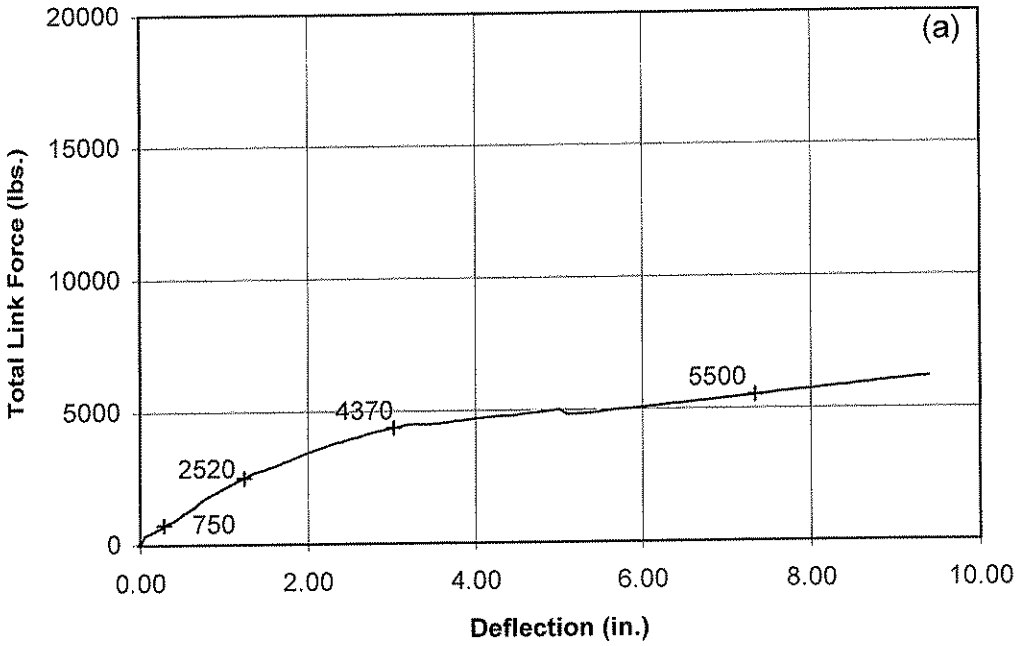


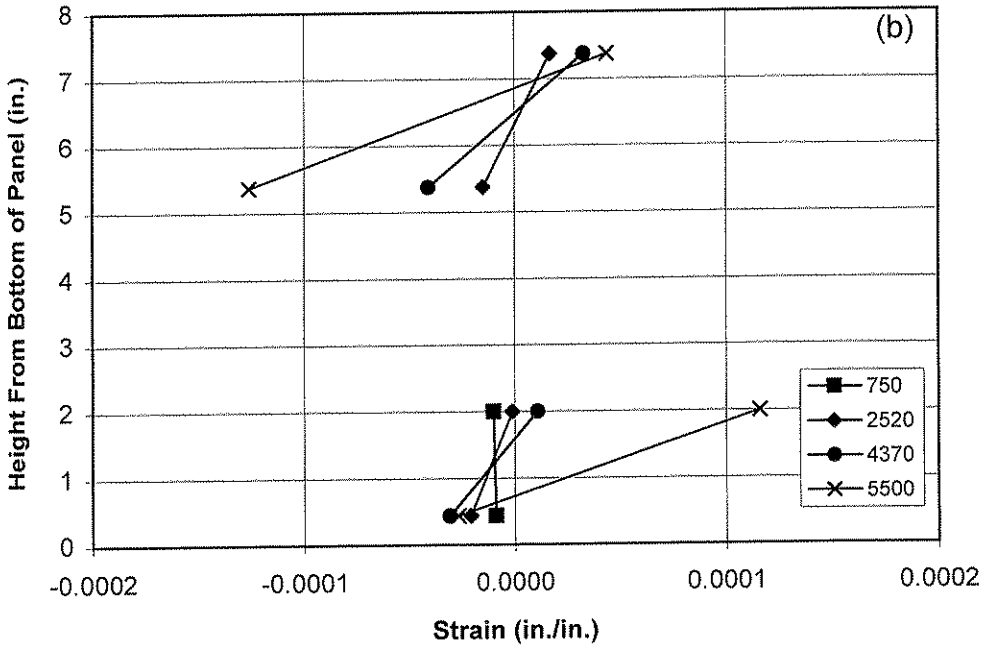


Figure 4.37 Strain distributions for Panel 4: (a) load-deflection plot showing points at which strain distributions are plotted; (b) strain distributions at Location I.

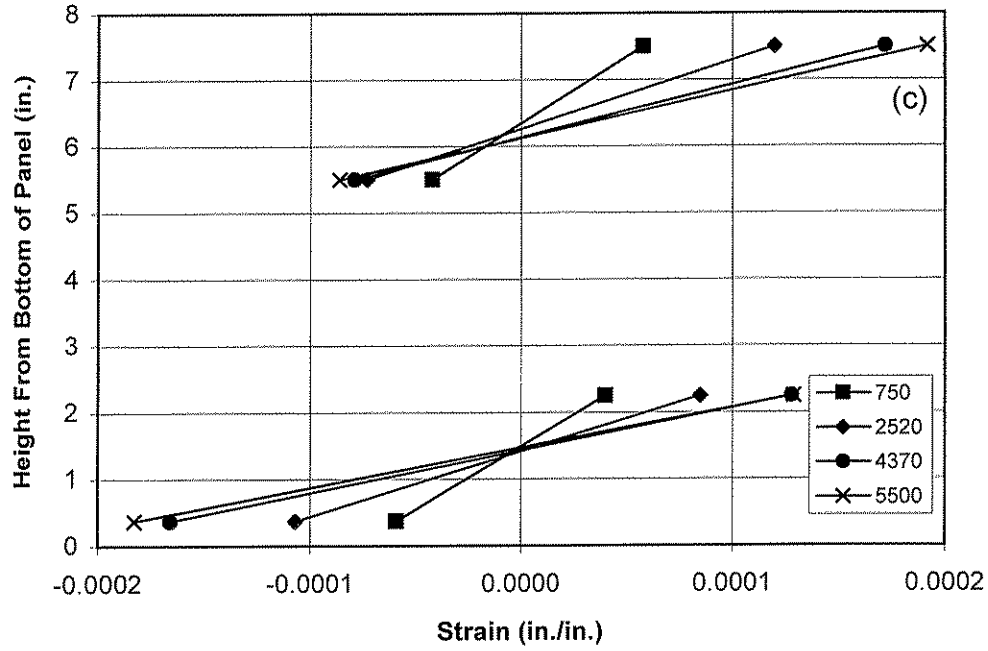


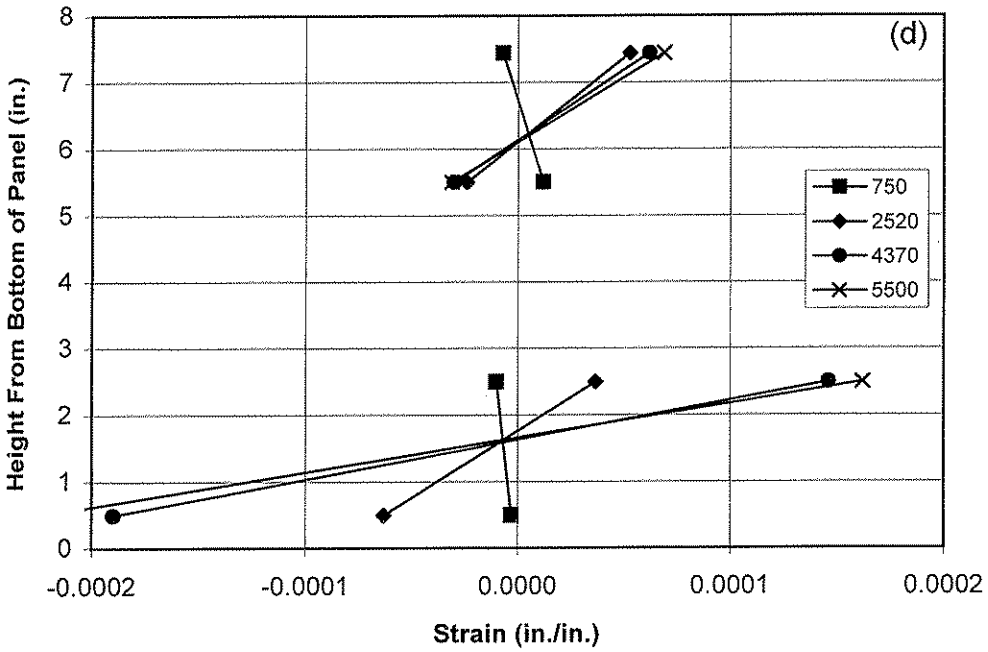


Figure 4.37 (c) strain distributions at Location II;
(d) strain distributions at Location III;

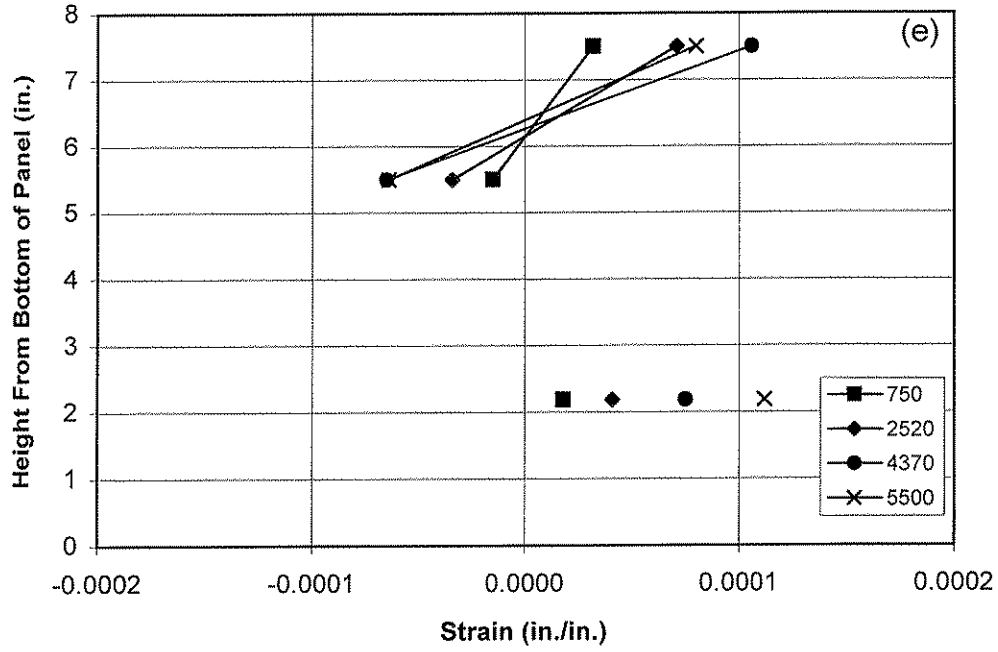


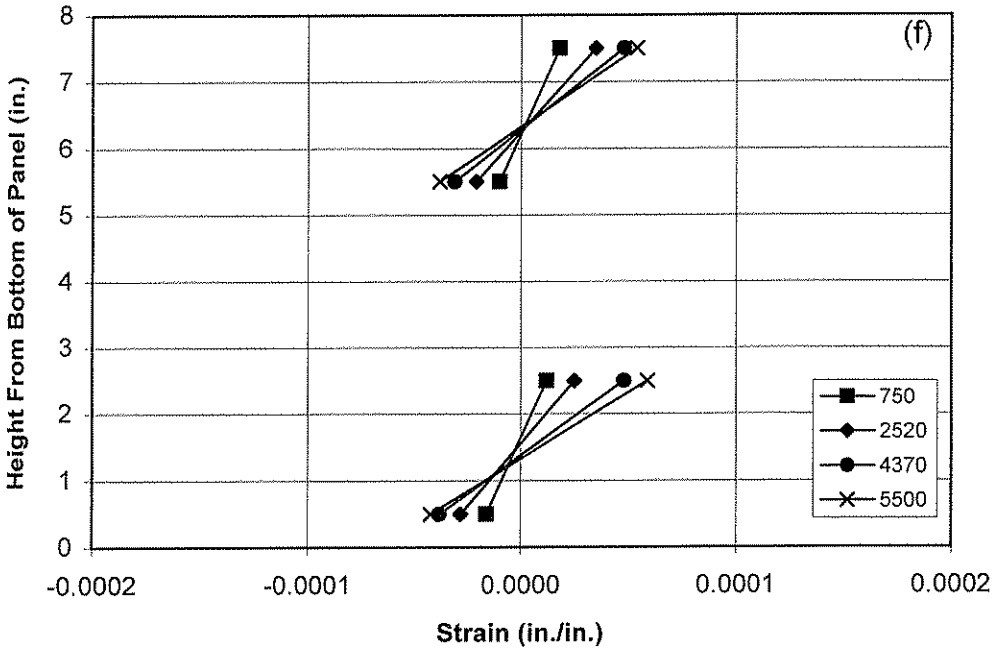


Figure 4.37 (e) strain distributions at Location IV;
(f) strain distributions at Location V;

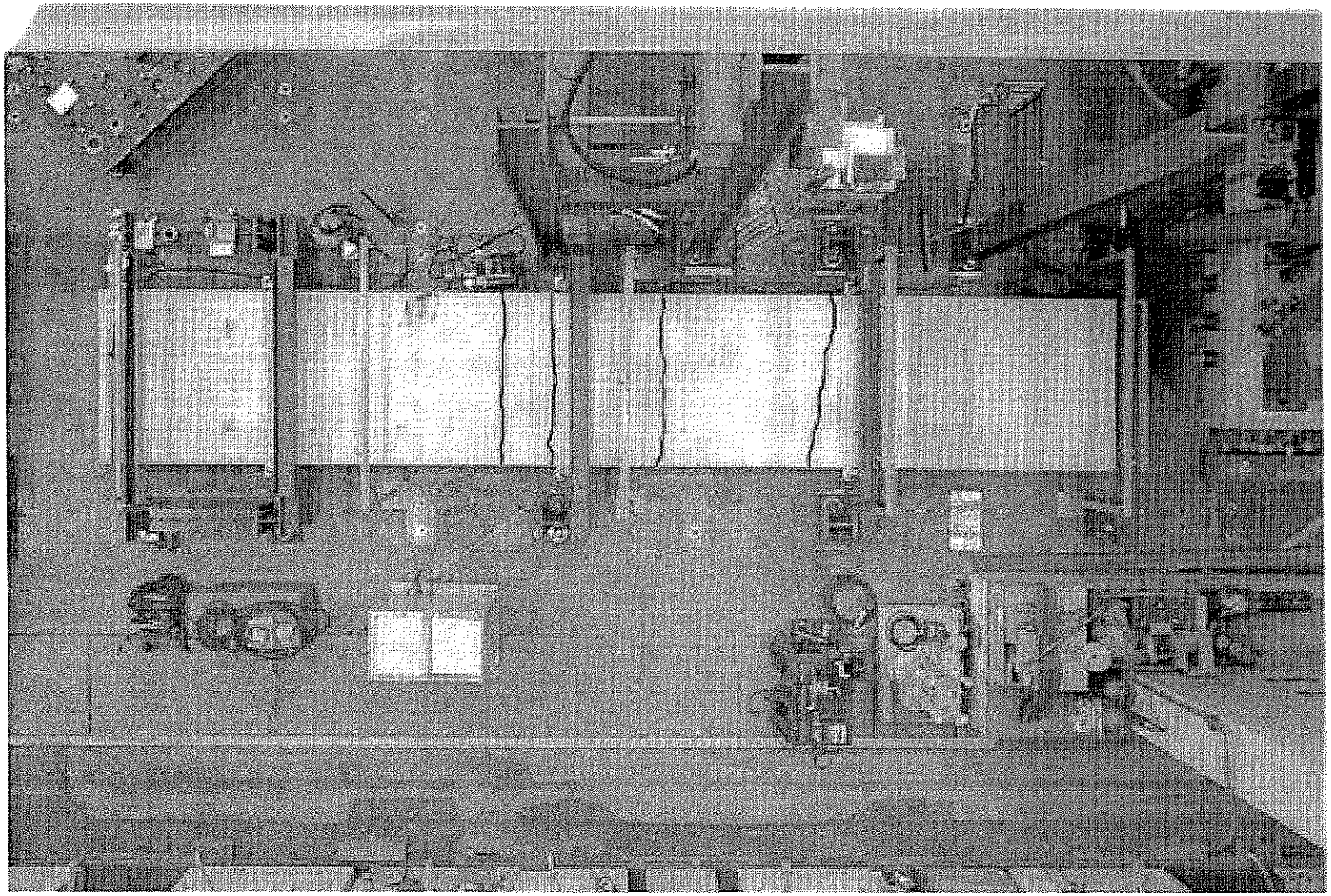

Figure 4.38 Post test photograph of Panel 4 showing crack locations.

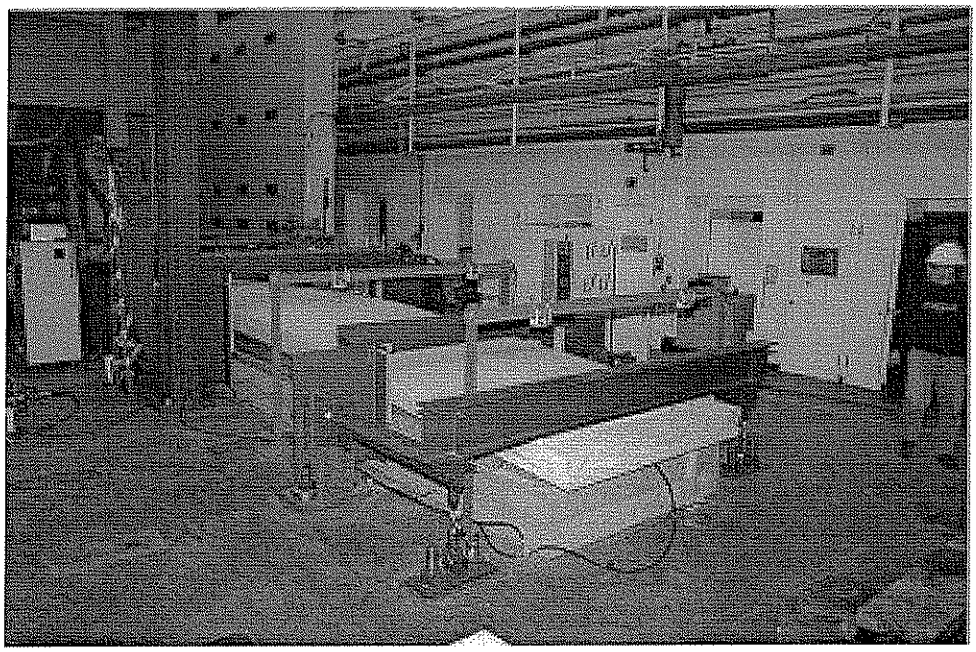

Figure 4.39 Deflected shape of Panel 4 at P=5960 lbs. and midspan deflection $\Delta$=8.75 in.

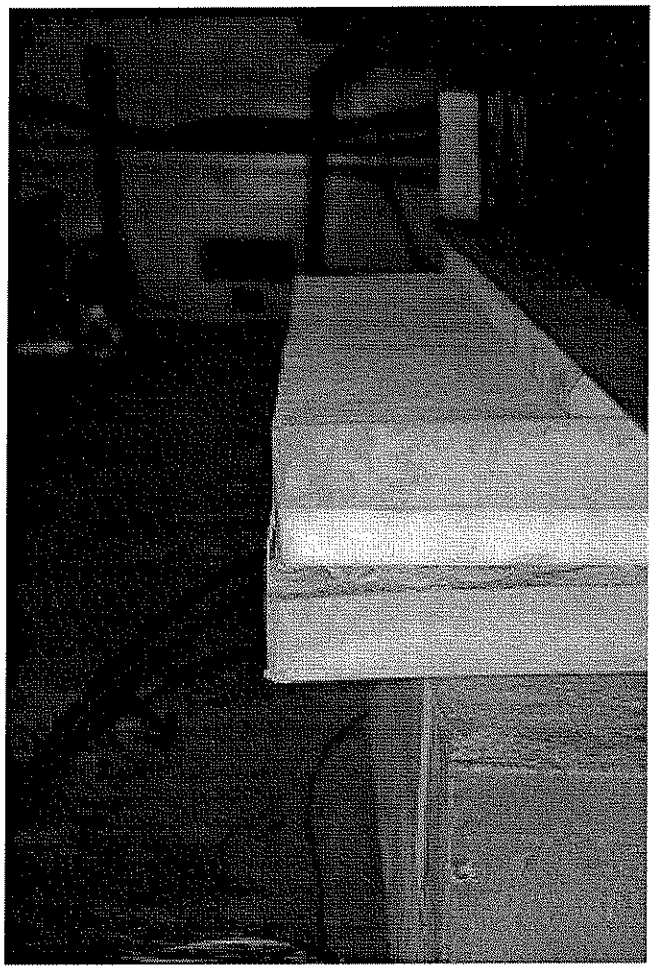

Figure 4.40 Relative displacement of wythes at the south end of Panel 4.

# CHAPTER 5
# ANALYSIS AND DISCUSSION OF RESULTS

## 5.1 INTRODUCTION

This chapter presents a detailed analysis and discussion of the results obtained from the experimental program. For simplicity in identifying the test panels, from this point forward all test panels are identified by their mechanism of shear transfer. Therefore, Panel 1 is identified as the Prototype panel, which contained all three mechanisms of shear transfer (solid concrete regions, M-ties, and bond); Panel 2 is identified as the M-tie panel; Panel 3 is identified as the Concrete panel; and Panel 4 is identified as the Bond panel.

Sections 5.2 and 5.3 compare the load-deflection behavior and the initial uncracked stiffnesses of the four test panels to each other, and also to theoretical fully composite and non-composite panels. Section 5.4 proposes an equation for calculating the percent composite action of a sandwich wall panel, and uses this equation to evaluate and compare the composite behavior of the four test panels to each other and to theoretical fully composite and non-composite panels. Section 5.5 compares the load versus relative displacement between wythes behavior of the four test panels, and Section 5.6 discusses the observed load-strain behavior of the four test panels. The performance of the Prototype panel is evaluated with respect to design requirements in Section 5.7. Section 5.8 discusses possible explanations for the bilinear load-deflection behavior of the Prototype and Concrete panels. Finally, Section 5.9 discusses flexural cracking behavior of the Prototype and Concrete panels.

## 5.2 LOAD-DEFLECTION BEHAVIOR

The load-deflection responses of the four test panels are shown in Figure 5.1. The Prototype panel exhibited the largest flexural stiffness of all the test panels. At the cracking load of 8710 lbs., the stiffness decreased slightly. Upon formation of the second flexural crack at a load of 10490 lbs., the stiffness of the panel began to degrade more rapidly. As more flexural cracks formed, the panel became progressively more flexible.

The Concrete panel exhibited load-deflection behavior similar to the Prototype panel. As shown in Figure 5.1, the initial stiffness of the Concrete panel was slightly less than the Prototype panel. The Concrete panel cracked at a load of 7080 lbs., which is slightly lower than the load at which the Prototype panel cracked. Similar to the Prototype panel, the stiffness of the Concrete panel decreased slightly upon formation of the first flexural crack. Flexural stiffness began to degrade significantly upon formation of the third flexural crack at a load of 10140 lbs. As in the Prototype panel, the stiffness degraded progressively as more flexural cracks formed.

The M-tie panel exhibited a load-deflection behavior that was dramatically different from the Prototype and Concrete panels. As shown in Figure 5.1, its initial flexural stiffness was much less than that of the Prototype and Concrete panels. The first flexural crack formed at a load of 2890 lbs. Unlike the Prototype and Concrete panels, flexural cracks were not associated with distinct drops in load. Instead, the stiffness of the panel appears to have degraded continuously

after the formation of the first flexural crack. Most of the stiffness degradation appears to have occurred over the range from first cracking, at a load of 2890 lbs., up to a load of about 6500 lbs.

The Bond panel exhibited behavior similar to the M-tie panel, and exhibited the smallest initial flexural stiffness of the four panels. The first flexural crack occurred at a load of 820 lbs. Similar to the M-tie panel, flexural cracks were not associated with distinct drops in load. The stiffness of the panel appears to have degraded continuously after the formation of the first flexural crack. Most of the stiffness degradation appears to have occurred over the range from first cracking, at a load of 820 lbs., up to a load of about 5000 lbs.

### 5.2.1 Comparison of Experimental and Theoretical Load-Deflection Behavior

Figure 5.2 compares the load-deflection behavior of the four test panels with theoretical load-deflection curves for fully composite and non-composite panels. These theoretical curves were generated using the equation:

$$\Delta = \frac{5wL^4}{384E_cI} \tag{5.1}$$

In Equation 5.1, $\Delta$ is the midspan deflection of the panel, w is the uniform load along the span, $E_c$ is the elastic modulus of the concrete, and I is the moment of inertia of the cross-section of the panel. Values of midspan deflection, $\Delta$, were computed for increasing values of load w (converted from the total link force in Figure 5.2). The elastic modulus of the concrete, $E_c$, was computed using an unconfined concrete compressive strength of 7230 psi, which was the average strength of cylinder tests for all test panels. The value of the moment of inertia substituted into Equation 5.1 varies after cracking, as discussed below.

Each of the theoretical composite and non-composite curves consists of two parts. The first part is the linear elastic part of the curve, during which the concrete remains uncracked. In this part of the curve, the full cross section of the panel contributes to resist bending. For the composite section, both wythes are assumed to act together to resist bending and for the non-composite section, the two wythes are assumed to act independently to resist bending.

The second part of the curve begins upon formation of the first flexural crack. The load at which the first flexural crack is expected to occur was computed for both the composite and non-composite sections, based on the section and prestressing parameters of the test panels. The calculated theoretical cracking loads were P=12960 lbs. and P=3710 lbs. for the composite and non-composite curves respectively. These cracking loads are indicated in Figure 5.2. These cracking loads correspond to equivalent wind loads (surface pressures) of 67.5 psf and 19.3 psf for the composite and non-composite panels, respectively.

Upon formation of the first flexural crack, an effective moment of inertia, $I_e$, is used to compute deflection. As cracking of the section progresses, the effective moment of inertia decreases. The effective moment of inertia for partially cracked prestressed beams is given by Nilson (1987) as:

$$I_e = \left(\frac{M_{cr}}{M_a}\right)^3 I_g + \left[1 - \left(\frac{M_{cr}}{M_a}\right)^3\right] I_{cr} \tag{5.2}$$

In Equation 5.2, $I_g$ is the moment of inertia of the gross concrete section, $I_{cr}$ is the moment of inertia of fully cracked transformed concrete section, $M_{cr}$ is the cracking moment, and $M_a$ is the maximum moment acting in the span.

Figure 5.2 shows that the Prototype and Concrete panels behave more similarly to a composite panel, while the M-tie and Bond panels behave more similarly to a non-composite panel. The Prototype and Concrete panels appear to have behaved almost as fully composite panels until the first flexural cracks occurred. Figure 5.2 also shows that the Prototype and Concrete panels cracked at values of load well below the predicted cracking load even though they appeared to initially behave as fully composite panels. This is discussed further in Section 5.9.

To illustrate the role of concrete strength on the theoretical load-deflection response, Figure 5.3 shows the theoretical fully composite and non-composite load-deflection curves which were generated using the lower and upper bounds of unconfined compressive strength. The lower and upper bounds of unconfined compressive strength of the concrete were 6240 psi and 8760 psi, which were the average unconfined compressive strengths of the concrete in M-tie panel (Panel 2) and Concrete panel (Panel 3), respectively. This figure shows that variations in concrete strength that exist between panels do not alter the discussion of the preceding paragraph.

## 5.3 INITIAL UNCRACKED STIFFNESSES

Figure 5.4 is a plot of load versus deflection for all test panels, plotted up to a deflection value of 3.00 in. Superimposed on each curve is a straight line, which represents the initial uncracked stiffness of each panel. For the Prototype, Concrete, and M-tie panels, the initial uncracked stiffness was determined by extending a line from the origin to the point at which the first flexural crack occurred for each panel. The line representing the initial uncracked stiffness for the Bond panel was extended past the point at which the first flexural crack occurred (820 lbs.), up to a load of 2520 lbs, since the load-deflection curve remains relatively linear up to this point.

Experimentally determined values of stiffness, $EI_{exp}$, were computed using Equation 5.3.

$$EI_{exp} = \frac{5wL^4}{384\Delta} \tag{5.3}$$

In Equation 5.3, w is the value of uniformly distributed load and $\Delta$ is the value of deflection that specifies the point that defines the line which represents the initial uncracked stiffness for each

panel. The uniformly distributed load, w, was converted from total load, P, and L is defined as the span length of the test panel. The experimentally determined values of initial uncracked stiffness, $EI_{exp}$, are presented in Table 5.1.

The straight lines which represent the initial uncracked stiffnesses for all test panels are replotted in Figure 5.5, without the experimental load-deflection curves. Two additional straight lines, representing the initial uncracked stiffnesses of theoretical fully composite and non-composite panels, are also shown in the figure. These lines were plotted using the same procedure as the theoretical composite and non-composite load versus deflection curves, which was explained in Section 5.2. The lines were discontinued at the point of the theoretical cracking load.

As shown in Figure 5.5, the initial uncracked stiffnesses for all test panels fell within the region bounded by the initial uncracked stiffnesses for the theoretical composite and non-composite panels. The Prototype panel behaved as a fully composite panel until the first flexural crack formed. The Concrete panel behaved essentially as a fully composite panel, with its initial uncracked stiffness being only slightly less than that of the Prototype panel. The M-tie panel exhibited an uncracked initial stiffness that was much less than either the Prototype or Concrete panels. The uncracked initial stiffness for this panel falls much closer to the line which defines non-composite behavior. The initial uncracked stiffness for the Bond panel is only slightly above that of the non-composite panel.

## 5.4 COMPOSITE BEHAVIOR

One of the results of primary interest in this research is the degree of composite action provided by each of the mechanisms of solid concrete regions, wythe connectors, and bond. In this report, Equation 5.4 is used to define the percent composite action, $\kappa$, achieved by each test panel:

$$\kappa = \frac{I_{exp} - I_{nc}}{I_c - I_{nc}}(100) \tag{5.4}$$

$I_{exp}$ is the experimentally determined moment of inertia of the test panel, and $I_c$ and $I_{nc}$ are the theoretical values of the fully composite and non-composite moments of inertia of the panel.

Equation 5.4 shows that the values of $I_c$ and $I_{nc}$ define the upper and lower bounds of percent composite action, respectively. For example, if $I_{exp}$, the experimentally determined moment of inertia of a panel is equal to $I_c$, then the panel exhibits 100 percent composite action. On the other hand, if the experimentally determined moment of inertia of a panel is equal to $I_{nc}$, then the panel exhibits 0 percent composite action. A partially composite panel with an experimentally determined moment of inertia between $I_c$ and $I_{nc}$, exhibits between 100 and 0 percent composite action.

The experimentally determined values of moment of inertia, $I_{exp}$, were computed from the slopes of the lines representing the initial uncracked stiffnesses for each panel, which were presented in Section 5.3.

The experimentally determined values of moment of inertia, $I_{exp}$, are computed by dividing the experimentally determined values of initial uncracked stiffness, $EI_{exp}$, by the modulus of elasticity of the concrete, $E_c$. The experimentally determined values of moment of inertia, $I_{exp}$, are shown in Table 5.2.

Table 5.2 shows the computed percent composite action, $\kappa$, for each test panel and for theoretical composite and non-composite panels. As shown in this table, the Prototype panel behaved as a fully composite panel, with 100 percent composite action. The Concrete panel behaved nearly as a fully composite with the solid concrete regions causing the panel to reach 92 percent composite action. The M-tie panel behaved nearly as a non-composite panel with the M-ties causing the panel to achieve only 10 percent composite action. The Bond panel also behaved nearly as a non-composite panel, with the bond causing the panel to achieve only 5 percent composite action.

## 5.5 RELATIVE DISPLACEMENT BETWEEN CONCRETE WYTHES

Figure 5.6 is a plot of load versus relative displacement between concrete wythes for the Prototype panel. The Prototype panel exhibited small values of relative displacements, which indicates a high degree of composite action during the test. Relative displacements were extremely small (less than 0.005 in.) while the panel remained within the linear elastic range. Upon formation of the second flexural crack, at a load of 10490 lbs, the flexural stiffness of the panel began to degrade significantly and the values of relative displacement began to increase at a slightly faster rate with increasing load.

Figure 5.7 shows plots of load versus relative displacement for the Concrete and Prototype panels plotted together for comparison. The Concrete panel exhibited relative displacement behavior similar to that which was observed for the Prototype panel. Initially, the Concrete panel exhibited small values of relative displacements, which indicates a high degree of composite action during the test. Relative displacements were extremely small while the panel remained within the linear elastic range. The values of relative displacement began to increase at a slightly greater rate upon formation of the first flexural crack at a load of 7080 lbs. After the third flexural crack formed at a load of 10140 lbs and the flexural stiffness of the panel began to degrade more significantly, the values of relative displacement began to increase even more rapidly with increasing load. At a load of 13580 lbs, instruments RD2 and RD3 began to indicate large values of relative displacement. Except at instruments RD2 and RD3, all other values of relative displacement remained similar to those observed in the Prototype panel.

Figure 5.8 shows plots of load versus relative displacement for the M-tie and Prototype panels plotted together for comparison. Throughout its entire response, the M-tie panel exhibited much larger values of relative displacement than the Prototype panel. Values of relative displacement approached or exceeded 0.25 in. at both ends of the panel. Photographs of this were shown earlier in Figures 4.21 and 4.22. While it is likely that the M-ties provided some resistance to relative displacement, Figure 5.8 shows that they are much more flexible than the solid concrete regions.

Figure 5.9 shows plots of load versus relative displacement for the Bond and Prototype panels plotted together for comparison. The Bond panel exhibited the largest values of relative displacement that were observed in the testing program. The largest values of relative displacement were observed at instruments RD1 and RD2, which were located at the south end of the panel. At the south end of the panel, a relative displacement of almost 0.5 in. was observed at instrument RD1. A photograph of this was shown earlier in Figure 4.40. Relative displacement values at the north end of the panel were much smaller, reaching a maximum of only about 0.08 in. at instrument RD5. Figure 5.9 shows that bond only contributes a small amount of resistance to relative displacement, and that this resistance degrades rapidly with loading.

## 5.6 STRAIN BEHAVIOR

As explained in Chapter 2, fully composite panels are expected to exhibit plane section behavior throughout their entire depth. As discussed in Section 5.4, load versus deflection data indicates that the Prototype and Concrete panels behaved initially as fully or nearly fully composite panels. However, the strain distributions for the Prototype and Concrete panels, presented earlier in the individual test summaries in Chapter 4, do not indicate plane section behavior through the depth of the panels.

It was thought that the cause of this discrepancy (load-deflection results indicate composite action, but the strain results do not indicate plane section behavior) arises from the fact that the face and back wythes are not connected continuously along the span of the panel, but instead are connected by solid regions at the top and bottom of the panel and by solid regions spaced apart along the span. This intermittent connection between concrete wythes may create localized stress concentrations that would disrupt plane section behavior through the panel and uniform strains across any particular section of the panel, even though in a global sense the panel may behave as a fully composite member.

To investigate this further, a linear elastic finite element analysis was performed to determine the distribution of strains in the Prototype panel under the action of lateral pressure. Figure 5.10 shows the quarter symmetry model that was used in the analysis. The coordinate axes for the model are also shown in Figure 5.10.

Finite elements representing the concrete and the insulation were included in the model, with the insulation perfectly bonded to the concrete. The model was constructed from a mesh of a total of 5328 8-node solid elements, with 74 elements along the x-axis, 6 elements along the y-axis, and 12 elements along the z-axis. All concrete elements measured x=3 in., y=1.5 in., z=3in. and all insulation elements measured x=3 in., y=1 in., z=3in. The moduli of elasticity for the concrete and the insulation were 4750 ksi and 1.35 ksi, respectively.

Restraint conditions along the two lines of symmetry and at the support are shown in Figure 5.10. The model was subjected to an arbitrary 1 psi load, which was applied across the full width and over the entire length between the support and the midspan line of symmetry.

Figure 5.11 shows the strain distributions from the finite element analysis at various locations along the length and width of the panel. Strain distributions were plotted at eight locations along the length of the panel. At each location along the length, strain distributions are plotted at three different locations across the width of the panel. These strain distributions are normalized with respect to the theoretical strain distributions, which were calculated at each location along the length, assuming a fully composite section and the same arbitrary 1 psi load. Consistent with beam theory, the theoretical strain distributions were assumed to be uniform across the width of the model. Each graph in Figure 5.11 shows a normalized theoretical strain distribution for that location along the span, as well as the strain distributions from the finite element analysis. Each strain distribution is identified by a letter and a number, which corresponds to a location specified by the markers on Figure 5.10.

Figure 5.11 shows that plane sections do not exist through the entire depth of the panel at all locations along the model. Behavior resembling plane section behavior only appears to exist at locations 3, 4, 6, and 8. The figure also shows that at some locations, the strain distributions were not uniform across the width of the panel.

Figure 5.12 shows the strain distributions at three locations (Locations I through III) where the strain gages were placed on the Prototype panel. These strain distributions also show that plane section behavior does not exist in the panel at the strain gage locations. Again, the strain distributions were not uniform across the width of the panel.

Based on the results presented above, it is concluded that the strain values measured in the experiment were highly dependent upon the placement of the strain gages. Therefore, the strain data obtained from the test panels appears to be of little use in providing information about the degree of composite action.

## 5.7 STRENGTH AND SERVICEABILITY OF THE PROTOTYPE PANEL

This section evaluates the performance the Prototype panel with respect to the strength and serviceability requirements for which it was designed. The key issues with regard to strength and serviceability are (1) strength versus factored load; (2) deflection at full service load; and, (3) flexural stresses at full service load.

### 5.7.1 Strength

The Prototype panel was designed for a service pressure of 32 psf. For the given panel area, this corresponds to a total wind load, W, of 6140 lbs. All factored load combinations were checked as required by the ACI 318 Code. The controlling load combination for the factored load, U, was computed as:

$$U = 0.9D + 1.3W \tag{5.5}$$

No axial service dead load, D, was considered in the design of the Prototype panel. Therefore, the controlling factored load was 7990 lbs., which corresponds to a pressure of 41.6 psf.

Figure 5.13 shows a plot of load versus deflection for the Prototype panel. Included on the figure are markers representing the service load and factored load. Figure 5.13 shows that the strength of the Prototype panel exceeded the factored load. In fact, as noted earlier, flexural failure by crushing of the concrete in the compression zone was not reached in the Prototype panel when the test was terminated.

The nominal moment capacity for the Prototype panel was computed using strain compatibility, assuming fully composite behavior, with the experimental concrete strength of 6930 psi. The computed nominal moment capacity was 910 kip-in. This nominal moment capacity was converted to an equivalent total force of P=15810 lbs. The design moment capacity was computed using the ACI strength reduction factor, $\phi$, of 0.9. The design moment capacity of the Prototype panel was 820 kip-in or an equivalent total force of P=14230 lbs. The Prototype panel was loaded to a load of 16340 lbs., which is well above the predicted design capacity of P=14230 lbs.

### 5.7.2 Deflection at Service Load

No deflection requirement was considered in the design of the Prototype panel. However, for the purpose of evaluating the performance of the test panels, deflections are evaluated at the full service load.

Deflection limits for precast wall panels can be found in Section 2.5.2 of the ACI Committee 533 Report. Deflections for non-load-bearing precast wall panel elements likely to be damaged by large deflection are limited to L/480, but not greater than 0.75 in. The maximum allowable deflection for the Prototype panel, with a span length of 35 ft., is controlled by the upper limit of 0.75 in.

The Prototype panel performed well with regard to deflection requirements, experiencing a deflection of only 0.43 in. at the full service load of 6140 lbs. As an aside, it is noted that the Concrete panel exhibited a similar deflection of 0.50 in. at the full service load, and that the M-tie and Bond panels experienced much larger values of deflection of 3.30 in. and 9.30 in., respectively, at the full service load. The values of deflection experienced by the M-tie and Bond panels are well beyond the allowable limit.

### 5.7.3 Cracking

The available experimental results can not be used to determine flexural stresses to see if these stresses remain within code limits under the full service load. However, insight into the behavior of the panels at the full service load can be gained by examining the cracking patterns of the test panels. According to Section 2.5.3.3 of the ACI Committee 533 Report, flexural tension stresses in prestressed wall panels should be limited to $5\sqrt{f'_c}$ to prevent cracking.

The performance of the Prototype panel can be evaluated with regard to allowable stresses by comparing the experimentally determined cracking load with the full service load. The Prototype panel cracked at a load of 8710 lbs., which is above the full service load of 6140 lbs.

Thus, at the full service load, the Prototype panel was still behaving in the linear-elastic uncracked range. Therefore, it is likely that the flexural tension stresses in the Prototype panel were within the allowable limit of $5\sqrt{f'_c}$.

## 5.8 BILINEAR LOAD-DEFLECTION BEHAVIOR

The load-deflection curves for the Prototype and Concrete panels, shown in Figure 5.1, are approximately bilinear, with the change in slope between linear segments occurring at a load of slightly greater than 10000 lbs. This section presents a discussion of two possible explanations for this behavior, which are: (1) failure of the solid concrete regions due to horizontal shear; and (2) yielding of the prestressing steel.

### 5.8.1 Horizontal Shear

The first possible explanation for the bilinear load-deflection behavior of the Prototype and Concrete panels is the failure of the solid concrete regions due to horizontal shear. As shown earlier, the solid concrete regions played a large role in developing composite action in these two panels. If the horizontal shear capacity of the solid concrete regions is exceeded, a sequence of events would occur which would lead to a loss of flexural stiffness. Upon failure of some or all of the solid concrete regions, there would be a loss of composite action between the two concrete wythes. This loss of composite action, in turn, would cause a decrease in the moment of inertia of the panel. Therefore, the decrease in moment of inertia would cause the lateral deflection of the panel to increase more rapidly with increasing load.

Calculations were performed for the Prototype panel to evaluate the horizontal shear force at a load of P=10490 lbs., which is approximately the load at which the change in slope in the load-deflection curve occurs. The calculated horizontal shear force was then compared with the predicted horizontal shear capacity.

The horizontal shear force was evaluated using a fundamental mechanics of materials approach. The horizontal shear force, H, is computed using the equation:

$$H = \frac{\Delta M(Q)}{I_c} \tag{5.6}$$

$\Delta M$ is the change in moment across the shear span, Q is the first moment of inertia of the composite section, and $I_c$ is the fully composite moment of inertia of the panel. The shear span is taken as half of the clear span of the panel. This calculation indicates that at a load of P=10490 lbs., the horizontal shear force, H, in the Prototype panel was equal to 90 kips.

The horizontal shear capacity, $V_{nh}$, was computed as outlined in Section 4.3.5 of the PCI Handbook using the equation:

$$V_{nh} = 80 A_{cs} \tag{5.7}$$

In Equation 5.7, $V_{nh}$ is in units of psi and $A_{cs}$ is the total area of concrete, in units of $in.^2$, resisting horizontal shear. Equation 5.7 assumes that the strength of unreinforced concrete due to horizontal shear is 80 psi. The Prototype panel had a total area of concrete, $A_{cs}$, equal to 1440 $in.^2$. Therefore, the Prototype panel had a predicted horizontal shear capacity of 115 kips.

The computed horizontal shear force, H, was only 78 percent of the horizontal shear capacity. Also, it is likely that the shear strength of unreinforced concrete is actually much greater than the value of 80 psi, which is given by PCI. Tests performed Hofbeck, Ibrahim, and Mattock (1969) indicate that the shear strength of initially uncracked unreinforced concrete is approximately 500 psi. This value is much higher than 80 psi, and therefore the actual horizontal shear capacity of the Prototype panel is likely much higher than 115 kips. Therefore, it is not likely that the failure of solid regions and loss of horizontal shear transfer occurred at this point in the loading, and is not the cause of the loss in stiffness in the load-deflection.

To further investigate the possible failure of the solid regions, several core samples were taken from the Prototype panel after testing. Four 5.75 inch diameter core samples were taken through the solid regions. One core sample was taken through one of the solid end regions, and three more core samples were taken from three of the 1 ft. square solid regions. For all core samples, except one, the solid regions appeared to be undamaged after testing. The one damaged core sample, which was taken from one of the 1 ft. square solid regions, was sheared off at the interface between the solid region and the bottom concrete wythe. However, this core sample only included a corner of the solid region, and it is thought that the coring machine may have damaged the core sample.

In summary, both the calculations and the core samples seem to indicate that the bilinear nature of the load-deflection curve is not due to the failure of the solid concrete regions due to horizontal shear.

### 5.8.2 Yielding of Prestressing Steel

The second possible explanation for the cause of the bilinear load-deflection behavior of the Prototype and Concrete panels is yielding of the prestressing steel. To investigate this, the theoretical load at which the prestressing strands yield was computed for the Prototype panel using strain compatibility. To perform the strain compatibility calculation, the strain in the prestressing steel was set equal to the yield strain and the concrete was assumed to remain linear-elastic. Losses were assumed to be 13 percent. From this calculation, the theoretical load at which the prestressing steel in the Prototype panel yields was computed to be P=12100 lbs. It was found in the calculation that the concrete stress remained below $0.5f'_c$, so the assumption that the concrete remained linear elastic was confirmed. Additional calculations were performed to investigate the effects of prestress losses on the load at which the panel yields. These calculations indicated that variation in losses has little effect on the load at which the prestressing steel yields.

The change in slope of the bilinear load-deflection curve for the Prototype panel occurred at a load of approximately P=10490 lbs. This is approximately 87 percent of the load at which the

prestressing steel was predicted to yield. It seems that yielding of the prestressing steel is the most likely cause of the bilinear nature of the load-deflection curves for the Prototype and Concrete panels.

The strain compatibility analysis assumes that the entire panel width is effective in compression in bending. As noted in Section 5.6, because of the intermittent placement of solid concrete regions along the span of the panel, at some sections along the panel the strain distributions are not uniform across the width of the panel. This is likely due to shear lag, or shearing deformations causing portions of the width of the section further removed from the solid concrete regions to experience less strain as compared to portions of the section closer to the solid concrete regions. This may contribute to some of the disparity between the observed and predicted values of yielding of the prestressing steel.

Finally, it is also noted that actual sandwich wall panels are often twice as wide as the test specimens treated in this study. This increased width will only increase any shear lag present in the panels. Additional tests should be performed on wider panels to study this issue. This is discussed further as part of future work in Section 6.5.

## 5.9 FLEXURAL CRACKING BEHAVIOR

Although both the Prototype and Concrete panels exhibited fully or nearly fully composite behavior, the one aspect of their behavior that was not consistent with the behavior of the theoretical fully composite panel was their flexural cracking behavior. The theoretical flexural cracking load for the theoretical fully composite behavior was P=12670 lbs. As noted earlier, the Prototype and Concrete panels cracked at loads of P=8710 lbs. and P=7080 lbs., respectively.

In general, the tensile strength of concrete in flexure is computed as $7.5\sqrt{f'_c}$. The experimental tensile strengths for the Prototype and Concrete panels, which were computed using the experimental cracking loads, were $3.8\sqrt{f'_c}$ and $3.6\sqrt{f'_c}$. These are somewhat lower than the theoretical value. Several possible causes of this low tensile strength were considered.

The first explanation that was considered was that the bending stresses in the panel increased subsequent to the failure of solid concrete regions due to horizontal shear. As explained in Section 5.8.1, if the solid concrete regions failed due to horizontal shear, composite action would be lost, and the moment of inertia would decrease drastically. This decrease in moment of inertia would cause the bending stresses in the panel to increase. This would cause cracking of the panel if the bending stresses exceeded the tensile strength of the concrete. However, as discussed in Section 5.8.1, it is not likely that the solid concrete regions failed at the load at which the first flexural cracks formed.

Another possible explanation that was considered was that the panels cracked at lower values of load due to stress concentrations near the edges of the solid regions. As shown in Figure 5.11, the finite element analysis results indicate that strains are especially high at Locations 5 and 7. These higher strain values indicate that large stress concentrations exist at the interfaces between the solid concrete regions and the top and bottom wythes. This can also be seen in Figure 5.12 at

Locations I and II. However, although several cracks did form immediately adjacent to the solid regions, these were not the first flexural cracks to form. Therefore, stress concentrations near the solid regions cannot be attributed to the early flexural cracking of the Prototype and Concrete panels.

A third possible explanation to the low flexural cracking loads of the Prototype and Concrete panels was that stresses were higher at midspan due to the lack of solid concrete regions near midspan. As shown in Figure 5.12, the finite element analysis indicates that plane section behavior does not exist at Location I, near midspan. Therefore, strains are higher than predicted at this location. The higher flexural stresses could cause flexural cracking at a lower load than predicted if the tensile strength of the concrete was exceeded. The flexural stresses at midspan were computed from the strains computed by the linear elastic finite element analysis with a 1 psi load. The stresses were also computed for a theoretical fully composite panel subjected to a 1 psi load using beam theory. It is noted that a 1 psi loading is a high value of load. The loading in these analyses is arbitrary. What matters is the ratio of stresses from these two analyses. The stresses computed from the results of the finite element analysis show that at midspan, flexural stresses are approximately 13 percent higher than the stresses computed for a theoretical fully composite panel. Therefore, it is likely that the higher stresses due to a localized lack of composite action at midspan contributed to the cracking of the Prototype and Concrete panels at loads somewhat lower than predicted. However, the Prototype panel cracked at a load approximately 31 percent lower than the predicted flexural cracking load. Therefore, the effects of a localized lack of composite action, contributes to, but may not fully explain the low cracking load behavior of the Prototype and Concrete panels.

| Panel Type | P (lbs.) | w (lbs./in.) | Δ (in.) | $EI_{exp}$ (psi) |
|---|---|---|---|---|
| Prototype | 8710 | 22.7 | 0.64 | 14360000 |
| Concrete | 7080 | 18.4 | 0.59 | 12660000 |
| M-tie | 2890 | 7.5 | 0.98 | 3110000 |
| Bond | 2520 | 6.6 | 1.24 | 2140000 |

Table 5.1 Experimentally determined values of initial uncracked stiffness.

| Panel Type | $EI_{exp}$ (psi) | $f'_c$ (psi) | $E_c$ (ksi) | $I_{exp}$ ($in.^4$) | κ (%) |
|---|---|---|---|---|---|
| Composite | - | - | - | 3024 | 100 |
| Prototype | 14360000 | 6930 | 4750 | 3024 | 100 |
| Concrete | 12660000 | 6240 | 4500 | 2814 | 92 |
| M-tie | 3110000 | 8760 | 5340 | 583 | 10 |
| Bond | 2140000 | 7000 | 4770 | 450 | 5 |
| Non-Composite | - | - | - | 324 | 0 |

Table 5.2 Computed percent composite action, κ, for all test panels, including values for theoretical fully composite and non-composite panels.

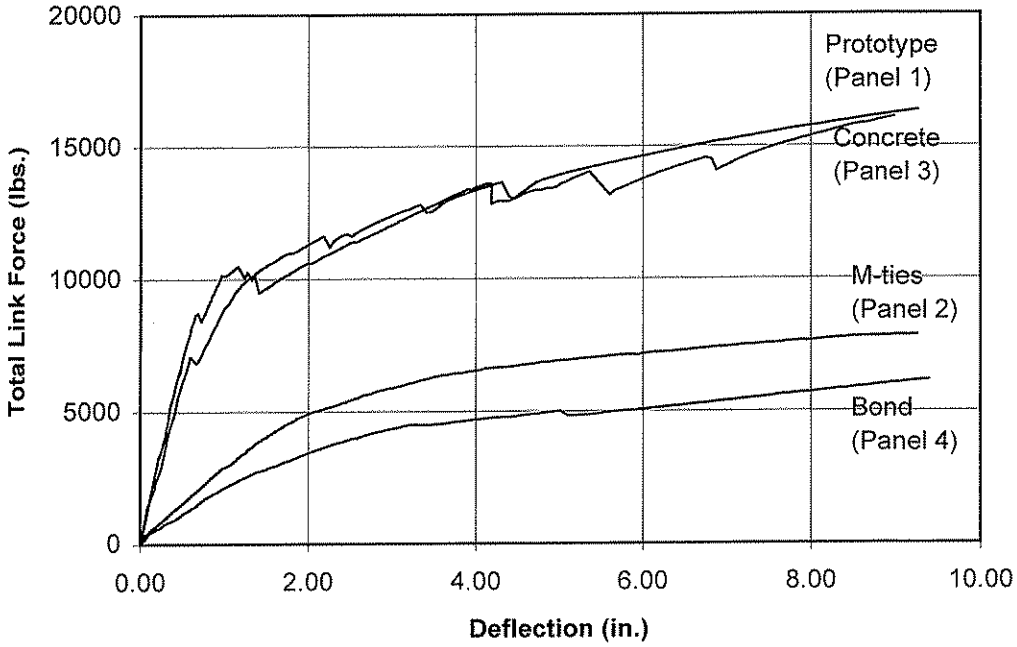


Figure 5.1 Plot of load versus deflection for all test panels.

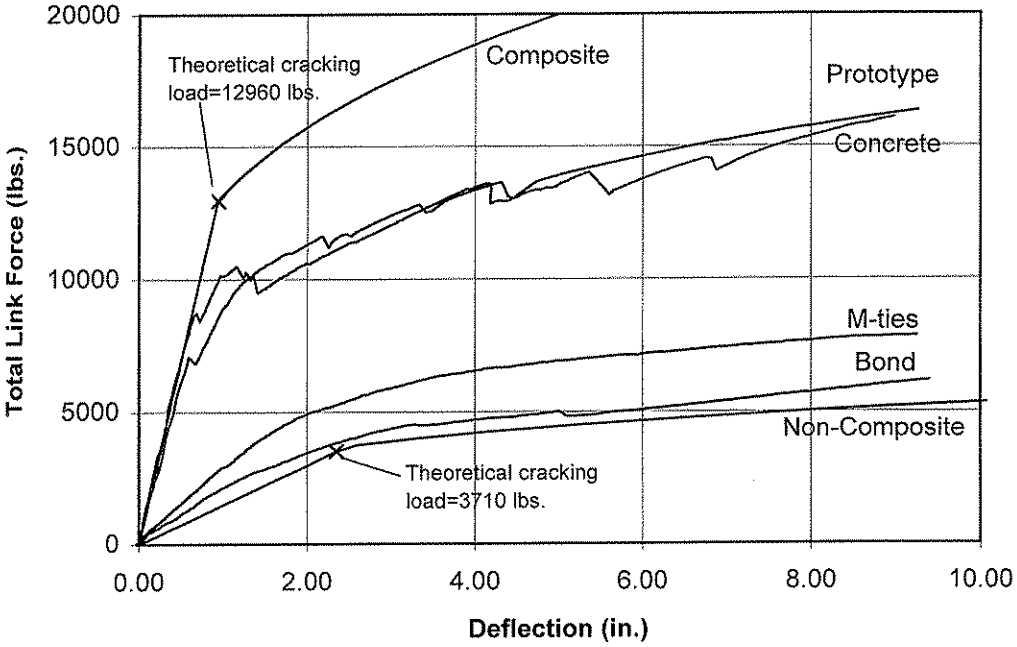


Figure 5.2 Plot of load versus deflection for all test panels, including curves for theoretical fully composite and non-composite panels.

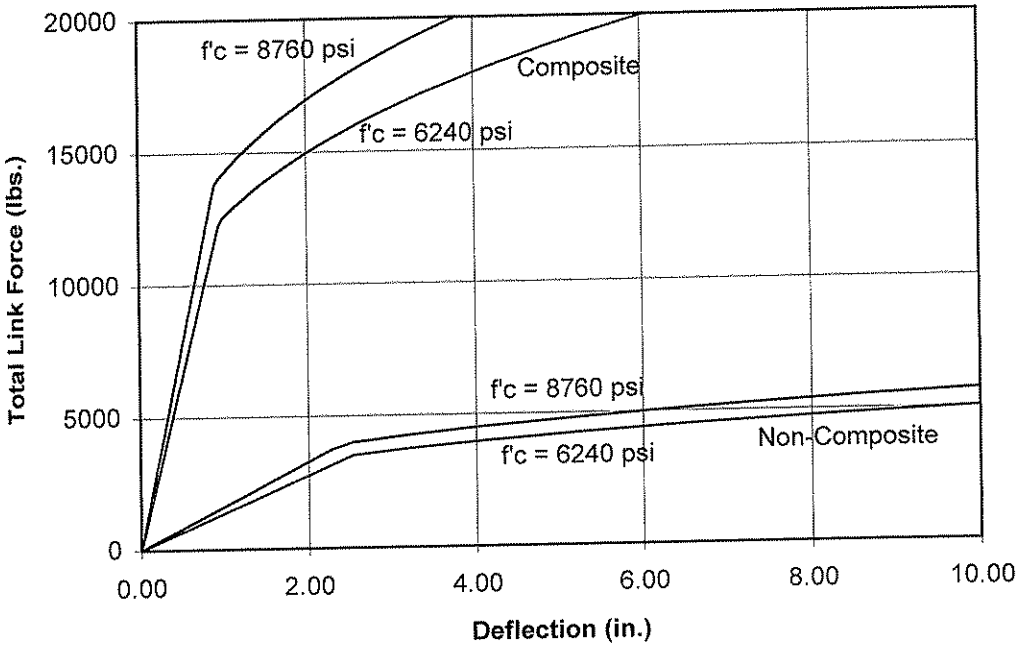


Figure 5.3 Plot of theoretical fully composite and non-composite load versus deflection curves, generated using the lower and upper bounds of unconfined compressive strength.

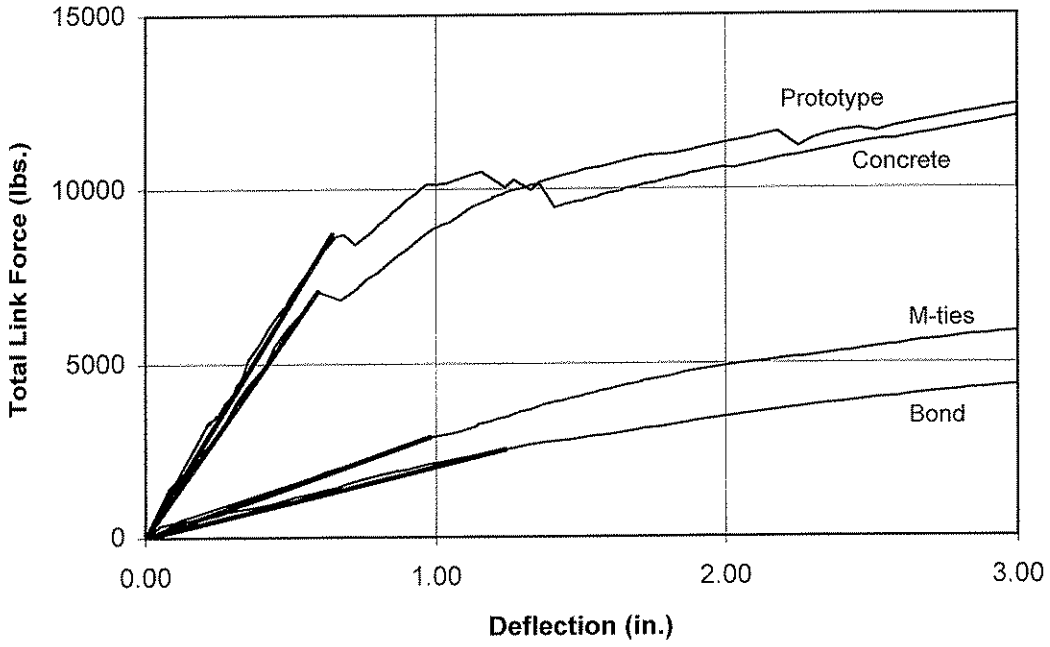


Figure 5.4 Load versus deflection for all test panels, and initial uncracked stiffnesses.

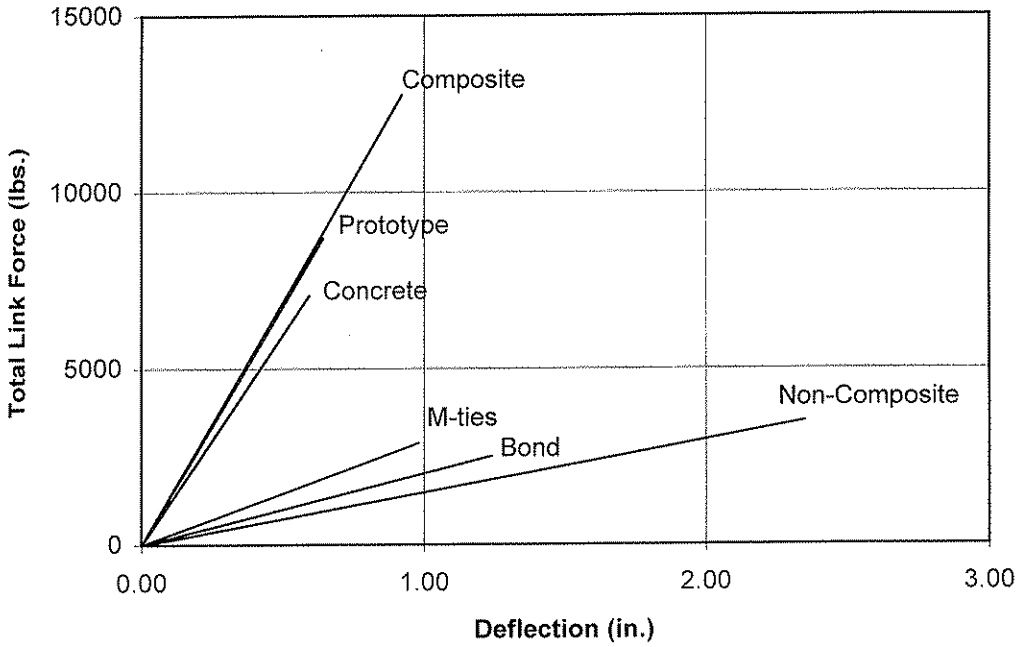


Figure 5.5 Initial uncracked stiffnesses for all test panels, including stiffnesses for theoretical fully composite and non-composite panels.

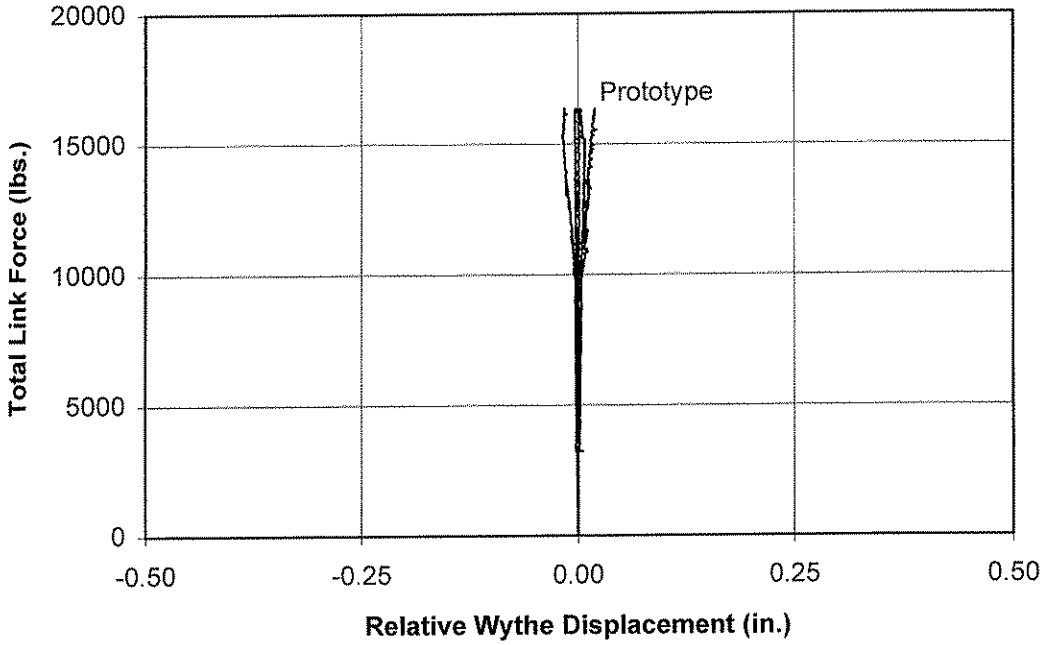


Figure 5.6 Plot of load versus relative displacement between concrete wythes for the Prototype panel.

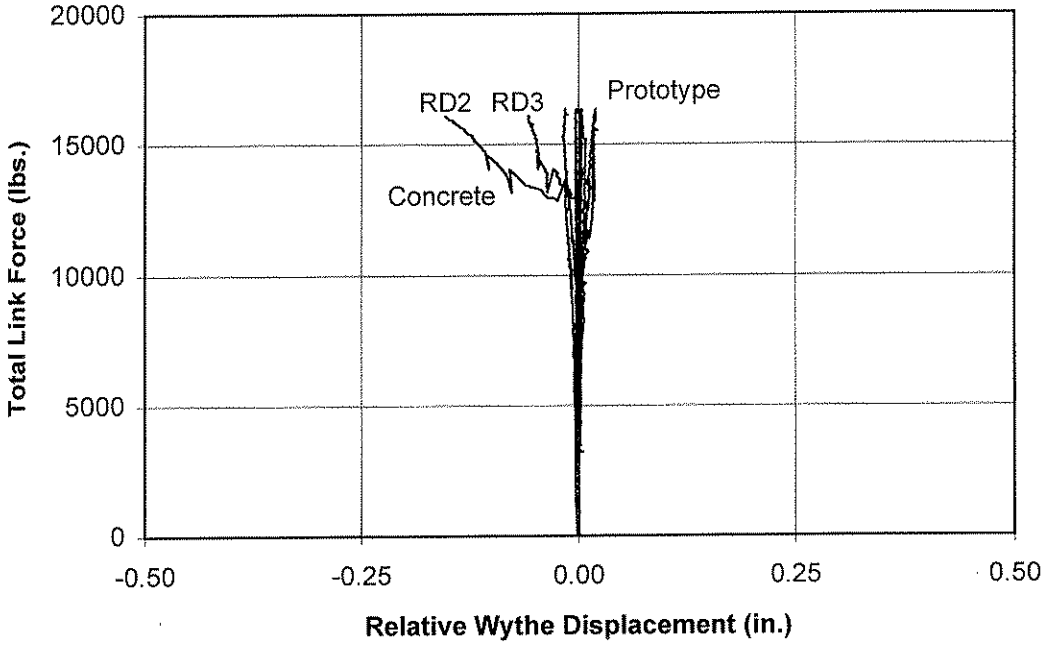


Figure 5.7 Plot of load versus relative displacement between concrete wythes for the Concrete and Prototype panels.

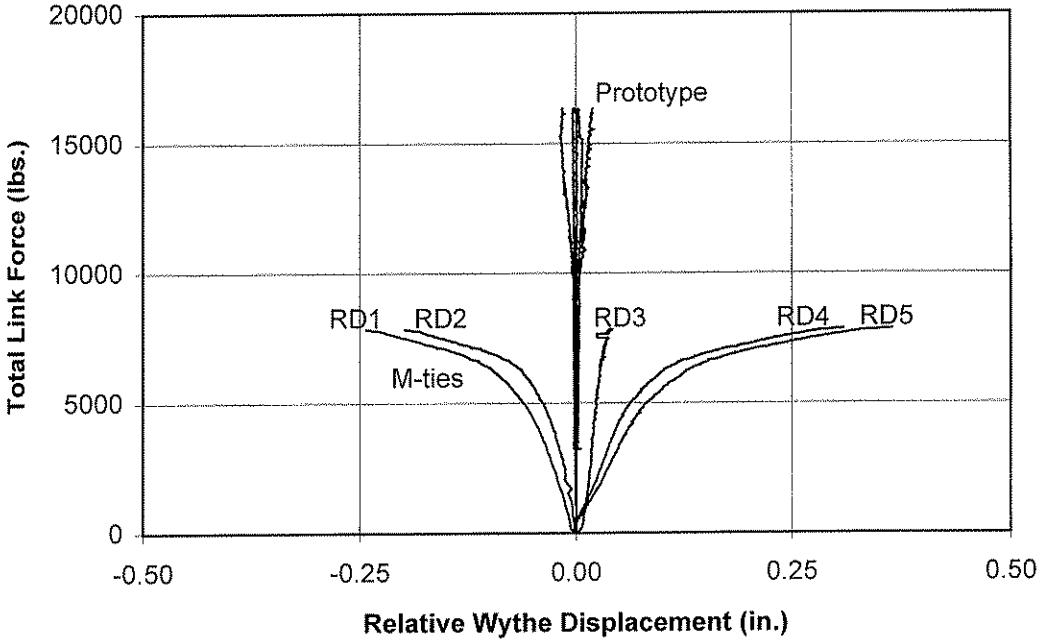


Figure 5.8 Plot of load versus relative displacement between concrete wythes for the M-tie and Prototype panels.

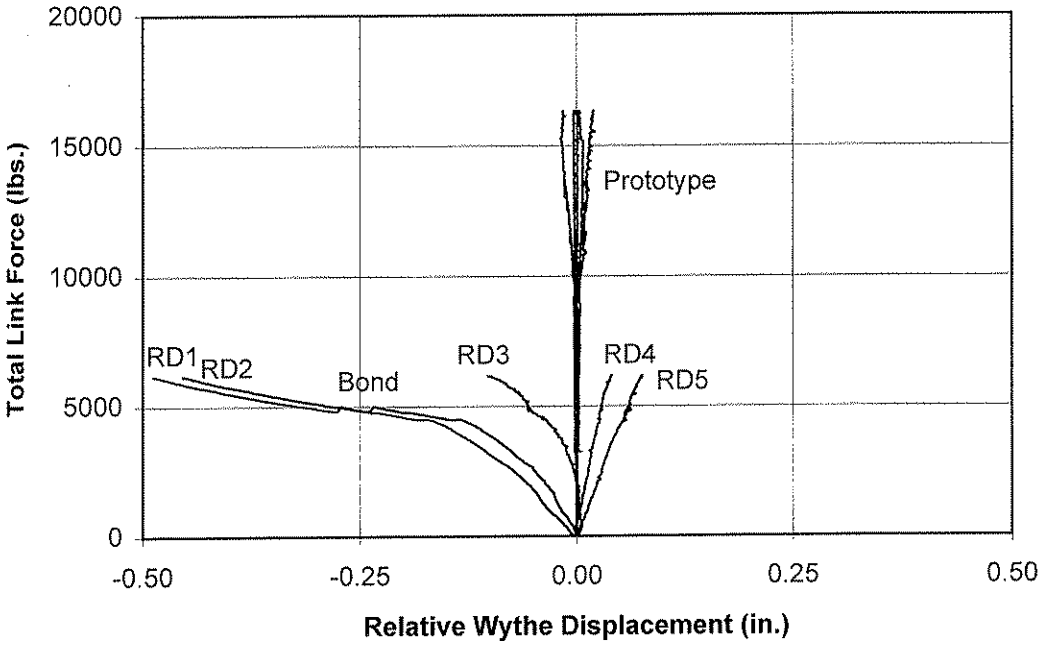


Figure 5.9 Plot of load versus relative displacement between concrete wythes for the Bond and Prototype panels.

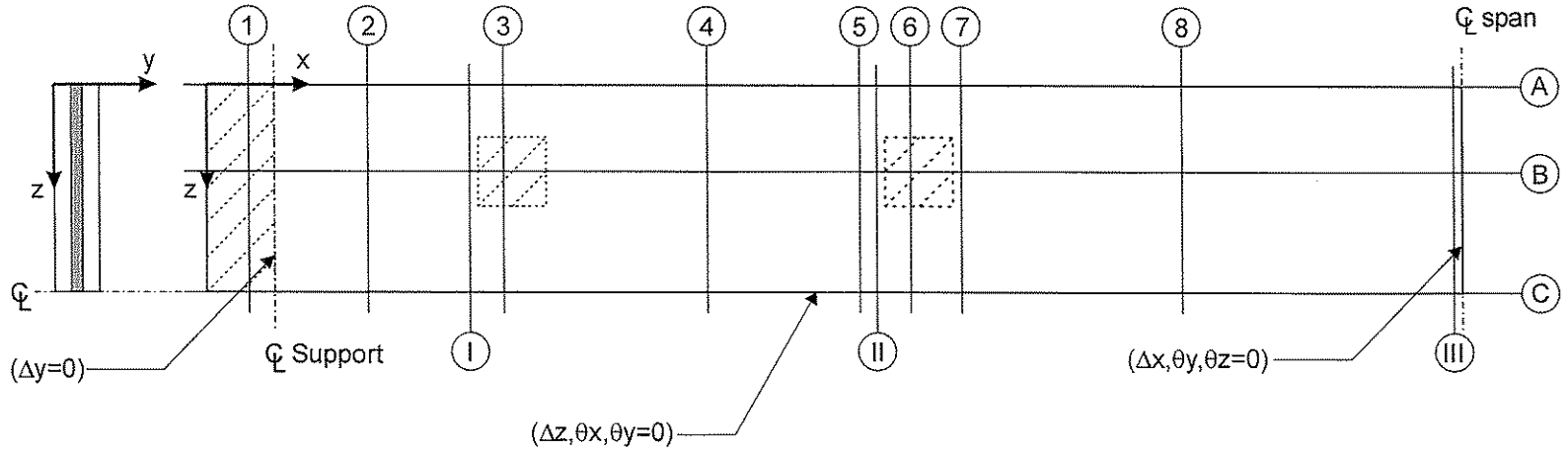


| Location | x (in.) | Location | z (in.) |
|---|---|---|---|
| 1 | 7.5 | A | 0 |
| 2 | 28.5 | B | 15 |
| 3 | 52.5 | C | 36 |
| 4 | 88.5 | | |
| 5 | 118.5 | | |
| 6 | 124.5 | | |
| 7 | 133.5 | | |
| 8 | 178.5 | | |
| I | 46.5 | | |
| II | 115.5 | | |
| III | 220.5 | | |

Figure 5.10 Geometry and boundary conditions of Prototype panel used for finite element analysis.

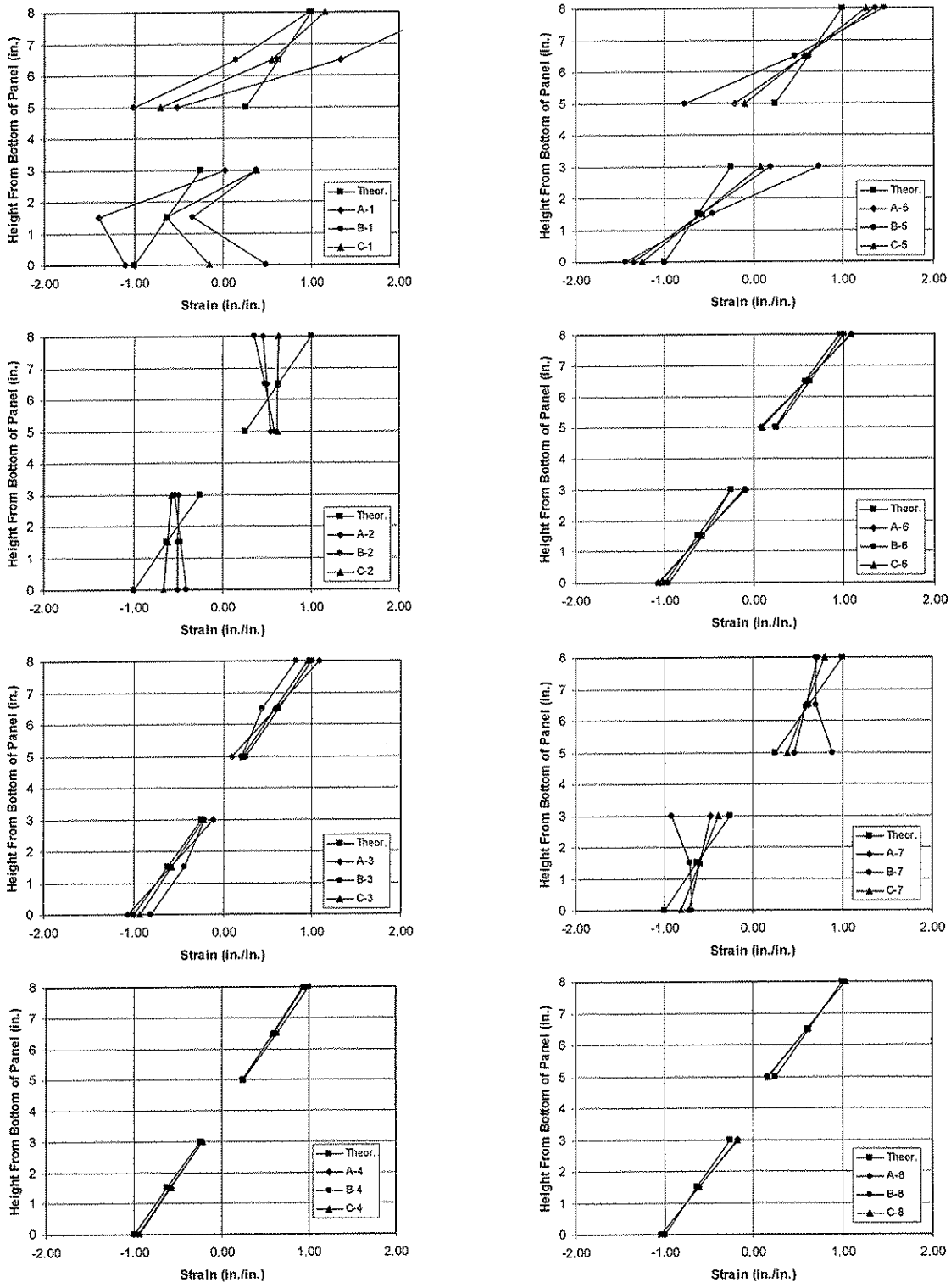


Figure 5.11 Normalized strain distributions from finite element analysis of Prototype panel at Locations 1 through 8.

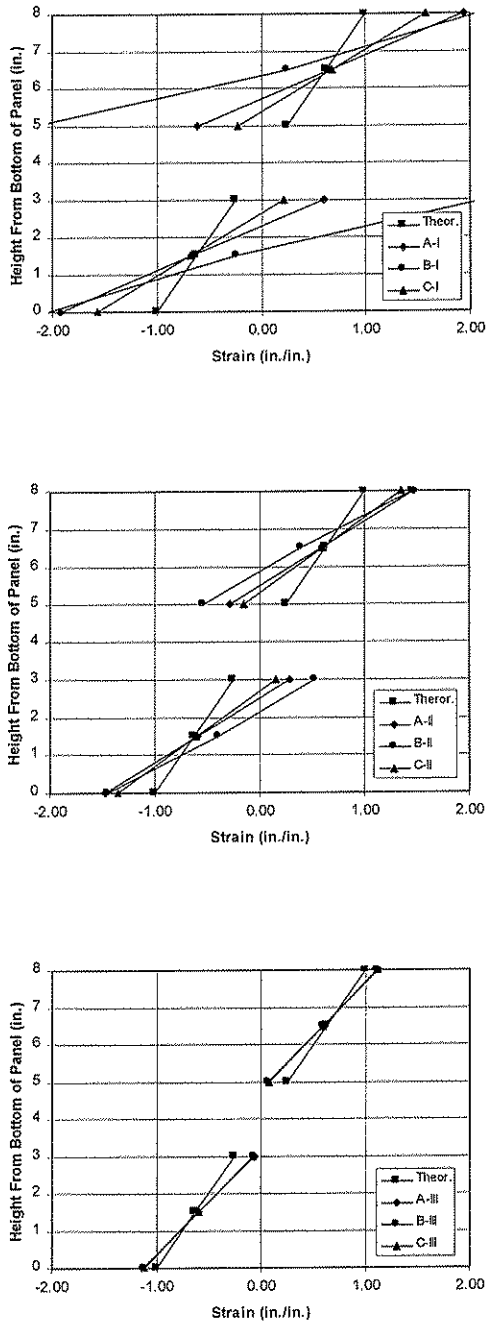


Figure 5.12 Normalized strain distributions from finite element analysis of Prototype panel at Locations I through III, the actual strain gage locations.

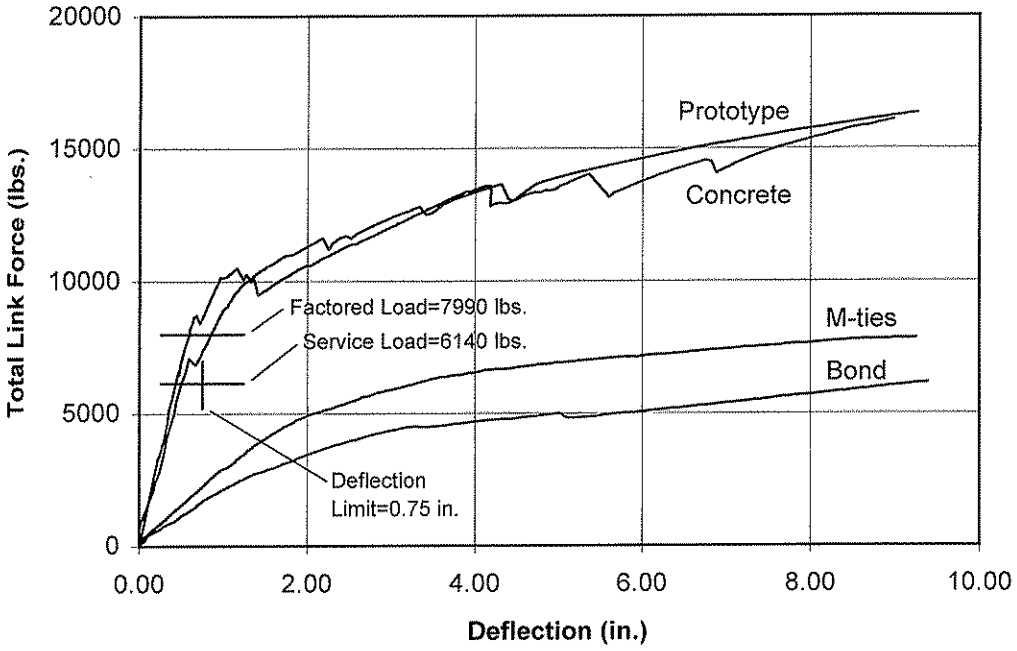


Figure 5.13 Plot of load versus deflection for all test panels showing the design loads for the Prototype panel.

# CHAPTER 6
# SUMMARY, CONCLUSIONS, AND DESIGN RECOMMENDATIONS

## 6.1 INTRODUCTION

There are at least three potential mechanisms of horizontal shear transfer which contribute to composite action in precast sandwich wall panels. These mechanisms are: (1) solid concrete regions; (2) mechanical connectors that pass through the insulation wythe; and, (3) bond between the concrete wythes and the insulation. The primary objective of this research was to investigate the flexural behavior of sandwich panels and the contribution to composite action provided by regions of solid concrete, wythe connectors, and bond.

Tests were performed on four full-scale precast sandwich wall panels. The first sandwich panel tested was a typical sandwich panel that would be produced for a building project. This panel included regions of solid concrete in the insulation wythe, metal wythe connectors, and no attempt was made to disrupt the bond between the concrete wythes and the insulation wythe. The degree of composite action developed by each of the different shear transfer mechanisms was then evaluated by testing three additional panels that included only one mechanism of shear transfer (solid concrete, wythe connectors, or bond).

A summary of the test results is presented in Section 6.2. The conclusions of the study are presented in Section 6.4, and design recommendations are presented in Section 6.4. Finally, recommendations for future research are presented in Section 6.5.

## 6.2 SUMMARY OF RESULTS

From the test results, it was determined that the Prototype panel behaved as a fully composite panel, with 100 percent composite action. The Concrete panel behaved nearly as a fully composite panel, with the solid concrete regions causing the panel to reach 92 percent composite action. The M-tie panel behaved nearly as a non-composite panel with the M-ties causing the panel to achieve only 10 percent composite action. The Bond panel also behaved nearly as a non-composite panel, with the bond causing the panel to achieve only 5 percent composite action.

Although the Prototype and Concrete panels behaved as fully or nearly fully composite panels in terms of load-deflection, plane section behavior was not observed. This is attributed to the intermittent placement of the solid concrete regions along the pan of the panel. Failure of all test panels occurred by yielding of the prestressing steel and by large deflection. Concrete crushing did not occur by the point at which testing was stopped.

## 6.3 CONCLUSIONS

The major conclusions from this research are as follows:

1. For the panel geometries and materials treated in this study, the solid concrete regions provide most of the strength and stiffness that contribute to composite behavior. Steel M-tie connectors and bond between the insulation and concrete contribute relatively little to composite behavior.

2. A precast concrete sandwich wall panel constructed similarly to the Prototype panel treated in this study will behave as a fully composite panel in terms of service load-deflection behavior and flexural strength.

3. Panels with solid concrete regions placed intermittently along the span develop stress concentrations at the solid regions, do not exhibit plane section behavior through the depth of the panels, and develop strains that are not uniform across the width of the panels. These effects seem to contribute to early flexural cracking at service loads. Non-uniformity of strains across the width of the panel may also contribute to a reduction in the value of bending moment at which yielding of the prestressing steel occurs.

## 6.4 DESIGN RECOMMENDATIONS

For design purposes, it is recommended that solid concrete regions be proportioned to provide all of the required composite action in a precast sandwich wall panel. If full composite action is required at service loads, the amount and arrangement of solid concrete regions similar to the amount provided in the Prototype panel will largely achieve this requirement. If flexural cracking at service load is a concern, allowance should be made for the expected reduced cracking stress that occurs in panels with intermittent placement of solid concrete regions along the span. Alternatively, the effects of intermittent placement of the solid concrete regions may be reduced or eliminated by designing a panel with a prismatic section (e.g. solid concrete ribs that run the entire span length of a panel). If full composite behavior is required at overload, the solid regions should be designed to provide adequate strength to resist the horizontal forces that develop at this overload, and the solid concrete regions should be arranged to minimize shear lag to ensure that the entire panel width is effective in compression. Current code approaches such as shear friction may be used to proportion the solid regions in this case.

One disadvantage of relying on solid concrete regions to provide composite action is that the thermal performance of the panel is adversely affected by the thermal bridges created by the solid concrete regions. In such instances, it may be required to eliminate the solid concrete regions and provide composite action through the wythe connectors and / or the insulation. If this is the case, then the connectors and insulation should be designed specifically for that purpose. For example, alternative configurations of wythe connectors, such as truss connectors, may be designed and evaluated as a means to provide composite action. Insulation materials with variable thickness (for example, stepped or corrugated profiles) that provide mechanical interlock with the concrete may be designed and evaluated as a means to provide composite action. In either case, the performance of the system should be verified by full-scale testing.

## 6.5 FUTURE WORK

Additional research is needed to address the role of panel width on the behavior of precast concrete sandwich wall panels that employ solid concrete regions placed intermittently along the span of the panel. The results presented in this report show that panels with solid concrete regions placed intermittently along the span develop stress concentrations at the solid regions, that the panels do not exhibit plane section behavior through the depth of the panels, and that strains are not uniform across the width of the panels. These effects seem to contribute to early flexural cracking at service loads. The panels treated in this research are narrower than many panels used in practice. It may be that these effects are even more significant in wider panels. Further, it is not unreasonable to suspect that any shear lag that contributes to nonuniform strains across the width of the panel may also have an effect on bending strength, since a reduced effective width in compression will result in a larger stress block depth, and thus a smaller internal lever arm and resulting bending moment capacity.

# REFERENCES

ACI Committee 318, "Building Code Requirements for Structural Concrete (ACI318-99) and Commentary (ACI 318R-99)," American Concrete Institute, Farmington Hills, MI, 1999.

ACI Committee 533, "Guide for Precast Concrete Wall Panels (ACI533-R93)," American Concrete Institute, Farmington Hills, MI, 1996.

Bush, T.D., Jr., and Stine, G.L., "Flexural Behavior of Composite Prestressed Sandwich Panels," M.S. Thesis, Department of Civil Engineering, University of Oklahoma, Norman, Oklahoma, 1992, 133 pp.

Bush, T.D., Jr., and Stine, G.L., "Flexural Behavior of Composite Prestressed Sandwich Panels With Continuous Truss Connectors," PCI Journal, Vol. 39, No. 2, March-April 1994, pp. 112-121.

Einea, A., Salmon, D.C., Fogarasi, G.J., Culp, T.D., and Tadros, M.K., "State-of the-Art of Precast Concrete Sandwich Panels," PCI Journal, Vol. 36, No. 6, November-December 1991, pp. 78-98.

Hofbeck, J.A., Ibrahim, I.O., and Mattock, A.H., "Shear Transfer in Reinforced Concrete," ACI Journal, Vol. 66, No. 2, February 1969, pp.119-128.

Nijhawan, J.C., "Insulated Wall Panels-Interface Shear Transfer," PCI Journal, Vol. 43, No. 3, May-June 1998, pp.98-101.

Nilson, A.H., Design of Prestressed Concrete, Second Edition, John Wiley and Sons, Inc., 1987, 592 pp.

PCI Committee on Precast Sandwich Wall Panels, "State-of-the-Art of Precast/Prestressed Sandwich Wall Panels," PCI Journal, Vol. 42, No. 2, March-April 1997, pp. 992-134, Vol. 42, No. 3, May-June 1997, pp. 32-48.

PCI Design Handbook – Precast and Prestressed Concrete, Fifth Edition, Precast/Prestressed Concrete Institute, Chicago, IL, 1999.

Pfiefer, D.W. and Hanson, J.A., "Precast Concrete Wall Panels: Flexural Stiffness of Sandwich Panels," Special Publication 11, American Concrete Institute, Farmington Hills, MI, March 1964, pp.67-86.

# APPENDIX A

Panel Design Parameters:

| | |
|---|---|
| Wind load | = 32 psf |
| Panel self weight | = 75 psf |

Assume panel behaves as 70% composite during service.

Allowable tension stresses:

The allowable tension stresses for wall panels are defined in Section 2.5.3.3 of the ACI Committee 533 Report.

| | | |
|---|---|---|
| Stripping and Handling | $= 5\sqrt{f'_{ci}}$ | = 0.296 ksi |
| Travel | $= 5\sqrt{f'_{c}}$ | = 0.387 ksi |
| Service | $= 7.5\sqrt{f'_{c}}$ | = 0.580 ksi |

Check stripping and handling stresses:

Forces imposed during stripping and handling are discussed in Section 5.2 of the PCI Handbook.

| | |
|---|---|
| Stripping multiplier | = 1.4 (controls) |
| Handling multiplier | = 1.2 |
| Factored panel weight = 1.4(75) | = 105 psf |

Check stress due to bending about x-axis (where the x-axis is defined as the axis along the length of the panel):

$+M_x = -M_x = 0.0054wb^2L' = 0.0054(105/1000)(6)^2(37)$ = 0.76 kip-ft.
= 9.1 kip-in.

Resisting width of panel:

(a) 15t = 15(8) =120 in.
(b) L/4 = 37(12)/4 = 111 in. (controls)

Effective section modulus:

| | | |
|---|---|---|
| $S_{eff}$ | = 756(111/72) | = 1166 in.$^3$ |
| $f_x = -f_{pe} + \frac{M_x}{S_{eff}}$ | = -0.350 + (9.1/1166) | = -0.342 ksi |

-0.342 ksi < 0.296 ksi, O.K

Check stress due to bending about y-axis (where the x-axis is defined as the axis along the width of the panel):

$+M_y = -M_y = 0.0062wbL'^2 = 0.0062(105/1000)(6)(37)^2$ = 5.17 kip-ft.
= 62.1 kip-in.

Resisting width of panel:
b/2 = 72/2 = 36 in.

Effective section modulus :
$S_{eff}$ = 756(36/72) = 378 in.$^3$

$f_y = -f_{pe} + \frac{M_y}{S_{eff}}$ = -0.350 + (62.1/378) = -0.186 ksi

-0.342 ksi < 0.296 ksi, O.K.

Check travel stresses:

Forces imposed during travel are also discussed in Section 5.2 of the PCI Handbook.

Stripping multiplier = 2.0 (more conservative than PCI value of 1.5)
Factored panel weight = 1.4(75) = 150 psf

Check stress due to bending about x-axis:

$+M_x = -M_x = 0.0054wb^2L' = 0.0054(150/1000)(6)^2(37)$ = 1.08 kip-ft.
= 12.9 kip-in.

$f_x = -f_{pe} + \frac{M_x}{S_{eff}}$ = -0.350 + (12.9/1166) = -0.339 ksi

-0.339 ksi < 0.387 ksi, O.K.

Check stress due to bending about y-axis:

$+M_y = -M_y = 0.0062wbL'^2 = 0.0062(150/1000)(6)(37)^2$ = 7.63 kip-ft.
= 91.7 kip-in.

$f_y = -f_{pe} + \frac{M_y}{S_{eff}}$ = -0.350 + (62.1/378) = -0.186 ksi

-0.186 ksi < 0.387 ksi, O.K

Nominal Moment Capacity:

The nominal moment capacity of the section is computed using the equation for $f_{ps}$, given in Section 18.7.2 of the ACI 318 Code.

$$f_{ps} = f_{pu}\left[1-\frac{\gamma_p}{\beta_1}\left(\rho_p \frac{f_{pu}}{f'_c}\right)\right], \qquad \text{where } \gamma_p=0.28 \text{ and } \beta_1=0.75$$

$$f_{ps} = f_{pu}(1-16.8\rho_p)$$

Assuming non-composite action:

$$\rho_p = \frac{A_p}{bd_p} = \frac{0.46}{72(1.5)} = 0.00426$$

$f_{ps}$ = 250.7 ksi

$$a = \frac{A_p f_{ps}}{0.85 f'_c b} = \frac{0.46(250.7)}{0.85(6)(72)} = 0.31 \text{ in.}$$

$$\phi M_n = \phi A_p f_{ps}(d_p - \frac{a}{2}) = 0.9(0.46)(250.7)(1.5-\frac{0.31}{2}) = 140.1 \text{ kip-in.}$$

$\phi M_n$ = 280 kip-in. (for 2 wythes)

Assuming composite action:

$$\rho_p = \frac{A_p}{bd_p} = \frac{0.92}{72(4)} = 0.00320$$

$f_{ps}$ = 255.5 ksi

$$a = \frac{A_p f_{ps}}{0.85 f'_c b} = \frac{0.92(255.5)}{0.85(6)(72)} = 0.64 \text{ in.}$$

$$\phi M_n = \phi A_p f_{ps}(d_p - \frac{a}{2}) = 0.9(0.92)(255.5)(4-\frac{0.64}{2}) = 778 \text{ kip-in.}$$

Design moment capacity of 70% composite panel:

$\phi M_n = 0.70(778-280) + 280 = 629$ kip-in.

Cracking Moment:

As given by Section 18.8.3 of the ACI 318 Code, the design flexural strength must be at least 1.2 times the cracking strength.

Section properties for 70% composite panel:
$I_{pc} = 0.70(3024 - 324) + 324 = 2214$ in.$^4$
$S_{pc} = 2214/4 = 553$ in.$^3$

$$M_{cr} = (f'_r + f_{pe})S_{pc} = (0.58 + 0.35)(553) = 514 \text{ kip-in.}$$

Check $\phi M_n > 1.2M_{cr}$
$\phi M_n/M_{cr} = 629/514 = 1.2$, O.K.

Ultimate Moment:

U = 0.9D + 1.3 W = 1.3(32) = 41.6 psf
w = 41.6(6) =250 lbs./ft. = 0.021 kip/in.

$$M_u = \frac{wL^2}{8} = \frac{0.021(35\times12)^2}{8} = 463 \text{ kip-in.}$$

$\phi M_n > M_u$, O.K.

Check Service Stresses:

w = 32 psf(6 ft.) = 192 lbs./ft. = 0.016 kip/in.

$$M_s = \frac{wL^2}{8} = \frac{0.016(35\times12)^2}{8} = 353 \text{ kip-in.}$$

$$f_s = -f_{pe} + \frac{M_s}{S_{pc}} = -0.350 + (353/553) = 0.288 \text{ ksi}$$

0.288 ksi < 0.580 ksi, O.K